UNCLASSIFIED

CONFIDENTIAL

NATIONAL AERONAUTICS AND SPACE ADMINISTRATION

Classification Changed to
UNCLASSIFIED
JPL-Letter to Authority NASA-Langley
on Nov. 4, 1970 signed by W. E. Stevens
Date
Jan. 4 1971
By
A. Castain

Space Programs Summary No. 37-38, Volume I

for the period January 1, 1966 to February 28, 1966

The Lunar Program

(Title Unclassified)

JET PROPULSION LABORATORY
LIBRARY
MAY 20 1966

Copy No. 454

CALIFORNIA INSTITUTE OF TECHNOLOGY

JET PROPULSION LABORATORY
CALIFORNIA INSTITUTE OF TECHNOLOGY
PASADENA, CALIFORNIA

March 31, 1966

LAB-C00873

CONFIDENTIAL

GROUP 4 Downgraded at 3 ... declassified after ...

UNCLASSIFIED

145911

Preface

The *Space Programs Summary* is a six-volume, bimonthly publication that documents the current project activities and supporting research and advanced development efforts conducted or managed by JPL for the NASA space exploration programs. The titles of all volumes of the *Space Programs Summary* are:

Vol. I. The Lunar Program (Confidential)

Vol. II. The Planetary–Interplanetary Program (Confidential)

Vol. III. The Deep Space Network (Unclassified)

Vol. IV. Supporting Research and Advanced Development (Unclassified)

Vol. V. Supporting Research and Advanced Development (Confidential)

Vol. VI. Space Exploration Programs and Space Sciences (Unclassified)

The *Space Programs Summary,* Vol. VI consists of an unclassified digest of appropriate material from Vols. I, II, and III; an original presentation of technical supporting activities, including engineering development of environmental-test facilities, and quality assurance and reliability; and a reprint of the space science instrumentation studies of Vols. I and II.

W. H. Pickering, *Director*
Jet Propulsion Laboratory

Space Programs Summary No. 37-38,Volume I

Copyright © 1966, Jet Propulsion Laboratory, California Institute of Technology

Prepared under Contract No. NAS 7-100, National Aeronautics & Space Administration

[redacted] contains information affecting the national defense of the United States, within the mean[redacted] 794, the tr[redacted]mission or revelation of which in [redacted]ner to an unauthorized person is prohibited by law.

UNCLASSIFIED
CONFIDENTIAL

Contents

I. *Surveyor* Project 1
A. Introduction 1
B. System Engineering 2
C. System Analysis 6
D. Launch Operations 16
E. System Testing 21
F. Flight Control 23
G. Electronics 30
H. Electrical Power Supply 32
I. Thermal Control 37
J. Engineering Mechanics 43
K. Propulsion 51
L. Spacecraft Vehicle and Mechanisms 75
M. SC-1 Transit Thermal Model 80
N. Aerospace Ground Equipment 84

Reference 85

UNCLASSIFIED
CONFIDENTIAL

CONFIDENTIAL

I. *Surveyor* Project

A. Introduction

Calculated to span the gap between the *Ranger* flights and Project *Apollo*, the *Surveyor* spacecraft is designed to take the next step in lunar technology by attempting soft landings on the Moon. The first launches will be engineering test missions to demonstrate system capability up to soft landing, and limited postlanding operations. The engineering payload includes elements of redundancy, diagnostic telemetry, touchdown instrumentation, and survey TV.

Following the engineering test missions, *Surveyor's* objectives are to extend our knowledge of lunar conditions and to verify suitability of *Apollo* landing sites.

Hughes Aircraft Company, Space Systems Division, is under contract to develop and fabricate the first seven spacecraft. The launch vehicle is a combination *Atlas/Centaur*. The JPL Space Flight Operations and Deep Space Network (Mission Operations System) will be utilized for flight control and tracking. The first launch is presently anticipated for the second quarter of 1966.

The major portion of the following material relating to the *Surveyor* spacecraft system was derived from material prepared by the Hughes Aircraft Company; articles prepared by the JPL Technical Sections are identified by footnotes to the article titles. The principal model designations and vehicles discussed are defined in Table 1.

Table 1. Model and vehicle designations

Designation	Description
SC-1—7	Flight spacecraft with engineering payload
SC-8—10	Flight spacecraft with scientific payload
A-21	Model designation for spacecraft with engineering payload (SC-1—7)
A-24	Model designation for spacecraft with scientific payload (SC-8—10)
T-21	Model A-21 prototype system test spacecraft
T-2	Simplified spacecraft for evaluation of terminal descent propulsion and flight control
S-2	Test spaceframe for vibration, shock, and static structural tests
S-6, -7	Test spaceframe for vernier propulsion system tests
S-9	Structural test model
S-10	Temperature control model

UNCLASSIFIED

UNCLASSIFIED
CONFIDENTIAL

B. System Engineering

1. A-21 Spacecraft Configuration

Model A-21 spacecraft, which will be used for the first seven missions, carry an engineering instrument payload to evaluate spacecraft performance and lunar soft landing characteristics. The current A-21 weight summary is shown in Table 2, a more detailed weight breakdown is given in Table 3, and the balance summary, showing the center of gravity (CG) location, is given in Table 4.

Table 2. Weight summary

Item	Current design weight, lb
Total separated weight	2194.00
Basic bus	708.13
Usable propellant	1422.37
Engineering payload	63.50

Table 3. Weight breakdown

Item	Current design weight, lb
Basic bus (total)	708.13
Flight control	56.28
Usable propellant (total)	1422.37
Engineering payload (total)	63.50
Survey Camera 3 and auxiliary	22.46
Auxiliary battery installation	28.49
Engineering instrumentation (added)	12.52
Buoyance—payload	0.03
Electronics	120.72
Electrical power	54.32
Mechanisms	29.70
Spacecraft vehicle	213.92
Spacecraft propulsion (not including usable propellant)	223.32
Ballast	9.36
Buoyancy—basic bus	0.51

Table 4. Weight and balance summary

Condition	Weight, lb	Vertical center of gravity Z[a], in.	Lateral center of gravity X, in.	Lateral center of gravity Y, in.
Total separated weight (after *Centaur* separation)	2194.00	11.97	+0.04	−0.18
Maximum touchdown weight	645.58	16.81	−0.03	−0.14
Minimum touchdown weight	619.35	17.28	−0.01	−0.11

[a] Inches above landing gear hinge line (spacecraft Station 47.48).

2. A-24 Spacecraft Configuration

Under contract Modification 56, A-24 is a new designation superseding A-21A and denoting a scientific instrument payload version of the spacecraft. All effort on the A-21A spacecraft has been stopped, except for a few key items applicable to the A-24 configuration.

The current weight summary is shown in Table 5; a more detailed weight breakdown is given in Table 6; and the balance summary, showing the CG location, is given in Table 7.

3. Reliability

a. System and Subsystem A Priori *Reliability.* The *a priori* reliability of the A-21 *Surveyor* spacecraft for the

Table 5. Weight summary

Item	Current design weight, lb
Total separated weight	2524.53
Basic bus	743.20
Usable propellant	1649.60
Scientific payload	131.73

Table 6. Weight breakdown

Item	Current design weight, lb
Basic bus (total)	743.20
Flight control	56.38
Electronics	117.85
Electrical power	54.72
Mechanisms	32.41
Spacecraft vehicle	229.38
Spacecraft propulsion (not including usable propellant	237.42
Weight tolerance and contingency	14.50
Buoyancy—basic bus	0.54
Usable propellant (total)	1649.60
Scientific payload (total)	(131.73)
Survey television experiment subsystem	43.31
Soil mechanics/surface sampling experimental subsystem	13.79
Alpha scattering instrument and auxiliary	21.63
Seismometer and auxiliary	11.58
Micrometeorite ejecta detector and auxiliary	6.98
Touchdown dynamics instrumentation subsystem	32.03
Nonremovable harness	2.35
Buoyancy—payload	0.06

UNCLASSIFIED

UNCLASSIFIED

Table 7. Weight and balance summary

Condition	Weight, lb	Center of gravity, in.		
		Vertical Z[a]	Lateral X	Lateral Y
Total separated weight (after *Centaur* separation)	2524.53	11.66	−0.32	−0.16

[a]Inches above landing gear hinge line (spacecraft Station 47.48).

flight and landing mission is 0.811. Estimates by subsystem are shown in Table 8. There have been no significant changes since the last reporting period.

b. Reliability Estimates for SC-1 Based on Test Data. The data-based reliability estimate for SC-1 is 0.61 for the flight and landing mission. The primary source of data for the estimate is system testing on SC-1. Unit flight acceptance test data or *a priori* estimates are utilized only when system testing does not provide data on a unit. Reliability estimates by subsystems are shown in Table 9. The increase since the last reporting period was primarily caused by an increase in failure-free test time.

Table 8. *A priori* reliability flight and landing mission

Subsystem	Reliability
Telecommunications	0.975
Vehicle mechanisms	0.986
Propulsion	0.922[a]
Electrical power	0.957
Flight controls	0.955
System	0.811

[a]Excludes vernier engine thrust chamber assemblies.

c. Components and Materials.

Summary of spacecraft trouble and failure reports (TFRs) with components designated as cause of failure. An analysis of spacecraft TFRs, having components designated as the cause of failure, has been completed in the form of a matrix correlating failed parts with the units in which they failed. Three categories of TFRs were presented, those dated 1964 and earlier, 1965 TFRs, and TFRs written during system test.

Three hundred and thirty-three TFRs were analyzed. There were 238 dated 1964 and earlier, 72 dated 1965 and 23 written during system test. Because of this study, the following parts were pointed out as potential component problems: (1) 988644 (resistor), (2) 988682 (potentiometer), (3) 988500 (capacitor), (4) 988809 (transistor)

Table 9. SC-1 subsystem reliability estimates based on test data, flight, and landing mission

Subsystem	Reliability
Telecommunications	0.936
Vehicle mechanisms	0.872
Propulsion	0.924[a]
Electrical power	0.935
Flight controls	0.860
System	0.61

[a]Excludes vernier engine thrust chamber assemblies.

(5) 988810 (transistor), (6) 236405 (variable resistor), and (7) 988114 (O-ring). Components (1) through (5) are under intensive investigation. Action to analyze components (6) and (7) was also initiated.

Aerospace ground equipment (AGE) TFRs with components designated as cause of failure. Component problems pertaining to AGE were also presented in matrix charts as follows:

(1) Components replaced in *Surveyor* AGE ground handling equipment.

(2) Components replaced in AGE-system test equipment assembly (STEA) only.

(3) Components replaced in *Surveyor* AGE common to STEA and command data handling console.

(4) Components replaced in *Surveyor* AGE-CDC only.

An analysis based on the above revealed that the AGE equipment had the following five possible generic types of component part problems:

(1) [1]Diode: 1N1355AR–CDC

(2) Transistor: 2N2538–CDC

(3) [1]Transistor: 2N1308–STEA and CDC

(4) Transistor: 2N1613–STEA and CDC

(5) [1]Switch: MH-6AT series–STEA and CDC

Revised tab-run listings of component TFRs. To improve visibility on the status of our component problems, revisions to the present method of EDP tabulations are being planned. The objective of such revisions is to permit rapid assessment of component problems so that engineering may concentrate on the most predominant problem areas. In addition, timely summaries of the

[1]Parts presently being diagnosed for assignable cause of failure.

CONFIDENTIAL
UNCLASSIFIED

UNCLASSIFIED
CONFIDENTIAL

large number of TFRs related to a component failure or mere replacement will be feasible. To perform the aforementioned task, the following series of sorting operations will be a part of EDP tab runs:

(1) Part number

(2) Family code

(3) Lowest assembly or module number

(4) Circuit symbol

(5) Date

Accomplishment of a component listing by this method will permit easier evaluation of a component problem that may be common to several control items or units. It will also provide better visibility regarding the number of problems in a particular component. The classification, test type, environment, cause, and relevancy codes are also necessary additions to the present tab runs to determine if the component was actually the cause of a failure.

The part number sort will show the desired summary of causes of component failures and location of failure by test type. This is needed to ascertain *where* the largest number of component failures are occurring and to obtain a further delineation as to the cause of failures related to components.

Specific component status presentation. To assure analyses in depth are performed on components having a significant number of failures, an analysis format highlighting the following five aspects was devised:

(1) A time phased histogram showing the number of TFRs reported against a specific component. Such histograms provide a broad assessment as to the quantity and trends of problems pertaining to a component. Also the effectiveness of corrective actions taken is easily visible.

(2) Location and quantity of failures indicating where the greatest number of problems are occurring. If such problems should occur in systems testing, a significant component reliability problem exists.

(3) A listing of the causes of failure coupled with the frequency of occurrence, number of parts analyzed, and corrective action taken.

(4) A section pertaining to the mode of failures, providing information as to the mechanism of failure and the best method of correction.

(5) A portion of the chart indicating the various applications of the TFRs as to specific units or control items and also the number of TFRs against each unit or control item. Presentation of this information permits a qualitative assessment as to the ratio of failures and quantity of applications. Also provided is a method of assessing if a particular unit is having problems because of a particular part and if such a part is a common problem among several units.

Environmental matrix. The specification for each component listed in the HAC Approved Parts Guide for *Surveyor* was reviewed and the environmental requirements called out were listed in matrix form. The matrix will be analyzed to determine if any spacecraft component is used in an application where its environmental requirements are exceeded.

Detailed analysis of component TFRs. A study of the 988808 transistor TFRs indicated that it would be desirable to determine if devices similar to the 988808 transistor were experiencing the same type of problems. Two such devices were the 988802 and 988810 transistors, which were produced from the same die or mask, the primary difference being their selection for specific performance parameters.

An analysis of 69 TFRs written on the 988802 transistor revealed the following failure categories:

(1) Faulty installation—14 TFRs

(2) Test equipment failure—12 TFRs

(3) Human error and test accidents—15 TFRs

(4) Poor workmanship and solder splashes—6 TFRs

(5) Failure caused by failure of another component—4 TFRs

(6) Transistor blamed for another component failure—7 TFRs

(7) Cause of failure not known—9 TFRs

(8) Circuit design problem—2 TFRs

Analysis of 25 TFRs written on the 988810 transistor revealed the following distribution:

(1) Circuit problem—9 TFRs

(2) Test error—9 TFRs

(3) TFR open—4 TFRs

(4) Workmanship—3 TFRs

UNCLASSIFIED
CONFIDENTIAL

CONFIDENTIAL

From this analysis it was concluded that no self-induced mode of failure existed in the 988802 and 988810 transistors. However, in addition to the above study, a reverse-bias test at high temperature will be performed on ten specimens of each of the transistors to supplement the study.

Surveyor potentiometers are presently susceptible to a high vacuum phenomenon of "cold welding," which is an intermetallic attraction between metals when there is no oxide film. This tendency has been reduced by redesign of wipers and use of solid lubricant. Problems are complicated by restrictions on lubricants not to outgas and not to compromise the electrical properties.

Molybdenum disulfide, a solid dielectric, has been tested as a lubricant without success in chambers at 4×10^{-11} torr. Actions to resolve the above problem are as follows:

(1) Continue investigation of solid lubricant for presently used wire-wound devices.

(2) Reconfigure wiper arm to reduce pressure.

(3) Investigate use of plastic film and Cermet devices.

(4) Use hermetically sealed devices.

(5) Use lubricated sintered compact materials for fabrication of wiper and carriages.

An investigation was made to determine acceptance criteria for standard DO-14 glass diode package (988723) with end seal chips and cracks. Hoffman 1N749A and 1N751A zener diodes and Raytheon 1N3730 high conductance diode were evaluated. Results of these tests indicated that diodes maintained their hermetic seal when exposed to standard military plus space environments and the cracks do not increase in depth nor propagate beyond their original limits.

Analyses of 105 tantalum-fixed solid electrolyte capacitor (988500) TFRs showed the following:

Shorted	35	
Leakage	8	
Open	3	
Damaged or defective	2	
Out of tolerance	1	
		49
Not part failure		48
Unknown		8
		105

Primary cause of the above failures was attributed to soldering techniques during assembly. Training programs have been initiated to ensure that assemblers use proper soldering techniques.

An analysis of cracks in the solder seal and lipping of solder around the lead wires was made. This analysis indicated cracking was caused by the ductility of tin-antimony which is less than nickel. All testing and examination to date has shown that the seal is not affected by either solder cracks or separation and that the bond quality is equal to any combination of solder and lead.

Materials. A study of the cause of solder splash failures occurring during initial terminal wiring or during repair operations has been completed. In this study special *Surveyor*-type circuit boards were fabricated with a glass plate bonded to the underside so that any subsequent solder splashes could be observed. The variables studied included the following: (1) type of terminal (2) type of circuit board plating, (3) method of terminal installation, (4) thickness of fused solder plating on circuit board, and (5) type of adhesive used to bond the insulator and glass plate to the circuit board. It was found that solder splashing could be minimized by using fused solder-plated boards having a minimum of electroplated solder and by using solder-coated terminals which are fused-in-place, rather than hand soldered to the circuit board.

A report has been made on qualification of Minnesota Mining and Manufacturing Company's velvet coating 101-C10 optical black. The material was found to possess satisfactory adhesion and flexibility on a variety of surfaces, exhibited a solar absorptance of approximately 0.97, and a normal infrared emittance of approximately 0.93. The coating was unaffected by ultraviolet exposure of 500 solar-equivalent hr and did not produce a visible condensate on 80°F glass chamber walls when tested for outgassing at 260°F and 10^{-6} torr. Materials Specification HMS15-1376 and Process Specification HP4-143 were written to cover its use on the *Surveyor* spacecraft.

The use of an ionized stream of air for removing static charges has been investigated. A great deal of Teflon and Mylar film is used on *Surveyor*, for both permanent thermal control purposes and for temporary protective wrapping. The static charge which can build up on these films could cause explosion of fuel during loading or cause premature ignition of squibs. In a series of tests, the films were rubbed respectively with bare hands, cotton gloves, and polyethylene coated nylon in a normal laboratory atmosphere and the charge measured. The tests were then repeated in each case with ionized air

UNCLASSIFIED

UNCLASSIFIED
CONFIDENTIAL

from a Simco Aerostat Model AS-20 blowing over the sample. It was found that the discharge rate in the presence of the Aerostate breeze is extremely rapid, complete discharge occurring within 1–3 sec in all cases. Additional studies indicated that the operation does not generate ozone or nitrous oxide in quantities considered dangerous.

A hard chrome plating is desired on aluminum alloy valves and connectors used in the vernier system to provide wear and galling resistance. A special requirement of this plating is that no undercoats such as copper, nickel, or zinc be used because they are not compatible with the monomethyl hydrazine and nitrogen tetroxide fuel and oxidizer involved. An evaluation has been made of the quality of 0.0002 to 0.0003 chrome plating applied directly to 6061 and 7075 alloys by two different vendors. Briefly, the quality of plating by one vendor was found to be poor in dimensional control, coverage, and wear resistance. The plating of the other vendor was satisfactory except that dimensional tolerances in the threaded area exceeded the 0.0001 specified in one case. Parts plated by the latter vendor are presently being tested for compatibility with the monomethyl hydrazine and nitrogen tetroxide.

A low temperature retraction test was conducted on a cured sheet of Raw Corning RTV-731 in accordance with ASTM D-1329-60. Briefly, the test consists of stretching the sample 100%, immersing it in a −70°F alcohol-dry ice bath, releasing the tension, then plotting recovery as the bath is warmed at 1.8°F/min back to room temperature. It was found that the material remains completely frozen until warmed to −65°F and that there is a rapid recovery of rubber-like qualities as the temperature passes between −50° and −40°F. The material has retracted 10% at −54°F, and at −40°F has retracted approximately 90%. Full retraction occurs at about −29°F.

A comprehensive report has been prepared covering the phenomenon of vacuum induced outgassing and its importance to vacuum technology and spacecraft reliability. The report, designated TM-843, is intended to serve as a general guide to those engaged in the design of spacecraft. Included are such subjects as (1) sources of outgassing, (2) types of materials that outgas, (3) rates of outgassing, and (4) the phenomenon of condensation in vacuum. Particular attention is given to sticking coefficients and their importance in the estimation of condensation effects. Various techniques for obtaining outgassing data at HAC and other companies are discussed and compared.

C. System Analysis

1. Radar Altimeter and Doppler Velocity Sensor

The following is an evaluation of spectral spreading loss for a Gaussian spectrum through the actual radar altimeter and doppler velocity sensor (RADVS) signal filter transfer functions. These losses are up to 1 db higher than a previous approximation which evaluated spectral spreading loss for a Gaussian spectrum through a rectangular passband. The results of this study are used to determine tracker signal power under various modes of RADVS operation.

The attenuation effect of the tracker filters on the signal, as a function of signal bandwidth, has been studied. The filter transfer functions are of the form

$$F(S) = \frac{1}{(1 + \tau S)^2} \tag{1}$$

where

$$S = j\omega = j2\pi f.$$

The values of filter constant τ are given in Table 10.

The signal is assumed to have a Gaussian power spectrum

$$P(\omega) = P(0)\, e^{-k\omega^2} \tag{2}$$

where ω is angular frequency. The filter power output is given by

$$P_0 = \int_0^\infty P(\omega)\,|F(\omega)|^2 d\omega \tag{3}$$

$$|F(\omega)|^2 = F(S)\,F(-S) \tag{4}$$

The signal power spectrum can be given in terms of the 3-db bandwidth,

$$\ln e^{-k\omega_3^2} = -k\omega_3^2 = \ln 0.5 = -0.693$$

$$k = \frac{0.693}{\omega_3^2} \tag{5}$$

Eq. (3) becomes

$$P_0(\omega_3, \tau) = \int_0^\infty \frac{P(0)\, e - \dfrac{0.693\,\omega^2}{\omega_3^2}}{[1 + (\tau\omega)^2]^4} d\omega \tag{6}$$

CONFIDENTIAL
UNCLASSIFIED

CONFIDENTIAL

Table 10. Filter characteristics

Filter	Use	Filter constant τ, sec	Estimated maximum signal bandwidth, kc
Radar altimeter			
Narrow-band	Altitude <1000 ft	3.32×10^{-4}	1.8
Wide-band	Altitude >1000 ft	5.11×10^{-5}	8
Doppler velocity sensor			
Narrow-band	After retrorocket burnout	3.32×10^{-4}	3
Wide-band	Before retrorocket burnout	6.11×10^{-5}	9

Eq. (6) is normalized to 100 by multiplying by $200\,(k)^{-1/2}\pi$ since

$$\int_0^\infty e^{-kx^2}\,dx = \frac{1}{2}\left(\frac{\pi}{k}\right)^{1/2} \tag{7}$$

The resulting equation is

$$P_0(\omega_3, \tau) = \frac{200}{\omega_3}\left(\frac{0.693}{\pi}\right)^{1/2} \int_0^\infty e^{\frac{-\frac{0.693\,\omega^2}{\omega_3^2}}{[1+(\tau\omega)^2]^4}}\,d\omega \tag{8}$$

The normalization was checked by setting $\tau = 0$ (unity transfer function). For various bandwidths (ω_3), the results were

$$P_0(\omega_3, 0) = 99.9912 \tag{9}$$

Fig. 1 shows plots of attenuation of filter power output in decibels versus full 3-db signal bandwidth (half-power point to half-power point). The values used are obtained from computer output. Table 11 shows the maximum attenuation expected for each filter.

Table 11. Maximum expected filter attenuation

Filter	Estimated maximum signal bandwidth, kc	Maximum attenuation, db
Radar altimeter		
Narrow-band	1.8	6.26
Wide-band	8	4.77
Doppler velocity sensor		
Narrow-band	3	8.38
Wide-band	9	6.24

2. Reduction of Launch Windows due to Earth Shadow Constraint for May–June and June–July 1966 Launch Periods

One of the constraints that must be applied to the design of *Surveyor* trajectories is that the spacecraft spend not more than ½ hr in the Earth's shadow during transit to the Moon. The effects of this constraint on the May-June through August 1966 launch periods have been investigated. It was found that for the May-June period 3 of the 7 days with launch windows greater than 20 min are essentially eliminated as possible launch days, and the available launch window is greatly reduced on another day. In the June-July period, 1 day is eliminated and on another the available launch window is reduced to 14 min. The spacecraft does not enter the Earth's shadow for any length of time during the July and August launch periods. The effect upon launch opportunity for the first two periods is summarized in Fig. 2, which shows the portions of the available launch windows during which the spacecraft spends more than ½ hr in the Earth's shadow during transit.

Fig. 3 presents detailed information for June 2 during which the spacecraft passes through the Earth's shadow. The upper portion of the figure shows the total minutes spent in the Earth's shadow versus launch time. The lower half presents the time of entrance and exit from the shadow (from launch) measured versus launch time. In the lower portion of Fig. 3, for example, if launch occurs June 2, 1966 at 18:00, the spacecraft will enter the Earth's shadow 152 min after launch and exit 236 min after launch. Total shadow time, from the upper portion of Fig. 3, is 84 min.

3. Characteristics of May–June 1966 Launch Opportunity

The May-June 1966 direct ascent launch period consists of a total of 9 possible launch days. Table 12 presents the launch windows and lunar landing conditions for these 9 days.

The launch windows reflect the available launch times which are based on a launch azimuth sector of 80 to 115 deg (which has been approved by the AFETR for the *Surveyor* direct ascent mission) and the current *Atlas/Centaur* payload capability with a 3-σ flight performance reserve of 210 lb of propellant. Seven of the nine days have acceptable launch windows (greater than 20 min). Improvements in *Atlas/Centaur* performance or use of the 3-σ reserve could result in increased windows at a rate of 0.07 min/lb.

CONFIDENTIAL UNCLASSIFIED

UNCLASSIFIED
CONFIDENTIAL

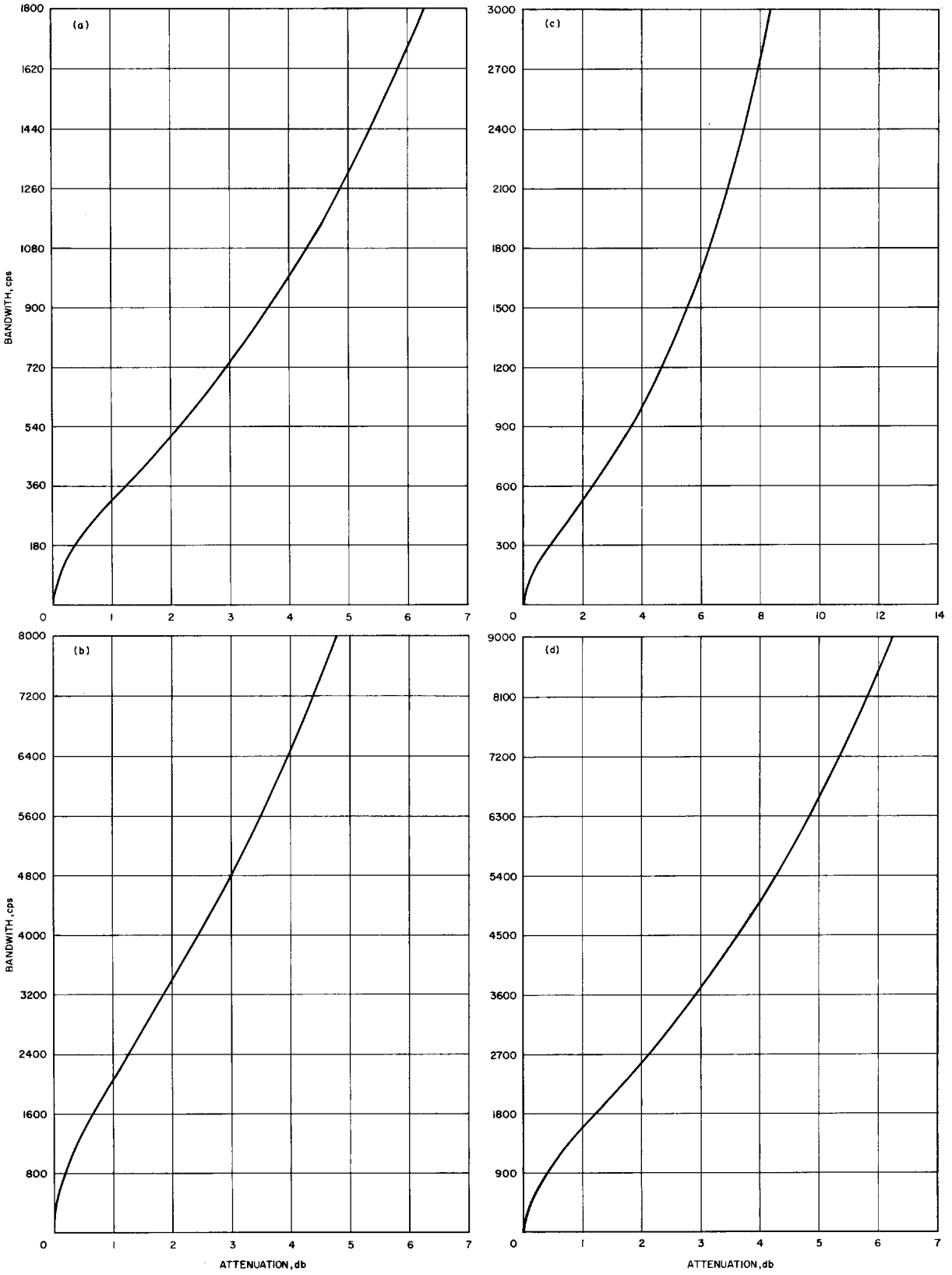

Fig. 1. Attenuation of filter power output (a) RA narrow-band; (b) RA wide-band; (c) DVS narrow-band; (d) DVS wide-band

CONFIDENTIAL
UNCLASSIFIED

UNCLASSIFIED
CONFIDENTIAL

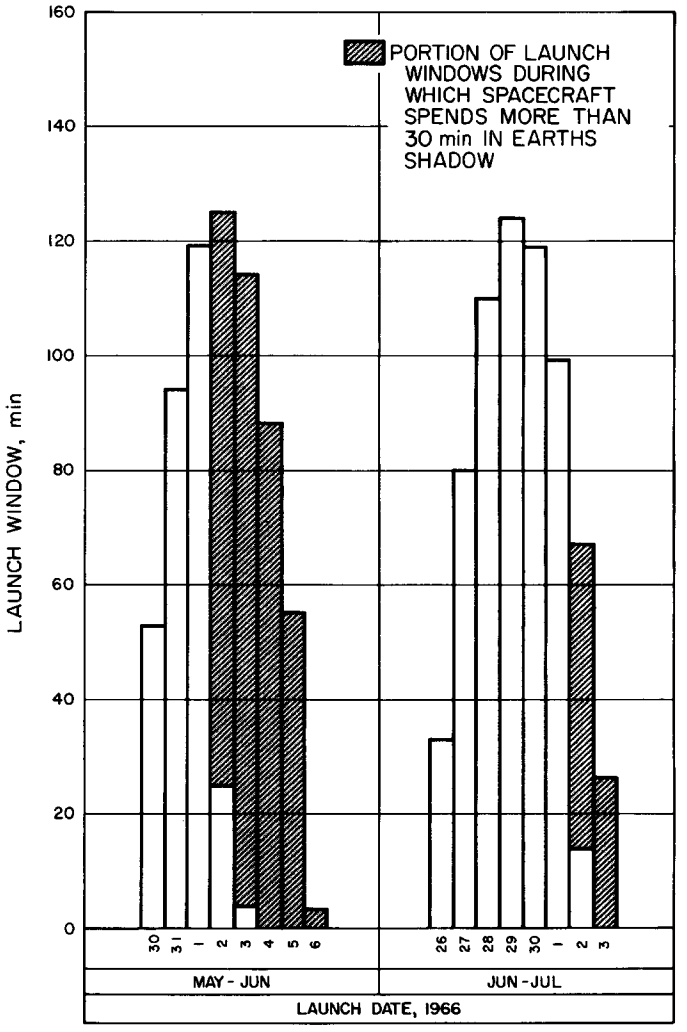

Fig. 2. Direct ascent launch windows May–June and June–July 1966

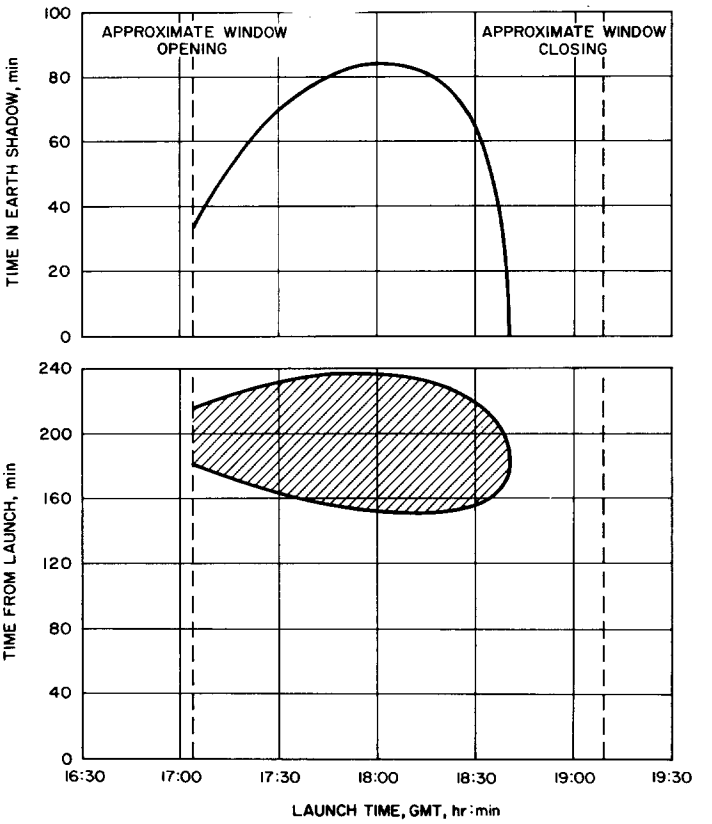

Fig. 3. Spacecraft time in Earth's shadow vs launch time June 2, 1966

The launch windows available will be additionally restricted by the spacecraft's ability to tolerate time spent in the shadow of the Earth during transit. This problem was investigated and it was found that in order to fully exploit the launch vehicle capability it would be necessary

Table 12. Characteristics of May–June 1966 *Surveyor* direct ascent launch period

Launch date	Launch window, min		Arrival date	Unbraked impact				Time to and from terminator, hr		Nominal operational duty cycle at landing, %	
1966	Launch vehicle capability	Spacecraft capability 1966	1966	Speed, m/sec	Selenographic location, deg		Angle, deg	From dawn terminator	To evening terminator	TV survey	Narrow-band engineering data transmission
					S. latitude	W. longitude					
5/29	1	1	6/1	2662	3.25	43.83	7	32	321	100	100
5/30	48	48	6/2	2662	3.25	43.83	6	57	296	100	100
5/31	83	83	6/3	2662	3.25	43.83	5	82	271	65	100
6/1	104	104	6/4	2662	3.25	43.83	4	107	246	42	100
6/2	108	31	6/5	2662	3.25	43.83	5	132	221	25	53
6/3	96	5	6/6	2662	4.00	36.83	3	171	182	10	27
6/4	71	—	6/7	2662	4.00	36.83	4	197	156	13	34
6/5	35	—	6/8	2662	4.00	36.83	5	222	131	27	57
6/6	4	—	6/9	2662	4.00	36.83	6	246	107	45	100

UNCLASSIFIED
CONFIDENTIAL

UNCLASSIFIED CONFIDENTIAL

for the spacecraft to be in shadow for upwards of 1.5 hr. The capability of the spacecraft to withstand the decreasing temperatures associated with shadow time is currently under investigation. The launch windows shown correspond to those trajectories which do not spend more than 30 min in the shadow. It should be noted that an increase in the *Centaur* payload capability, or use of the 3-σ flight performance reserve will not increase the launch windows, as the remaining window (after consideration of shadow time) is limited by the upper launch azimuth limit of 115 deg.

The target criteria for the May-June launch period have been selected. They include an unbraked impact speed of 2662 m/sec and the landing locations shown in Table 12. All locations are near the vertical impact site; the maximum unbraked impact angle is only 7 deg.

The lunar lighting conditions for this period are excellent, ranging from a landing 32 hr (approximately 16 selenocentric deg) after the dawn terminator on the first day to a landing 107 hr (54 selenocentric deg) before the evening terminator on the last day. The landings during the middle portion of the lunar day result in reduced duty cycles for the TV survey and narrow-band engineering data transmission due to the spacecraft's inability to dissipate the heat generated by a 100% duty cycle.

4. Parking Orbit Trajectory Characteristics, January–December 1968

The following ground rules were used in generating the data for this study.

(1) The boost vehicle was the *Atlas/Centaur.*

(2) Launches were assumed to take place from Cape Kennedy with launch azimuth restricted to between 80 and 115 deg east of true north.

(3) The coast time was constrained to between 2 and 20 min.

(4) The parking orbit altitude was 90 n mi.

(5) Arrival at the Moon had to occur 20 hr after lunar sunrise and 150 hr before lunar sunset for a fixed landing site of 45 deg W longitude.

(6) Arrival at the Moon had to occur between 2 hr after Goldstone rise and 3 hr before Goldstone set.

(7) Flight times of the order of 66 hr were assumed.

Fig. 4 shows the variation of parking orbit unbraked lunar impact speed for the year 1968. The top of the bar for each day indicates the impact speed expected for earliest arrival and minimum launch azimuth for that day. The bottoms of the bars represent expected impact speed for latest arrival and maximum launch azimuth for each day. Fig. 5 shows the launch windows for parking orbit trajectories for the same time period.

5. Surveyor System Test TV Linearity Evaluation

The system test linearity evaluation determines final correctability of raw TV data by use of the linear reseau correction technique and by appropriate lens distortion corrections. Twenty linearity test chart control points, selected from all portions of the TV frame, were utilized in the error analyses. These points are the intersections of horizontal and vertical lines on a test pattern. This test target is of a size such that, when used in conjunction with available system test collimators, it approximately fills the TV raster. The distance between adjacent lines is an accurate 0.20375 in.

Of the three normal mode, narrow angle, survey camera linearity films analyzed, the two obtained during group (subsystem) tests easily met the linearity requirements specified in the Functional Requirements, whereas the single telecommunications film was a borderline case.

Of the three group and one telecommunications approach camera linearity films, one group film failed to meet the linearity acceptance criteria, while the remainder satisfied them by a wide margin.

The borderline and failure cases mentioned were, however, subject to readout errors of the reseau and data points because of the limited quality of their films.

6. Updated Prediction of Pretouchdown Conditions for SC-1

The pretouchdown Monte Carlo simulation has been modified to show the effect of biasing the cutoff range circuitry such that, in the presence of T-2H noise levels, the cutoff range will be nominally 14 ft instead of the 16 ft range previously assumed. A 5000 trial Monte Carlo study was performed and resulted in the joint probability density histogram for pretouchdown lateral velocity and incidence angle shown in Fig. 6. The stability boundary superimposed on this figure separates the region of stable and unstable landings. Since there are no simultaneous occurrences of lateral velocity and incidence angle in the unstable region, the probability of a stable landing is greater than 0.999. The marginal probability distribution

UNCLASSIFIED CONFIDENTIAL

UNCLASSIFIED

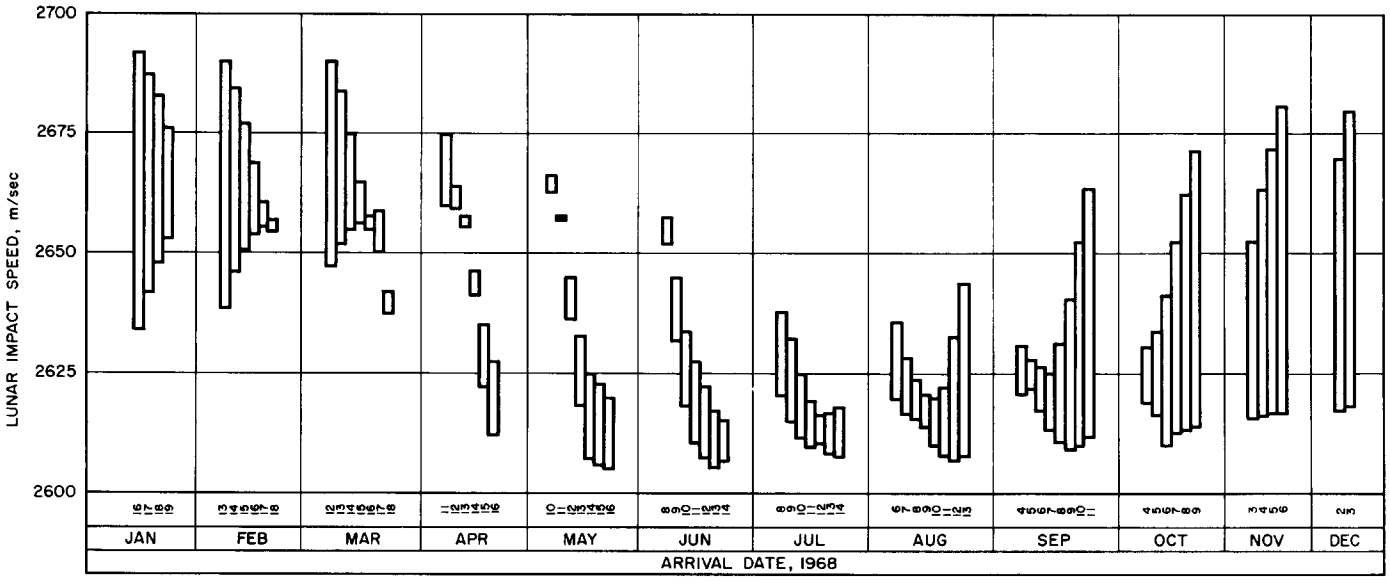

Fig. 4. Variations of parking orbit lunar impact speed, 1968

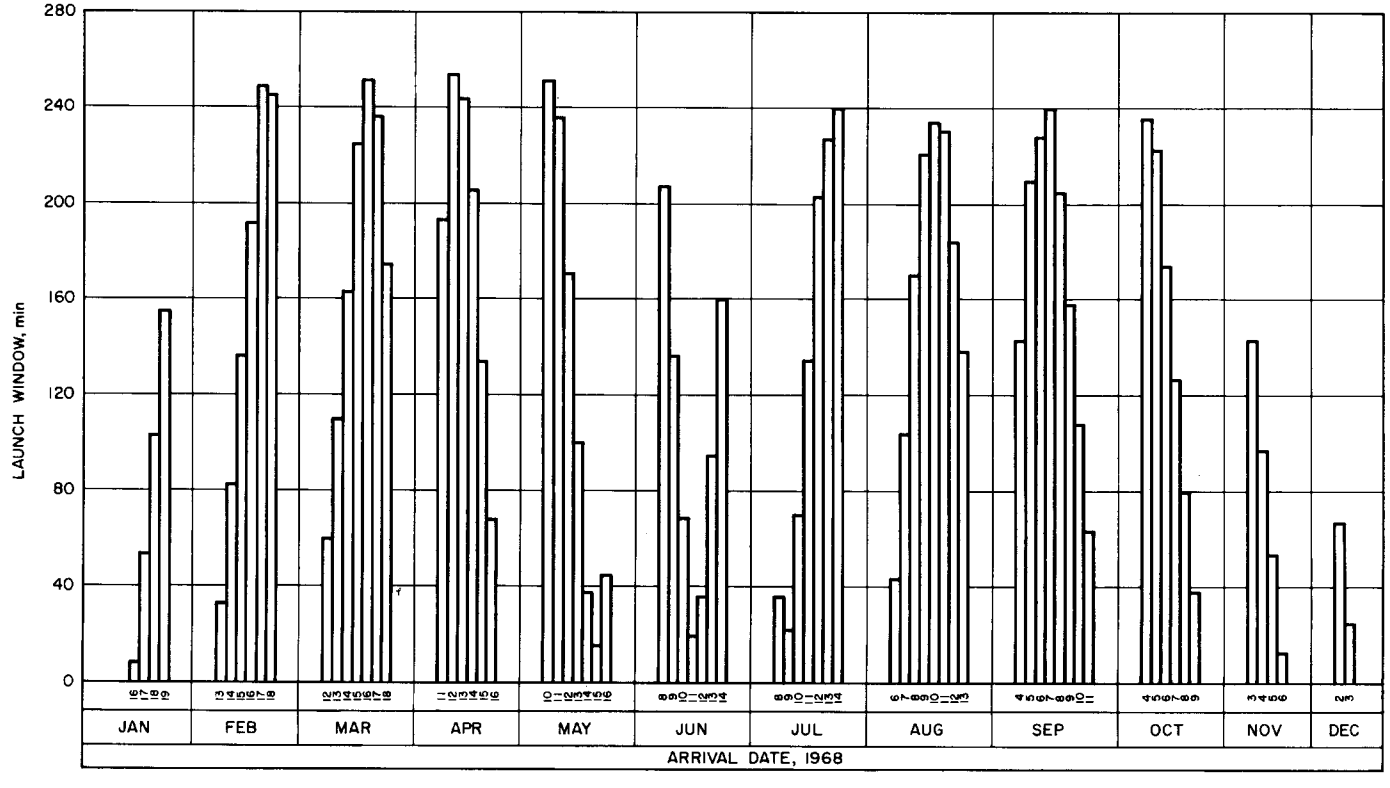

Fig. 5. Parking orbit launch windows, 1968

CONFIDENTIAL
UNCLASSIFIED

UNCLASSIFIED

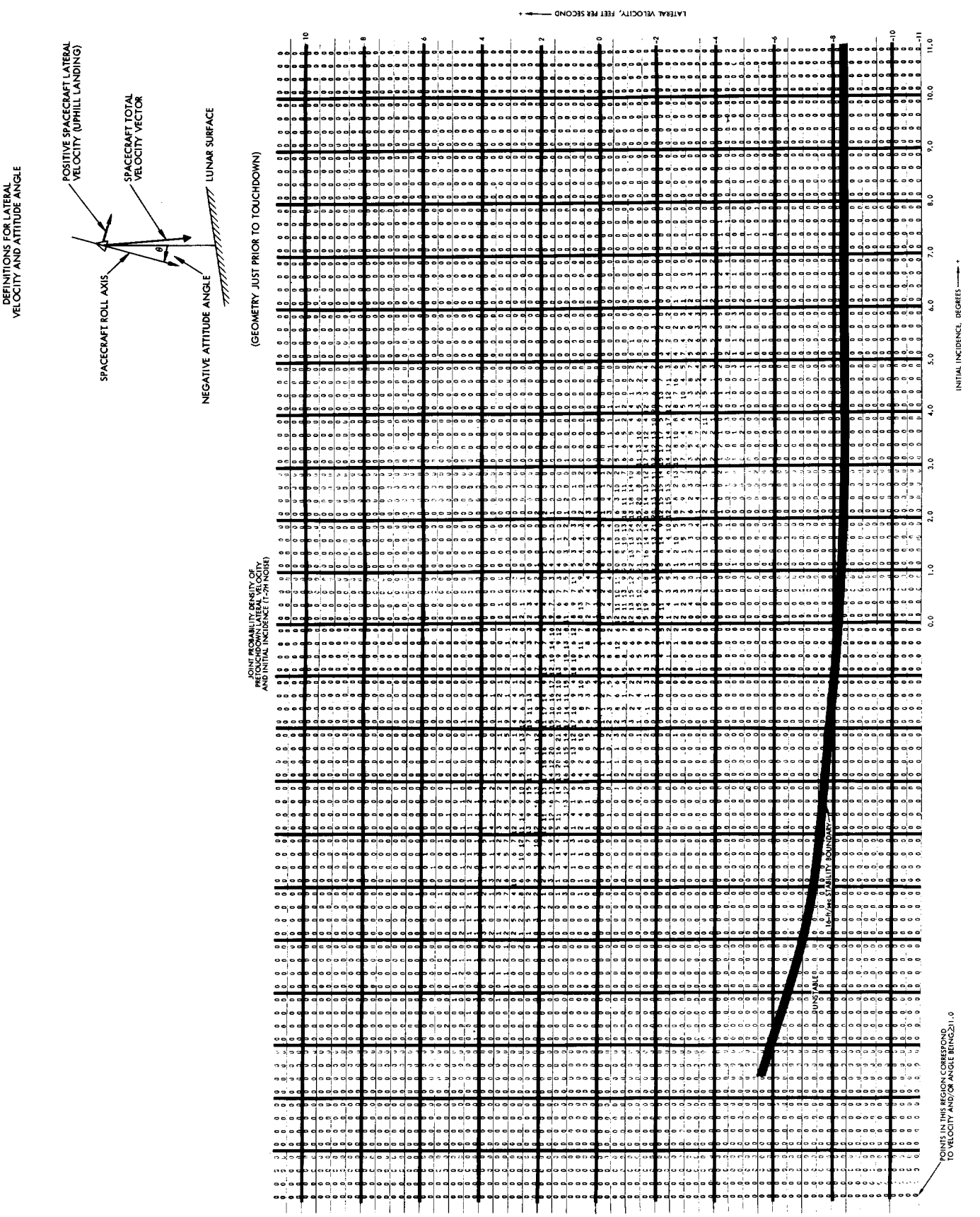
DEFINITIONS FOR LATERAL VELOCITY AND ATTITUDE ANGLE
POSITIVE SPACECRAFT LATERAL VELOCITY (UPHILL LANDING)
SPACECRAFT TOTAL VELOCITY VECTOR
LUNAR SURFACE
SPACECRAFT ROLL AXIS
NEGATIVE ATTITUDE ANGLE
(GEOMETRY JUST PRIOR TO TOUCHDOWN)
JOINT PROBABILITY DENSITY OF PRETOUCHDOWN LATERAL VELOCITY AND INITIAL INCIDENCE (1-2H NOISE)
LATERAL VELOCITY, FEET PER SECOND
INITIAL INCIDENCE, DEGREES
16-ft/sec STABILITY BOUNDARY
POINTS IN THIS REGION CORRESPOND TO VELOCITY AND/OR ANGLE BEING ≥11.0

Fig. 6. Joint probability density of pretouchdown lateral velocity and initial incidence

UNCLASSIFIED

UNCLASSIFIED
CONFIDENTIAL

functions for lateral velocity, vertical velocity, incidence angle and angular velocity are also program outputs and show that

$$Pr(V_{lat} \leq 5.0 \text{ ft/sec}) = 0.99$$
$$Pr(V_{ver} \leq 14.4 \text{ ft/sec}) = 0.99$$
$$Pr(\theta \leq 6.8 \text{ deg}) = 0.99$$
$$Pr(\omega \leq 3.2 \text{ deg/sec}) = 0.99$$

where

$Pr(X \leq X_0)$ denotes the probability that $X \leq X_0$

V_{lat} = magnitude of pretouchdown lateral velocity

V_{ver} = magnitude of pretouchdown vertical velocity

θ = magnitude of pretouchdown incidence angle

ω = magnitude of pretouchdown angular velocity

Fig. 7 shows plots of the marginal density and distribution functions for vertical landing velocity.

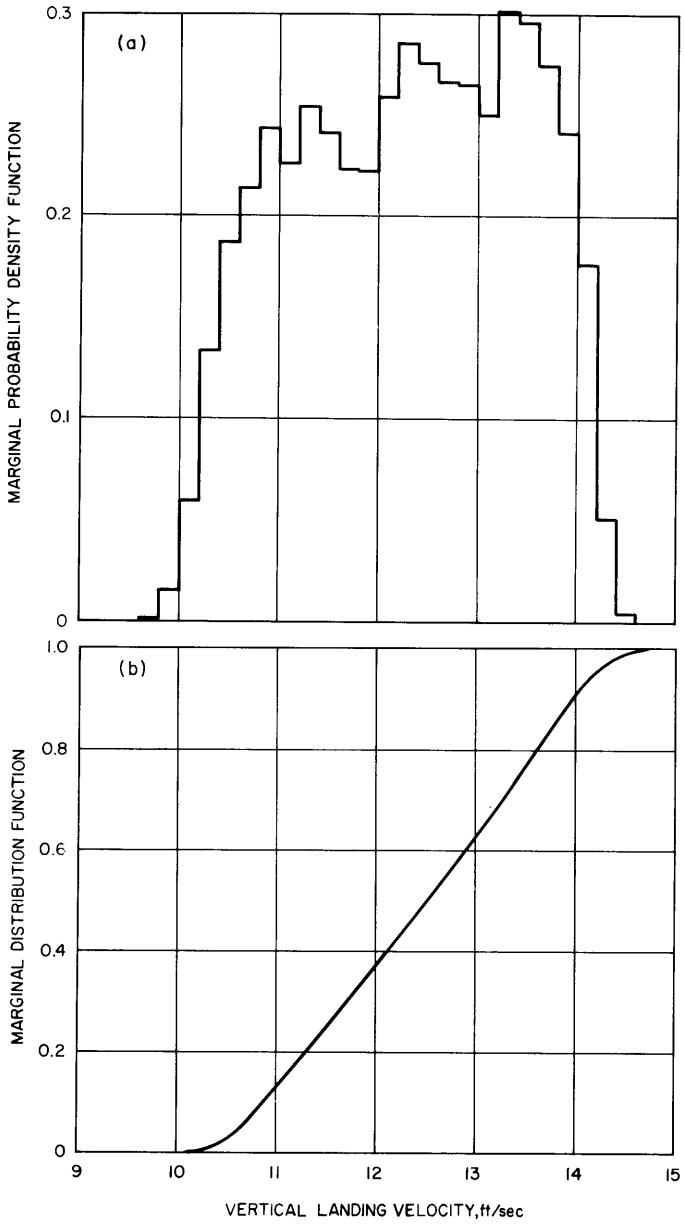

Fig. 7. Marginal density and distribution functions for vertical landing velocity; (a) marginal probability density function vs vertical landing velocity; (b) marginal distribution function vs vertical landing velocity

7. A-24 Retrorocket Engine Separation Tradeoff

As a result of the increase in spacecraft weight and decrease in retrorocket engine inert weight from the A-24 design, it is apparent that the relative acceleration between the A-24 spacecraft and retrorocket during separation will be substantially reduced from that obtained in the A-21 design. The purpose of this study is to develop the tradeoffs associated with possible changes to the present A-24 design to improve retrorocket separation performance.

The following changes were investigated

(1) Increase the high thrust vernier engine command current during separation.

(2) Change the duration of the separation interval.

(3) Change the time when the thrust command is increased to correspond to a delayed time following the acceleration switch signal.

a. Increase high thrust command. The high thrust level of the vernier engines delivered for installation on flight spacecraft is very near the lower boundary of the engine specification. Thus, the command current level of 48 ±5 ma, which was designed to produce a minimum total thrust of 280 lb from the three engines, must be reexamined. At the lower boundary, the required vacuum thrust delivered by a vernier engine is 88 lb (264 lb total for three engines).

The desirable features of increasing the high thrust command are twofold: to increase the relative acceleration between the retroengine and the spacecraft during separation and to reduce the retrorocket propellant requirement. Since the A-21A spacecraft is heavier and the

UNCLASSIFIED
CONFIDENTIAL

UNCLASSIFIED
CONFIDENTIAL

retroengine inerts are lighter, the relative acceleration has decreased from the A-21 design for the same thrust levels as indicated by the following equation

$$a_{S/C-R} = \left[\left.\frac{T}{W}\right|_{S/C} - \left.\frac{T}{W}\right|_{R}\right] g$$

An increase in relative acceleration reduces the possibility of retrorocket engine contact with the spacecraft during separation (possible snagging) and increases the separation distance during the period when radar control of the spacecraft is being established (Fig. 8).

The relative increase in relative acceleration for a corresponding increase in thrust is given by

$$\frac{\frac{\Delta a}{a}}{\frac{\Delta T_{S/C}}{T_{S/C}}} = \frac{1}{1 - (a_R)\left(\frac{W_{S/C}}{T_{S/C}}\right)}$$

where

a = acceleration of spacecraft minus acceleration of retrorocket engine

$T_{S/C}$ = thrust of spacecraft

$W_{S/C}$ = weight of spacecraft at separation time

a_R = acceleration of retrorocket engine produced by its thrust

Substituting in the above equation representative values for the A-21A design yields

$$\frac{\frac{\Delta a}{a}}{\frac{\Delta T_{S/C}}{T_{S/C}}} = \frac{1}{1 - \left(\frac{6.8}{32.2}\right)\left(\frac{856}{274}\right)} = 3$$

The percentage increase in relative acceleration is three times the percentage increase in thrust. For an increase in thrust command from 48 to 66 ma and a corresponding average increase in vernier engine thrust from 91.4 to 101.3 lb (a 11% increase), as determined from flight engine data, a 33% increase in relative acceleration is obtained.

Since the specific impulse of the vernier and retrorocket engine is approximately equal, this improvement in relative acceleration is obtained with no loss in payload. It is expected that if precise calculations were performed, a slight increase in payload capability would result. The increase in vernier propellant required is directly offset by the decrease in required retrorocket propellant.

A disadvantage associated with increasing the vernier thrust level is the decrease in unsaturated pitch/yaw moment capability of the vernier engine system. This capability varies as a function of the direction in which the capability is required, the direction the center of gravity is displaced from the spacecraft roll axis, the distance from the center of gravity to the roll axis, and the difference between the thrust command and the maximum

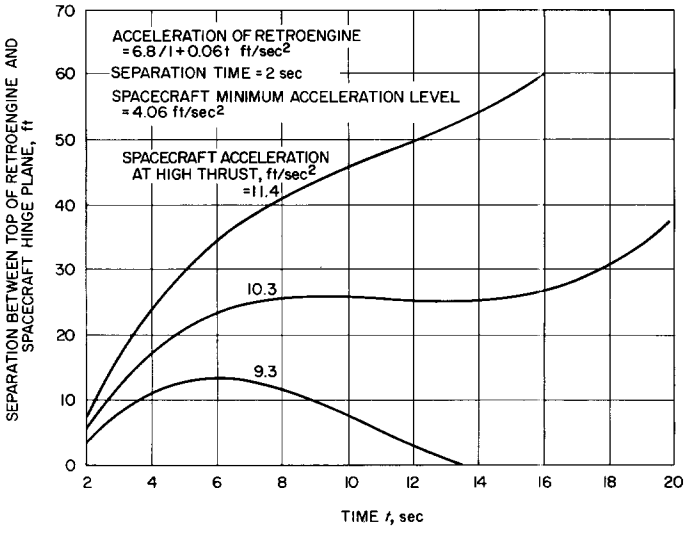

Fig. 8. Effect of spacecraft acceleration level on retrorocket separation

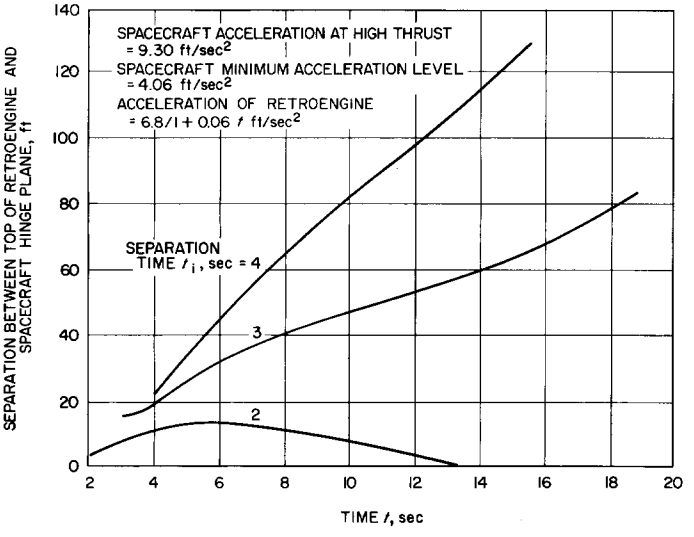

Fig. 9. Comparison of effects of t_1 = 2.0, 3.0, and 4.0 sec

UNCLASSIFIED
CONFIDENTIAL

UNCLASSIFIED

thrust of the vernier engine. For the worst direction of the center of gravity displacement and the moment disturbance, the unsaturated moment capability limit is given by

$$M = \Delta t\left[\frac{3}{2}R + 3D\right] - 312D$$

where

Δt = difference between maximum thrust and commanded thrust level for vernier engine, pounds

R = radius from roll axis to vernier engine thrust, inches

D = displacement of center of gravity from roll axis, inches

For a center of gravity displacement of 0.5 in. and a thrust command level of 66 ma, the moment capability is 206 in.-lb.

b. Increase Separation Time. As indicated in Fig. 9 for the A-21 separation time of 2 sec (t_1), complete separation does not occur with the assumed model for retrorocket thrust decay of

$$a_R = \frac{6.8}{1 + 0.06\,t_S}\ \text{ft/sec}^2$$

where

t_S = time starting at the instant the explosive bolts holding the retrorocket are fired.

If the separation time is increased to 3 sec, complete separation is obtained and for 4 sec additional margin and separation velocity is obtained.

The effect on the vernier propellant required is determined from

$$\delta W_V = \frac{T_{S/C}\,\delta t_S}{I_{SP}}$$

$$= \frac{(274)\,(1)}{271} = 1.0\ \text{lb}$$

using average thrust performance of delivered flight engines, an increase in separation interval of 1 sec and the -3-σ value for specific impulse (I_{SP}).

Owing to the additional vernier impulse, the burnout velocity is decreased from the previous design value by

$$\delta V_{BO} = \left[\frac{T_{S/C}}{W_{S/C}}(32.2) - 5.32\right]\delta t_S$$

$$= \left[\frac{274}{856}(32.2) - 5.32\right](1) = 5.0\ \text{ft/sec}$$

Since the retrorocket propellant load is selected to result in a desired burnout velocity, the retrorocket propellant weight is adjusted to achieve the initial burnout velocity. The change in burnout velocity as a function of change in retrorocket propellant weight for a fixed weight at retrorocket ignition is determined from the classical rocket equation and is given by

$$\frac{\partial V_{BO}}{\partial W_R} = \frac{-I_{SP}\,g_e}{W_0 - W_P}$$

where

I_{SP} = specific impulse of retrorocket engine and vernier engines

ge = 32.2 ft/sec^2

W_0 = initial weight at retrorocket ignition

W_P = weight of propellant burned

This expression assumes that the specific impulse of the vernier engines and the retrorocket engines is equal. For the present A-24 design, the value of this ratio is -9.55. The change in weight of the required retrorocket propellant is calculated as

$$\delta W_R = (\delta V_{BO})\frac{\partial W_R}{\partial V_{BO}} = -0.5\ \text{lb}$$

Since the weight of the payload is the only remaining weight variable to keep the total vehicle constant, its weight must be reduced by $(\delta W_R + \delta W_V) = 0.5$ lb. If other extensions of the separation interval are considered, the change in the appropriate weights can be determined by multiplying the above values by the increase in time selected.

c. Delay command of high thrust. The principal reason for delaying the high thrust command is to allow the potential retrorocket maximum disturbance to decrease to a value that is substantially less than the unsaturated moment capability of the vernier system. Attitude loop limit cycling can occur when this condition is not established. The maximum vehicle weight when the acceleration switch signals burnout is approximately 1000 lb. The corresponding retrorocket thrust level is (1000) (3.5) = 3500 lb, neglecting the vernier thrust of 200 lb. Assum-

CONFIDENTIAL UNCLASSIFIED

UNCLASSIFIED
CONFIDENTIAL

ing the 3-σ specified thrust to combined center of gravity offset of 0.18 in., the moment disturbance is 630 in.-lb. Assuming a similar thrust decay for the A-24 retrorocket as compared to the measured A-21 retrorocket decay (Fig. 10), the disturbance in 2 sec could be expected to decrease by a factor of 3.5. If a delay of 8 sec were selected, the retrorocket thrust could be expected to be less than 40 lb and the maximum disturbance equal to 7 lb.

Accompanying a delay in commanding high thrust is a reduction in vernier impulse and vernier propellant weight. The retrorocket propellant weight change is opposite to that of the vernier propellant and essentially equal in magnitude, which allows the payload weight to remain constant.

d. Tradeoff data. Although an increase in high thrust level causes the unsaturated moment capability to fall below the maximum expected moment disturbance at retrorocket burnout (3.5 g point), the margin for the present design is less than 25%. When the high thrust command is delayed for 8 sec, this margin becomes greater than 2 orders of magnitude for no increase in thrust and a factor of 30 for a change in thrust command to 66 ma. The increase in relative acceleration up to 33% for an increase in high thrust up to 11% is a significant improvement.

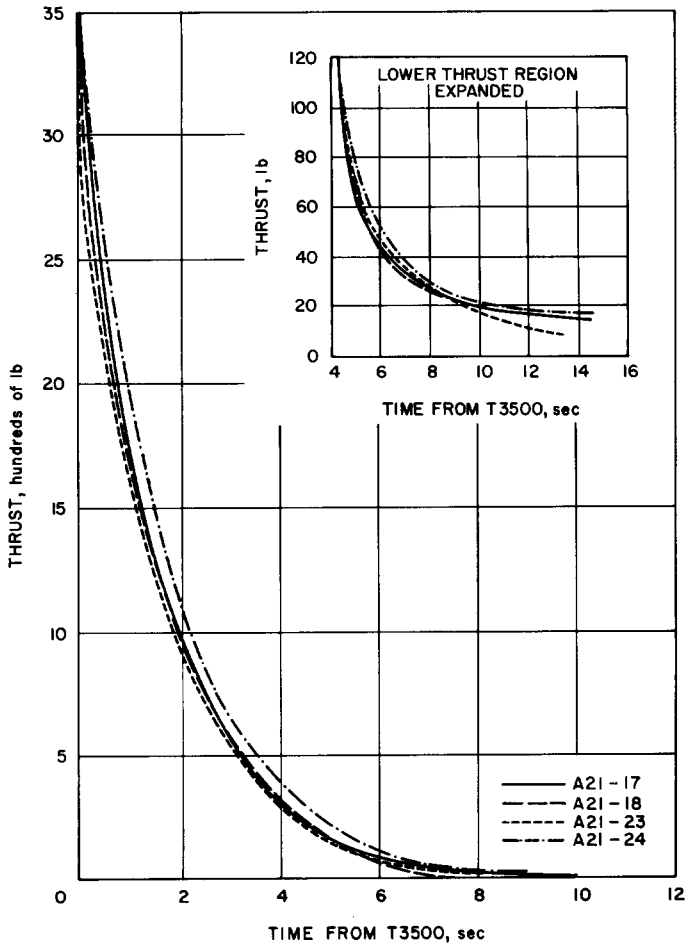

Fig. 10. Engine performance curves thrust tailoff

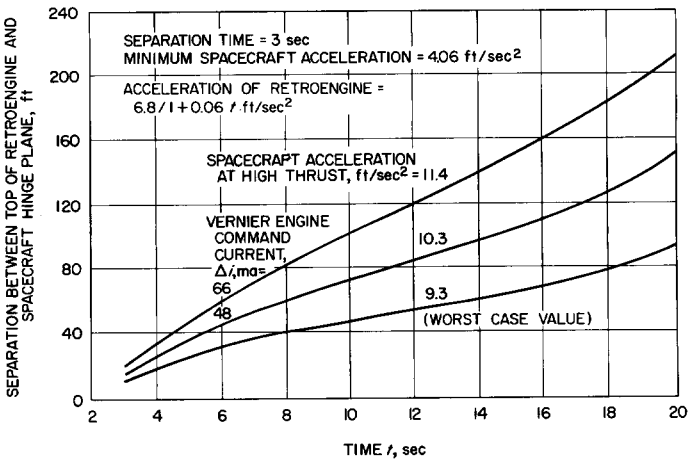
SEPARATION TIME = 3 sec
MINIMUM SPACECRAFT ACCELERATION = 4.06 ft/sec²
ACCELERATION OF RETROENGINE = 6.8/t + 0.06 t ft/sec²
SPACECRAFT ACCELERATION AT HIGH THRUST, ft/sec² = 11.4
VERNIER ENGINE COMMAND CURRENT, Δi,ma=
66
48
10.3
9.3
(WORST CASE VALUE)
SEPARATION BETWEEN TOP OF RETROENGINE AND SPACECRAFT HINGE PLANE, ft
TIME t, sec

Fig. 11. Effect of increase in high thrust level (t = 3 sec)

An increase in separation interval of 1 sec appears adequate per Fig. 10 and the payload weight penalty of 0.5 lb/sec increase is significant. An increase in high thrust level should provide sufficient margin for design (Fig. 11).

The delay in high thrust command of 8 sec, as indicated previously, offers a major margin between expected maximum disturbance and moment capability. If the increase in retrorocket propellant loading is undesirable, a delay of 4 sec could be selected which would provide adequate moment margin and result in a retrorocket engine propellant increase of less than a pound. The maximum extrapolated moment disturbance would be 72 in.-lb.

D. Launch Operations

Air force eastern test range. In the period mid-November to mid-January, two *Surveyor* cleanliness documents were generated, "AFETR Test Plan, for Determination of Nose Fairing Mobile Temperature Control Unit (MTCU) and Pad Air-Conditioner Contamina-

UNCLASSIFIED
CONFIDENTIAL

UNCLASSIFIED
CONFIDENTIAL

tion," HAC document 288481, and "SC-1 AFETR *Surveyor* Cleaning Operations," HAC document 288483. Previous shroud contamination level tests were run on the shroud furnished by NASA Lewis Center, using a spacecraft mockup for the latter tests in that early series. The above test plan designated the second series of tests to be performed on the AC-7 shroud designed for use on SC-1. The spacecraft mockup was not used in this later series.

Studies to establish requirements for the cleanliness of the exterior surfaces of the spacecraft justified evaluation of the other possible areas of contamination for *Surveyor*: namely, MTCU and pad air-conditioning systems, and the shroud used for encapsulating the spacecraft.

Additional effort will be required to define and maintain shroud and air-conditioning system cleanliness levels. The average total number of particles and fibers of 50μ or larger that fell out in the AC-7 shroud during GD/C tanking tests was $1345/ft^2$. The report of August 9, 1965, on the "Susceptibility of *Surveyor* Spacecraft to Free Particles" indicates $1000/ft^2$ of particles 50μ or larger as the maximum allowable for area contamination.

Fabrication of the modified site for installation of the microwave antenna on Building AO (spacecraft checkout facility) is completed. Following antenna installation, its tracking capability will be checked, and alignment and test of the spacecraft checkout facility/propellant loading building (SCF/PLB) RF link is planned.

A STEA spacecraft school was conducted to familiarize personnel with operation of the STEA equipment for the purpose of improving their efficiency.

Refurbishing of the propulsion carts has been completed.

Communications plan for combined system test facility operations. Present plans provide that *Surveyor* spacecraft be processed through the combined system test facility (CSTF) for joint flight acceptance composite tests checkout prior to AFETR operations. During spacecraft testing at CSTF, analytical support will be furnished by computer data system analysts; the computer, printers, and most system analysts will be based at El Segundo. Launch operations has established a communications link (both voice and data) between the test team at CSTF and the analysts at El Segundo.

Figure 12 shows the communications block diagram. Telemetry data will be taken from the STEA 3 command data handling console decommutator, at the telemetry data patch panel phone jack, through an interface unit to the telephone company data set. The data set will transmit the pulse-code modulation to a receiving set in El Segundo, through an interface unit (in the receive mode), and finally to the STEA 4 decommutator. The present STEA 4/command data system configuration provides the proper data input to the computer. HAC will be responsible for the following functions:

(1) Designing and fabricating the interface units to be compatible with the electrical requirements of the command data handling console and the phone company data sets.

(2) Performing the engineering to provide the proper electrical interface for inputting the received PCM to the STEA 4 decommutator.

(3) Supervising and incorporating command data handling console modifications, if required.

(4) Acquiring data phone service for transmitting and receiving the PCM data.

Command information will be transmitted to El Segundo via a route similar to that of the PCM data: the telemetry data patch panel to the interface unit to the data set (transmit) to the data set (receive) to the interface unit to route. The command information interface units will be of the same design as that carrying PCM data, but will operate in the command send mode at the point of origin. When received, the commands will be processed directly to the command data system computer, since no decommutator action is required.

Intercommunication will be provided through the use of equipment as determined by phone company and FCC requirements. Intercom connection at CSTF will be made at a specially provided missile operational paging system panel (Fig. 13). Launch operations will arrange for installing phone company equipment at CSTF and El Segundo for two-way missile operational paging system intercom, and will define requirements as to quantity and placement of equipment such as intercom stations and loudspeakers, at El Segundo. Direct phone and TWX communications are presently in place and require no additional implementation. Table 13 lists the equipment that is to be obtained to implement the plan, and the responsibility of the interested departments.

Mass model program. Analysis indicates that under worst case conditions (a very unlikely occurrence) the transponder can operate for about 5 hr before reaching 125°F, assuming a prelaunch temperature of 85°F. Every

UNCLASSIFIED
CONFIDENTIAL

UNCLASSIFIED

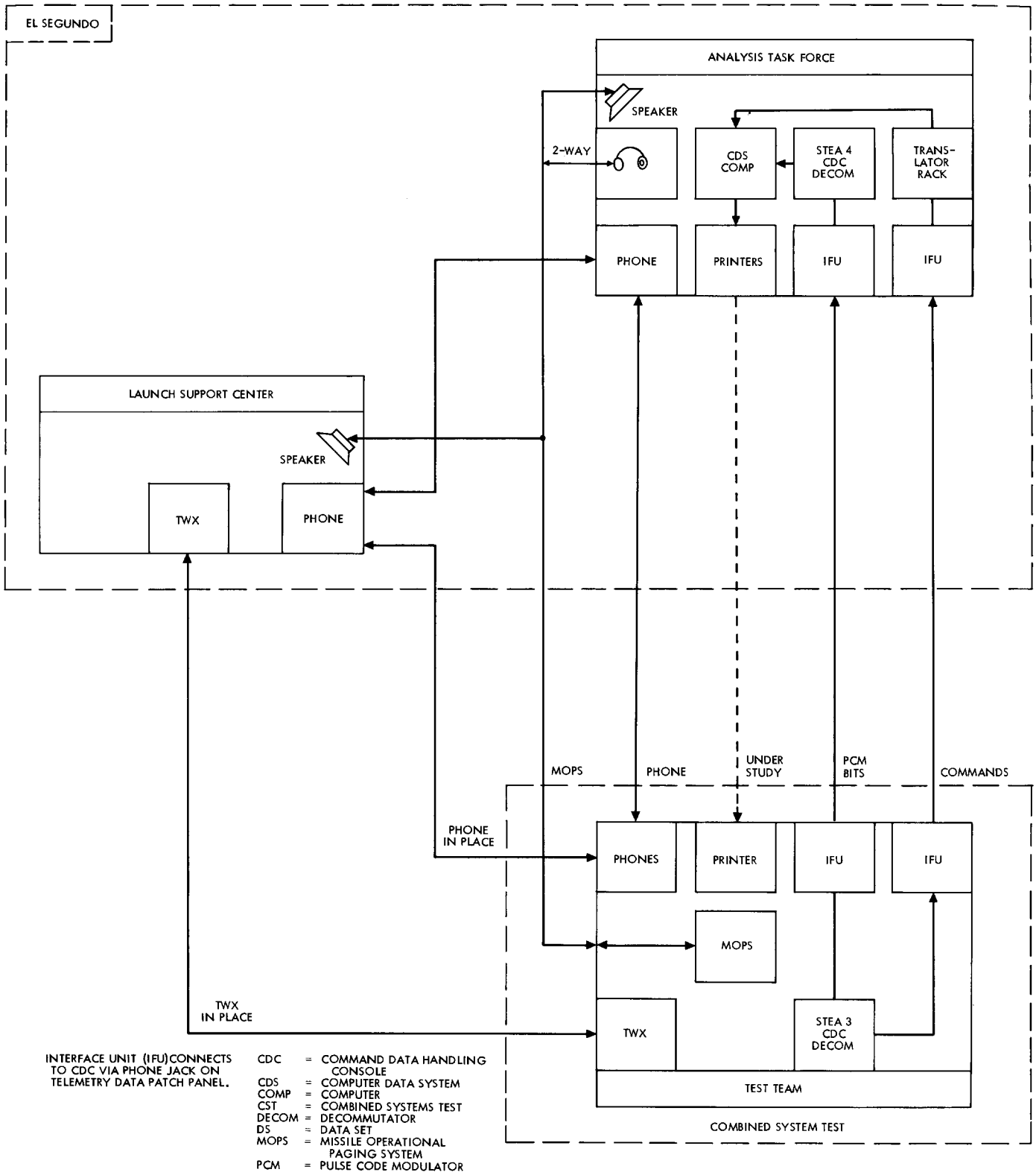

Fig. 12. Launch operations SC-1 CSTF/El Segundo communication plan

UNCLASSIFIED

UNCLASSIFIED
CONFIDENTIAL

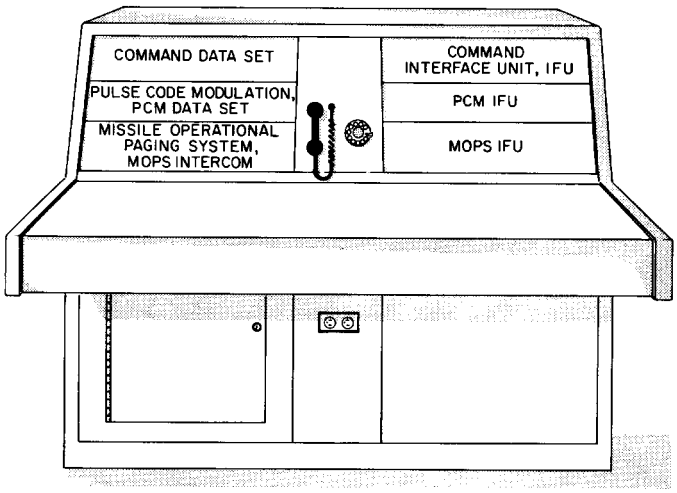

Fig. 13. Communications console

5 deg the prelaunch temperature is lowered will increase the time by about 1 hr. NASA/Lewis Research Center has decided to go ahead, based on this minimum time, and is considering lowering prelaunch temperature to 65°F to assure about 9- or 10-hr operation.

The flight acceptance test of the AC-8 payload (mass model) was successfully completed December 20, 1965. Postflight acceptance test checkout of the transponder on December 21, 1965 showed no abnormal performance.

Table 13. Required equipment

Type	Quantity	Responsibility
Communications console	1	Launch operations will provide the console and handle installation at CSTF. It will house all the CSTF-required communication equipment and will be located in the STEA 3 area (Figs. 13 and 14).
Interface unit SK12345	4	Space flight operations will design and fabricate the units according to Bell Systems specifications. Two will be located in the communications console at CSTF and two will be placed at each data set location at El Segundo.
Data set, Model 202C	4	Launch operations will make arrangements for acquiring sets and leasing lines. At CSTF, two will be installed in the communications console; at El Segundo, one will be at the computer site (with its interface unit) at column 19H, Building 350, and the other at the STEA 4 command data handling console.
MOPS intercom equipment		
Interface at CSFT Intercom at El Segundo	1 set	Launch operations will make arrangements for installation at CSTF (in the communications console) and leasing line. At El Segundo, the intercom tie-point will be at column 19H, Building 350, to provide the needed flexibility for rerouting should scheduling difficulties with SC-2 arise.

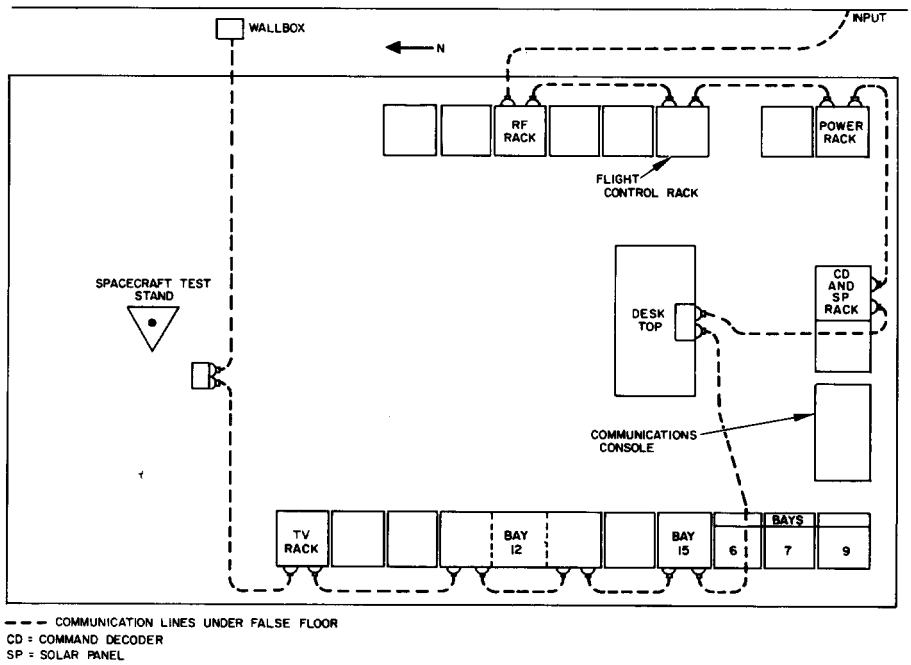

Fig. 14. Complete combined system test communications layout at GD/C

CONFIDENTIAL
UNCLASSIFIED

UNCLASSIFIED
CONFIDENTIAL

Interim combined systems test started December 27, but HAC was not required to participate until January 3, 1966 when simulated countdowns involving the transponder were run. Interim combined system test was completed successfully with transponder performance completely normal. On January 7, 1966 a postcombined systems test checkout of the transponder was successfully completed.

During this period, the transponder for AC-9 (SD-spare 1) was shipped to GD/C. It was match-mated to the AC-9 mass model during the week of January 10. During the week of January 17, the upgraded transmitter became available and was shipped to GD/C. It was installed in the transponder and successfully checked out on January 21. The transponder is now in combined system test stores at GD/C awaiting the start of AC-9 test operations, which will probably not occur before June.

The launch operations test directive for AC-8 mass model, document 288473, was completed and delivered to JPL during this report period. During this report period, first issues of the following test procedures were completed:

288467	AC 8/9 countdown test procedure.
288470	AC 8/9 J-FACT test procedure.
288474	Transponder system functional test procedure (AC-8 & 9) data book.
288475	AC 8/9 Simulated countdown test procedure.

At a meeting January 11, 1966 at JPL, agreement was reached on the contents of the frequency data to be supplied by HAC to JPL for use by DSN personnel during

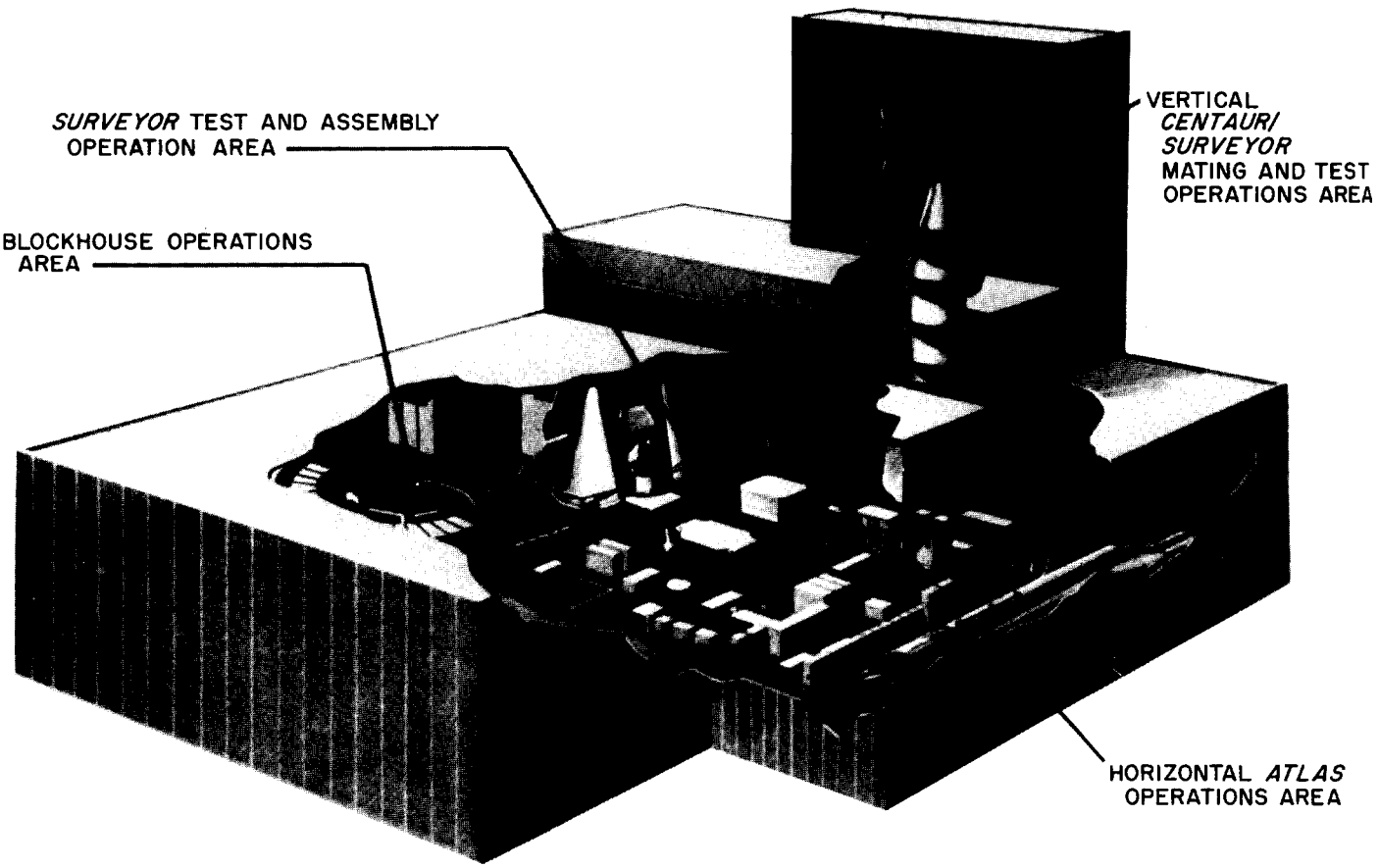
SURVEYOR TEST AND ASSEMBLY OPERATION AREA
BLOCKHOUSE OPERATIONS AREA
VERTICAL *CENTAUR/ SURVEYOR* MATING AND TEST OPERATIONS AREA
HORIZONTAL *ATLAS* OPERATIONS AREA

Fig. 15. Combined systems test facility

CONFIDENTIAL
UNCLASSIFIED

CONFIDENTIAL
UNCLASSIFIED

the AC-8 mission. Mutually agreeable delivery dates were also established.

Combined system test facility activation. Combined system test consists of checking performance of the *Surveyor, Centaur,* and *Atlas* vehicles while the vehicles are interconnected (Fig. 15). This test will uncover any incompatibility existing within the vehicle. The combined system test is performed at GD/C.

The planned schedule was to incorporate all the changes in the equipment in San Diego prior to the completion of the T-21 drop tests which were being conducted in El Segundo using the trailer-mounted STEA 3 Goldstone configuration. The schedule was met. An initial list of 33 mandatory changes was compiled December 1. This list has since expanded to 54 changes with additional changes to be added.

El Segundo. During this report period, compatibility tests were conducted with the T-21 spacecraft. The test proved successful, and only slight modifications to the container were required.

X-rays of Multipin connectors. At the request of the spacecraft operations and planning section, a series of X-ray pictures was taken using polaroid film on 19-pin Bendix connectors in an effort to determine the ability to find connector troubles from this type of photograph. Inspection from the outside did not indicate anything wrong with such a connection. It was determined that connector troubles could be easily isolated by the use of X-ray techniques.

E. System Testing

T-21 lunar landing shock tests. This final test phase of the T-21-type approval spacecraft was performed in the HAC space simulation laboratory by dropping the T-21 a prescribed distance onto an inclined wooden platform, which was studded with wooden rock-simulating blocks under the footpads. The objectives of this test phase were to evaluate the spacecraft functionally and structurally, and to evaluate the telemetry phase-lock situation at lunar touchdown.

Prior to this test, computer studies were conducted to develop the effects of an Earth-gravity impact. Over 120 worst-case lunar landing conditions were evaluated to determine peak loads on various components for various landing parameters. The four worst-case lunar landing conditions are shown in Table 14. The first three drops at 15 ft/sec represent the 3-σ expectancy of lunar landing conditions, while the fourth drop at 20 ft/sec represents the 10-σ expectancy. These were then converted to Earth-gravity conditions, as shown in Table 15, after another series of 120 computer cases were analyzed.

The shock instrumentation configuration consisted of special instrumentation accelerometers and flight accelerometers and strain gages. The flight strain gage bridges and accelerometers were hard-lined directly to the recording instrumentation. In addition, the shock absorber strain gages delivered output signals to the telemetry system.

All drops were performed per operational procedure 227146. Phase jitter, shock absorber strain gage channels, and selected power parameters were monitored during the drop. Flight control thrust phase power was on, as was radar altimeter and doppler velocity sensor (RADVS) power. Five seconds after impact, flight control thrust phase power was commanded off. Fifteen seconds after impact, the spacecraft was raised until clear of the drop platform and a cycle print of all commutators performed. After each drop, functional integrity of the spacecraft was verified by repeating the short system confidence check procedures.

Functional test results were satisfactory throughout the test. Phase error was reasonable and was caused primarily by omnidirectional antenna movement and not by shock on the transmitter itself. Phase lock was not lost on any of the three drops. No degradation of the survey camera (TV-3) could be noted from the quick-look data on any of the drops. Squib circuits and mechanisms functioned normally, with the exception of an antenna solar panel positioner (A/SPP) elevation axis failure on Drop 1. This failure was predicted because of extreme stress on (A/SPP), especially in elevation axis in this drop configuration.

Solar thermal vacuum test of SC-1. A dry run was conducted December 15 and 16 in preparation for Subphase A (low Sun) of the solar thermal vacuum test. During the terminal descent, noise was encountered; further investigation showed that the noise was due to a recorder problem in the test equipment. On December 28, 1965, the spacecraft was exposed to the low Sun condition. Although some anomalies were encountered, the test was successful.

The Subphase B (high Sun) was run immediately following the low Sun exposure of Subphase A without chamber pressure change. Anomalies observed during

CONFIDENTIAL
UNCLASSIFIED

UNCLASSIFIED
CONFIDENTIAL

Table 14. Worst-case lunar landings conditions

Condition	Spacecraft orientation (single leg in plane of symmetry)	A/SPP position (polar angle), deg	Worst-case lunar landings				Components with worst peak loads
			Touchdown velocity, ft/sec		θ_0,[a] deg	Slope of surface, deg	
			Longitudinal	Lateral[b]			
1	Leg 1 downhill	0	15	0	0	15	A/SPP
2	Leg 3 uphill	36½	15	−5.5	10.8	15	Components A and B, omnidirectional antenna B
3	Leg 2 downhill	36½	15	−0.3	0.4	15	TV-3 solar panel
4	Leg 3 below horizon	36½	20	4.9	− 2.7	15	Components A and B,[c] omnidirectional antenna B, omnidirectional antenna A

[a] θ_0 is initial incidence of spacecraft, positive for single leg above horizontal.

[b] For lunar landing, lateral velocity is positive in the direction of the single leg.

[c] Of 60 cases the one combination of most components approaching peak loads was selected.

Table 15. Landing shock environment[a]

Drop	Spacecraft orientation (single leg in plane of symmetry)	A/SPP position (polar angle), deg	Equivalent Earth drop tests (without horizontal velocity)				TV mirror position
			Vertical touchdown velocity, ft/sec	θ_0,[b] deg	Slope of surface, deg	h[c] ft	
1	Leg 1 downhill	0	13	0	15	2.62	Closed
2	Leg 3 uphill	36½	15.1	10.8	15	3.54	Closed
3	Leg 2 downhill	36½	13.2	0	15	2.70	Closed
4	Leg 3 below horizon	36½	17.5	−16.7	0	4.75	Open view of Leg 3 footpad

[a] For all conditions, the crushable blocks impacted on flat surface; the footpads impacted on a surface of 2-in. wooden blocks.

[b] θ_0 is initial incidence of spacecraft, positive for single leg above horizontal.

[c] h is the minimum vertical distance between the test article and the surface prior to release.

this test phase involved the improper cycling of the vernier line heater, noisy temperature telemetry, excessive rise in the boost regulator temperature, rise in battery main pressure due to shorted cells, and erratic magnitude register during receiver threshold sensitivity checks. Since this test phase operates on system test equipment assembly (STEA) power, the battery condition was attributed directly to spacecraft operation. The Subphase B test was successfully completed January 3, 1966.

Preparatory to the Subphase C or plugs-out test, a system readiness test was run January 16, 1966. The test was successfully concluded and on January 18, 1966, an ambient dry run was performed for approximately 25 hr prior to the actual environmental exposure.

The Subphase C test was initiated January 21, 1966 and successfully completed in approximately 35 hr.

Vibration test phase. The SC-1 vibration flight acceptance test was performed January 20 to February 4, 1966. The Z-axis series of tests 9A, 10A, and 10B were performed January 30 and 31, 1966. The lateral axes of vibration tests were deleted by mutual agreement between HAC and JPL in order to deliver the SC-1 to San Diego to perform combined system test as scheduled and also to preserve the launch date. A quick review of functional and environmental data indicates satisfactory spacecraft operation.

Vernier engine vibration test. Extensive changes have been made to the specification covering this test phase. The test has been expanded to include verification that

UNCLASSIFIED
CONFIDENTIAL

UNCLASSIFIED
CONFIDENTIAL

the RADVS beams would not lock onto a false signal while functioning in a search mode without a STEA closed loop configuration and while subjected to random vibration of 20-lb rms level at each dummy vernier engine. This is double the vibration level specified for the closed loop midcourse and the closed loop terminal descent.

SC-2 flight acceptance tests. The A-21 mission sequence electromagnetic interference test specification 224822 was revised and review copies issued. In the revision, the number of tests was reduced from five to three for the standard mission sequence. To support the tests, the flight acceptance MS/EMI test phase Volume 1, Volume 2 (parts 1, 2, and 3), and Volume 3 were revised and issued for review.

Flight acceptance tests. Group testing of hardware during this period was limited by the lack of a boost regulator for use on the GT-1 vehicle. In addition, delays in hardware delivery and overall program changes have slipped the group test dates for SC-3 and up.

F. Flight Control

The flight control subsystem is comprised of spacecraft units that provide velocity and attitude control during the transit and landing phase of the *Surveyor* mission. These units, which include optical sensors, inertial instruments, attitude controls, and flight control electronics, are discussed in this section. Although the lunar radar and propulsion subsystems are functionally included, they are also covered in other sections of this *SPS*.

1. Systems Design

The third S-6C live firing was successfully completed. As in the two previous firings the S-6C (vernier propulsion system) test vehicle at Placerita was tied via six telephone lines to the flight control system dynamics simulator at the Space Systems Division analog computer facility and throttled in normal closed-loop operation. The firing involved portions of simulated vernier descents from five different main retrorocket engine burnout flight conditions, ranging from minimum to maximum nominal A-21 burnout velocity.[2]

[2]The roll actuator was not exercised during the closed loop testing, as a part of the total closed loop control, during simulated vernier descents.

Performance of the vernier engines operating within the simulated flight control system was entirely satisfactory in each of the five descent runs. Attitude and velocity control system performance was nominal in comparison with "baseline" analog-computer-only checkout runs.

All test objectives of the planned S-6C three-firing sequence have been met. The data are being analyzed in detail.

The principal purpose of the third firing was to verify stability and performance of the attitude and lateral velocity control loops under conditions of sustained low-thrust operation and maximum dissolved helium in the propellants. These conditions are known to produce maximum sluggish engine response to throttling commands.

The third firing consisted of a rapid sequence of five vernier descents, each from a different main retrorocket burnout flight condition. Initial conditions used are listed in Table 16 and range from minimum to maximum nominal A-21 burnout velocities.

Table 16. S-6C test firing three simulated burnout flight conditions

Run No.[a]	Slant range R, ft[b]	Longitudinal velocity V_z, ft/sec	Lateral velocity, ft/sec	
			V_x	V_y
1	17,320	247	0	−36
2	21,530	342	0	−72
3	28,340	437	0	−108
4	37,160	531	0	−144
5	46,110	624	0	−180

[a]For each run, the spacecraft roll axis was initially aligned to lunar vertical.
[b]15-deg lunar surface slope in each case.

Each of the five runs consisted of the following phases of operation (Fig. 16):

(1) Initial attitude maneuver to align the spacecraft roll axis with the total velocity vector.

(2) Minimum deceleration (0.9 g_m) descent to the line-segmented command profile (sustained, low-thrust operation).

(3) Segment acquisition.

(4) Segment tracking (except Run 4).

Due to the limitation on total test time, only a representative portion of segment tracking operation was possible for each run. Simulated radar altimeter and doppler velocity sensor (RADVS) noise (four channels,

UNCLASSIFIED
CONFIDENTIAL

UNCLASSIFIED CONFIDENTIAL

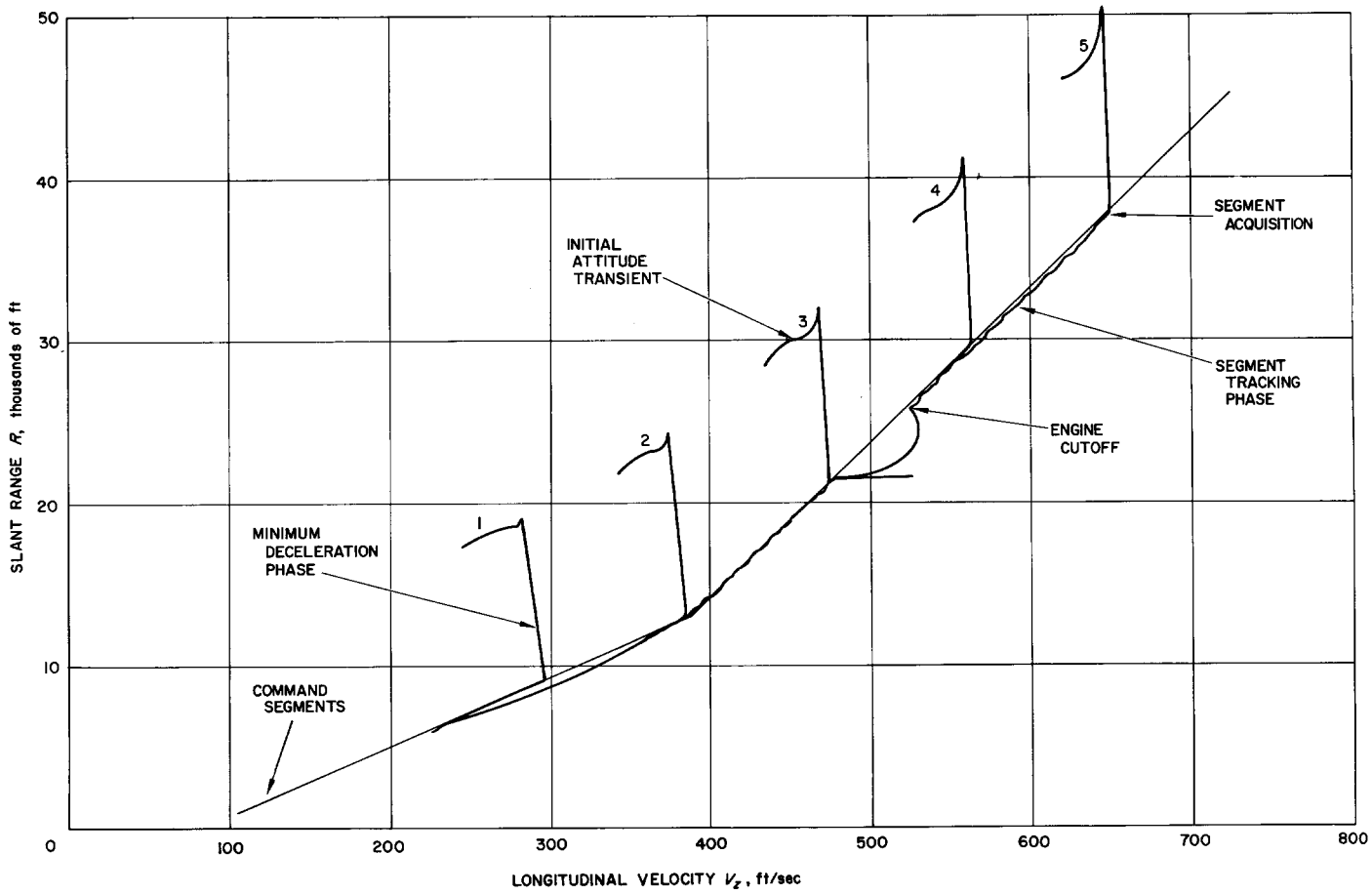

Fig. 16. S-6C closed-loop firing 3

T-2H level) was included in all five runs. Total duration of the third firing was 220 sec.

The S-6C test vehicle was preconditioned to expected vernier propulsion system conditions during the *Surveyor* terminal descent phase. This involved:

(1) Approximately 50-hr hold at full (755 psig) helium pressure.

(2) Temperature conditioning of three tank-pairs:

Leg 1 $80 \pm 10°F$.

Leg 2 $30 \pm 10°F$.

Leg 3 $70 \pm 10°F$.

Fig. 16 was traced by an X-Y plotter in real time during the live firing. Spacecraft slant range, R (measured along the roll axis), is plotted versus longitudinal velocity V_z, for the five simulated descent runs. Also shown are the two uppermost command descent segments. Fig. 17 is identical to Fig. 16, except that it was traced during a pretest analog computer checkout run which utilized idealized transfer functions in place of the actual vernier engines.

It can be seen that the traces of Fig. 16 and 17 are virtually identical and that, therefore, nominal velocity control performance was obtained with the live vernier engines.

Inspection of Brush recordings made during the test shows that attitude and lateral velocity control functions were also performed in a nominal manner. In all cases, the initial attitude maneuver aligned the spacecraft roll axis to the total velocity vector in less than 2.5 sec (9 sec allowed), and without overshoot. Pitch and yaw attitude response to RADVS noise inputs was less than 1.0 deg peak-to-peak in each axis, well below the 10-deg gyro limits.

2. T-2N Tests

The optical tracking data from the first tether descent test of the T-26-1 test vehicle have been reduced. Com-

UNCLASSIFIED CONFIDENTIAL

UNCLASSIFIED
CONFIDENTIAL

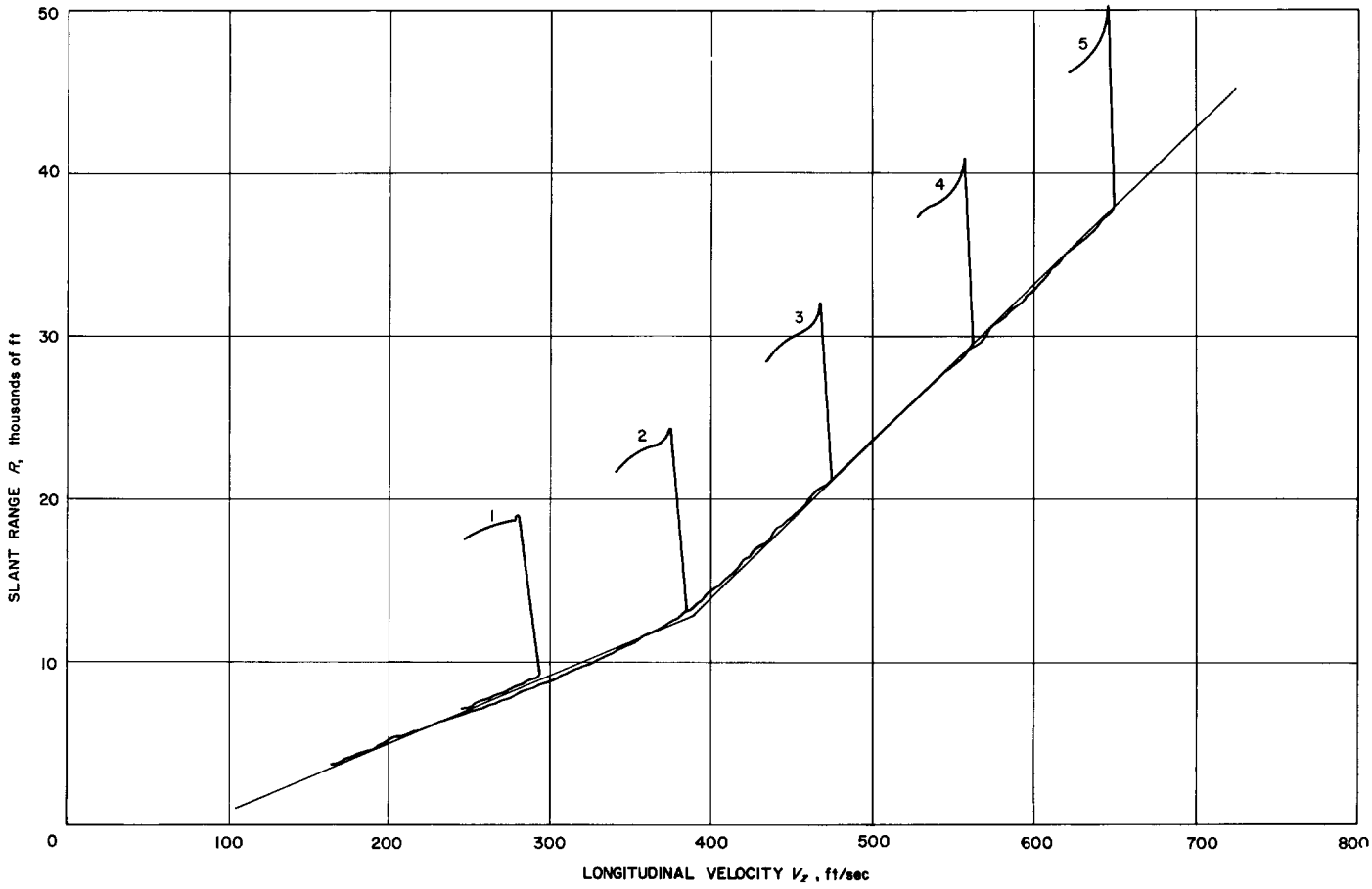

Fig. 17. S-6C pretest closed-loop simulation for firing 3

parison of optical and telemetered data showed good correlation for most signals, the largest discrepancy occurring between optically measured and radar-measured range. By fitting a least square straight line to the radar range versus optical range data, the relationship obtained is: Radar range = 41.7 + 0.923 × optical range, where 41.7 is the range bias and 0.923 is the range slope. Since radar range is a significant variable in predicting the "time of mission at 5 ft/sec," new radar range values based on optical range measurements and the above relationship were used to calculate a corrected time at 5 ft/sec. The new predicted time at 5 ft/sec is nominally 4.03 sec (down 1.57 sec from the previous prediction of nominally 5.60 sec), which correlates with the actual mission time at 5 ft/sec of 4.5 sec.

The result of this data evaluation is to increase the confidence in the analytic methods being used to predict a successful *Surveyor* mission.

Two soft landings of a T-2N test vehicle are required to fulfill Phase II of the T-2N program. It is impractical to shut off the vernier engines via the RADVS 14-ft mark, as is done in the flight spacecraft, since the larger (approximately six times lunar) Earth gravity would cause the vehicle to land at an excessively high velocity. Therefore, it is planned to supply a 1 gravity command at the 14-ft mark, resulting in a constant velocity descent until a touchdown probe contacts the Earth at 2-ft altitude, at which time the vernier engines will be shut off. These functional changes can be accomplished with only minor changes to the flight control hardware.

In order to evaluate this touchdown scheme, thorough analog computer studies were conducted. The effect of each known error source on the critical mission parameters of (1) altitude at which 5 ft/sec is attained, (2) total propellant used, and (3) maximum thrust required was determined. By assuming that the 3-σ value of each error source is equal to its specification limit and *rss*-ing these errors, the following values of mission parameters were determined:

Altitude at which 5 ft/sec is attained 31.2 ± 22 ft.

CONFIDENTIAL
UNCLASSIFIED

UNCLASSIFIED

Total propellant used	35.0 ± 7.2 lb.
Maximum thrust required	222 ± 5.5 lb.

Since these values are within the capabilities of the T-2N test vehicle, a successful touchdown test phase is predicted.

3. Flight Control Electronics Unit

During this report period, the following circuit improvements were incorporated in the flight control electronics units for SC-1 and SC-2:

(1) The reliable operate radar altimeter (RORA) signal was added as a logic signal to activate Switch 13, the above 1000 ft' RADVS controlled-descent switch. Present implementation now provides for Switch 13 to be closed via either RORA or RODVS (reliable operate doppler velocity sensor) and Switch 11 to be closed via RORA, thus assuring that the input (via Switch 13) to the descent amplifier will always precede or be simultaneous with switching (via Switch 11) amplifier output to the acceleration control circuit.

(2) The gas jet amplifiers have been desensitized to voltage noise on the spacecraft +29 vDC flight control bus, which is the B+ supply for the amplifier.

(3) During solar-thermal-vacuum testing of SC-1, an inadvertent setting of RADVS ON and BURNOUT latch occurred. In the instrumentation configuration for the solar-thermal-vacuum test, these two signals are not used at the RADVS STEA; therefore, the lengthy signal lines to the RADVS STEA are not connected. The output lines of these two latches have been electrically isolated to protect them from any potential disturbances on the test lines.

(4) The reset Group 4 output (AR01) was added as a logic signal to reset the clock enable latch (Z22). This provides the capability of resetting this latch in flight by a command instead of by the previous undesirable method of commanding all flight control power off and then on.

(5) The initial condition circuit has been desensitized to $\pm$15-v peak 500-μsec wide pulses on the $\pm$29-vDC flight control bus and the magnitude transfer line has been desensitized to $\pm$20-v peak pulses from the normal signal states.

4. Inertial Sensors

Fourteen of the eighteen gyros ordered in the third gyro procurement have been delivered. Only Gyro 63 was returned to the vendor, as previously reported, and it has since been redelivered and accepted.

The investigation of the decreasing transfer function in a number of gyros is continuing. Inertial Reference Unit 5, previously on SC-1, was replaced by Inertial Reference Unit 8, primarily because of the continuing decrease in the transfer function of Gyro 58. Calculations of the effect or torquer cup miscentering and distortions on damping did not account for the magnitude of changes in transfer function that have been experienced. These calculations are being extended to include the paddle damping effect; however, the analytic solution to the equations is not to be found in the literature.

Kearfott's tests on Gyro 54 and a HAC test on Gyro 41 have shown the copper loss heating in the torquer to have no measurable effect on transfer function. During the HAC test, 95 ma were applied to the torquer for 100 hr. The temperature rise of the torquer was established at approximately 4°F. A similar test on Gyro 40 was run at JPL and showed an apparent change in transfer function over the 100 hr. This gyro will be returned to HAC for further testing.

The physical chemistry investigation of the damping fluid at HAC is being conducted to:

(1) Determine if the polymeric viscosity improver is in true solution in the base stock fluid.

(2) Determine changes in viscosity of the fluid after a simulated degassing cycle.

(3) Investigate tendency of the viscosity improver to separate from the base stock after degassing. Loss of volatile components may alter the solvent power of the base stock.

There is renewed interest in possible changes in the signal generator as a cause of the changing transfer function. One gyro undergoing special transfer function testing began to show a very erratic signal generator signal. Also, changes in voltage output at the gyro stops have been detected in the history data of some gyros. Good repeatability can be expected for stop angle and stop voltage measurements; these parameters will now be tracked, as well as the transfer function.

Three gyros have been selected and assembled into a prototype inertial reference unit and a thermal vacuum

UNCLASSIFIED

UNCLASSIFIED
CONFIDENTIAL

test started as the first phase of a test planned to last a 200-hr minimum. The purpose of these tests is to reveal the effects of inertial reference unit environments on gyro transfer function. Gyros 54 and 58, which have exhibited a decrease in transfer function, were assembled into the inertial reference unit along with Gyro 38, which has had a relatively stable transfer function.

A fifth accelerometer was subjected to type approval test (TAT) using a new nonresonant vibration fixture after the two successful and two unsuccessful TAT previously reported. Satisfactory completion of testing was followed by a teardown inspection. A bulged diaphragm, indicative of air in the fluid, was noted. The vendor has recently instituted a new fill procedure to greatly reduce this risk, but, until confidence has been established, an X-ray examination will be made of every accelerometer from SC-1 up.

Inertial Reference Unit 9 was delivered and allocated to SC-3. Unit 5, which previously was allocated to SC-1, will have all three gyros and its accelerometer replaced and will be allocated to SC-4 upon redelivery.

5. Gas Jet System

The regulated pressure and lockup pressure on Gas Supply 6 showed an unacceptable upward shift between the end of flight acceptance testing and testing at spacecraft assembly. An investigation has revealed that this shift was due to deformation of the Nylon poppet valve, which is caused by excessive pressure loading of the valve during thermal coating at high temperature (250°F) and vapor depositing of aluminum at vacuum. This excessive pressure loading occurs when gas is trapped downstream of the regulator poppet valve and the pressure increases due to temperature changes and vacuum after the gas supply tank is down-loaded prior to thermal coating. Test procedures are being revised to: (1) check the pressure control regulator pressure for change due to pressure relief valve tests prior to assembling it to the tank, and (2) down-load the tank prior to thermal coating by reducing the pressure via the regulator discharge to a value that will cause the regulator valve to remain open during the thermal coating of the gas supply.

Gas Supply Regulator 6 has had the poppet replaced and retested, as required. Gas Supply 7, although the regulated pressure shift is acceptable, will be reworked and retested. Gas Supply 3 for SP-1 was tested and found to be satisfactory. The gas supplies on SC-1 and SC-2 will be tested for lockup pressure and replaced if found to be unacceptable.

Tests of jet valve armatures incorporating a new plating procedure have shown unsatisfactory results. In these armatures, a nickel flash was substituted for the copper flash undercoat required for a decorative chrome wearing surface. Tests are now in progress using a hard chrome-plate, which has been used in similar space applications with success.

Armature coils on order will have new lead wires complying with the revised specification to eliminate the gold-colored cover. The cover has been susceptible to flaking.

The spacecraft landing gear leg flexible line flexure tests and "B" nut tests were rescheduled, due to delays in providing the necessary hardware.

A total system gas leakage test, using the total spacecraft plastic enclosure procedure, was performed on Spacecraft S-7 at Placerita, using the vernier propulsion system helium tank. Results indicated this procedure to be satisfactory for the gas jet attitude system.

6. Roll Actuator

A redesign effort to provide a ±12-deg range roll actuator (designated Model B) has been approved and work is now in progress. The new design is an outgrowth of an earlier extended range design (Part No. 284600), with major exceptions: that the Size 15 motor will be replaced with the Size 11 motor, in the present design, and the pin puller will be relocated. The motor change, with an additional stage of gearing to match the present reduction ratio, permits the use of the present electronics with no major changes. Modification of the housing will be necessary to accommodate the Size 11 motor, relocate the pin puller, and decrease the weight of the unit.

The design changes relative to incorporation of the Size 11 motor will be directed toward simplicity in installation and interchangeability with the Size 15 motor, if the electronics for the larger motor become available. This can be accomplished by using separate motor mounting plates for each size motor and making the mounting plate for the Size 11 motor a subassembly containing the necessary reduction gear stage.

Several locations are available for mounting the pin puller on the roll actuator housing; however, the location that is most advantageous in weight and simplicity of design is in a congested area on the spacecraft. Further interference studies are under way to determine the best pin-puller location.

CONFIDENTIAL
UNCLASSIFIED

UNCLASSIFIED

The approximate weight of the earlier 284600 design was 2 lb. The redesigned unit is expected to weigh approximately 1.75 lb. This 0.25 lb reduction of weight will be obtained by the difference in weight between the Size 11 and Size 15 motors, elimination of the pin-puller thermal shield, and removal of excess material on parts.

7. Performance Evaluation of the Guidance Accelerometer[3]

Part of JPL's direct support of the *Surveyor* project involves special evaluation of certain components from *Surveyor* systems. Such an evaluation has been made of the guidance accelerometer of the flight control sensor group, inertial reference unit. This accelerometer (a Systron-Donner Corporation Model 4310) was evaluated for overall performance capability rather than for a go-no-go type of acceptance testing, as is usually done in preflight acceptance testing.

The Systron-Donner Model 4310 accelerometer is an analog, pendulous, linear force balance type of instrument which uses a D'Arsonval meter movement for the basic transducer. The meter pointer is eliminated and a pendulous mass substituted for use as a seismic element. The position pickoff is a variable reluctance type which effects the amplitude and frequency of a 2-to 5-Mc oscillator. The oscillator output is rectified, filtered and DC amplified to provide a rebalance current to the torquer. Damping can be provided by either electronic means or by fluid filling, depending on the application.

The suspension system employs a conical "pivot and jewel" arrangement. The materials are selected on the basis of the specified vibration and shock environments.

[3]Prepared by JPL Technical Section 344

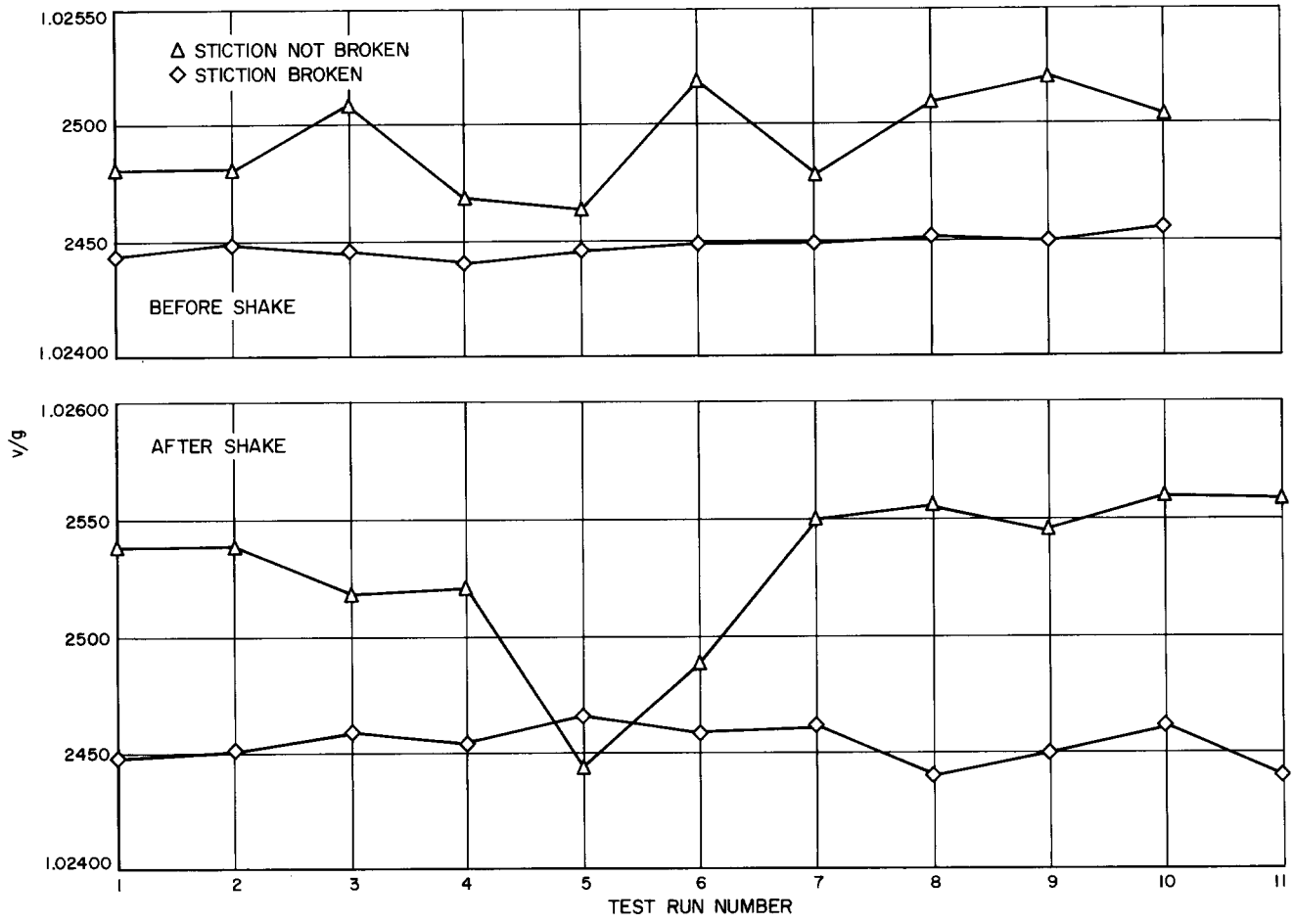

Fig. 18. Tapping stiction effect on scale factor

UNCLASSIFIED

CONFIDENTIAL
UNCLASSIFIED

The case was oil filled for damping and the pendulousity had been increased to provide a full range of ±0.75 g. A nominal scale factor of 33 v/g is required for the *Surveyor* system. For the JPL evaluation, this was divided down by means of Leeds and Northrup precision resistors to provide a scale factor of 1 v/g for use with the Tinsley precision potentiometer.

A series of long term performance and environmental tests were performed on instrument serial number 9254F. This unit was the initial unit obtained by Hughes Aircraft Co. (HAC) from Donner with the bidirectional capture capability. It was converted by Donner from a former unidirectional type, which had been the previous *Surveyor* design.

Tests were performed to determine the level of so called "tapping stiction." In this test the dividing head is first rotated slowly to the proper orientation and a reading is taken with the Tinsley potentiometer and recorded. The face plate of the dividing head is then tapped once with a small plastic screwdriver handle, and the reading repeated with the Tinsley.

Fig. 18 illustrates the effect of this type of stiction on the indicated scale factor, as determined at the ±0.5 g input points. Similar, although slightly smaller, standoff errors were experienced at the null positions. Fig. 18 also points out the degradation of this stiction effect after the vibration tests. The minimum level of vibration or shock input required to break the stiction is not known; however, it is assumed by HAC that the *Surveyor* vernier rocket engines will produce sufficient vibration to keep the stiction at a low level. The stiction effect plots shown in Fig. 18 may also be construed to be an indication of the short term stability of the accelerometer.

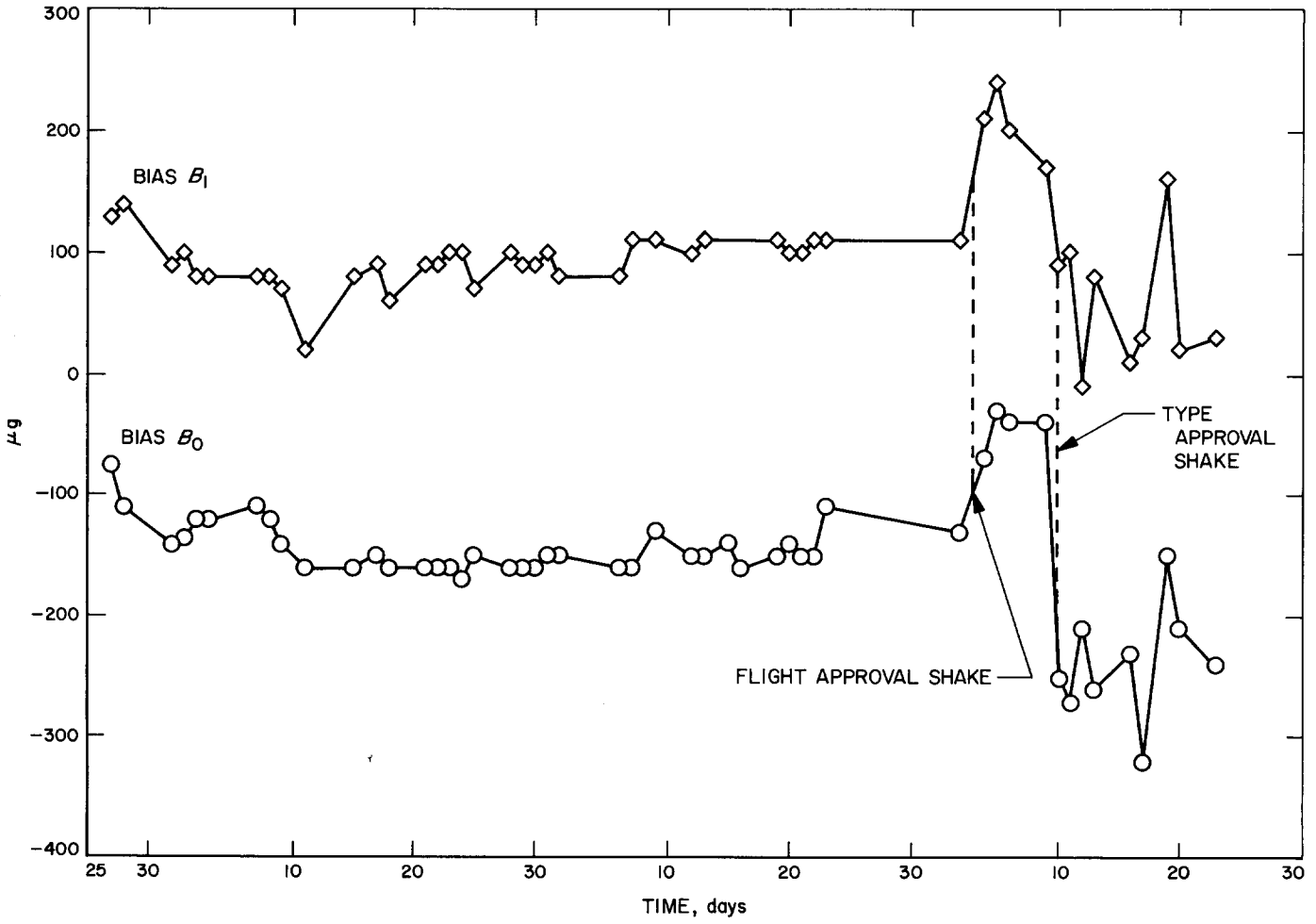

Fig. 19. Bias vs time

UNCLASSIFIED

UNCLASSIFIED CONFIDENTIAL

The test was conducted such that all ten data points could be recorded in one day. Approximately 2 hr warm up time was allowed, and then approximately 6 hr were required to take the data. The accelerometer temperature remained stable to less than 0.5°F over this interval.

Fig. 19 is a plot of the bias errors over a three month period. Bias B_0 is the bias obtained at the zero or null position, while bias B_1 is the bias obtained at the ±0.5-g input position. All data were obtained at 180°F, and with the stiction broken at each test point. Bias discrepancy $(B_0 - B_1)$, while large, is not excessive for an instrument of this class. No specification is placed on this parameter by the *Surveyor* system. The degradation of the bias error from vibration is also clearly shown in Fig. 19. Prior to vibration the most impressive thing about the data of Fig. 19 was the lack of any significant long term drift trends in the bias errors. In general, scale factor performance was excellent throughout the entire period covered in Fig. 19.

The vibration tests referred to in the preceding paragraph were performed with the accelerometer mounted on a solid aluminum block, which was attached to a C-126 shaker. No power was applied to the accelerometer during the running of a complex wave vibration program. This program consists of a 6-sec 9-g rms noise burst, then 200 sec of 3-g noise plug 6-g swept sine followed by another 6 sec 9-g noise burst. This was performed once along each of the three principal axes of the accelerometer. Higher vibration levels were then applied as follows: 18 sec of 14-g rms noise; 600 sec at 5-g noise plus 9-g swept sine and 18 sec of 14-g noise. These levels are similar to present *Surveyor* TAT vibration levels.

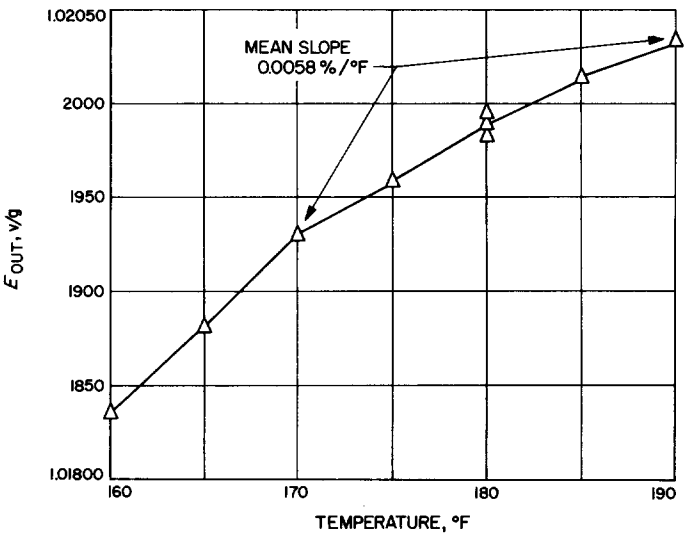

Fig. 20. Scale factor vs temperature

The effects of changing temperatures on the bias and scale factor parameters were also evaluated. Fig. 20 is a plot of scale factor at ±0.5 g versus temperature. The slope over the range covered is +0.0058%/°F. Bias error change with temperature was only −30 μg over the entire range of 30°F.

G. Electronics

Product design engineering. During this report period an intensive effort was made by the product design engineering section to complete the design of the A-24 digital equipment on or before schedule. New packaging techniques and interconnection concepts were initiated. These designs were distributed to HAC and JPL personnel for review via the preliminary design review, DR File 2942.40/200. The preliminary design review was effective in examining and exchanging views regarding the new *Surveyor* equipment design. Verbal and written responses indicated that some of the engineering design aspects will require additional analysis and review and described the improvements made on A-24 over A-21 equipment.

In addition to these important milestones, product design made a concerted effort to revaluate the weight of each control item. Subsequently every scrap of material was reexamined from a functional and a reliability standpoint. Weight charts were generated with a complete breakdown of all the materials as given in IDC 2942.40/245. Several weight reductions were made and reported to the personnel involved. This exercise will become a continuous function for all equipment.

The product design engineering section participated in the overall *Surveyor* program redirection. Estimates for incorporating several ECAs/ECRs were submitted in addition to the total cost of the A-21 program completion. The ECAs/ECRs reflect some of the critical problems encountered, which are categorized as follows:

(1) Central signal processor.—Two series of clamping diodes were added to each of the ten timing signals (total of 20 diodes for SC-1 and SC-2 per ECA 112322). These diodes were added to an existing terminal board area.

UNCLASSIFIED CONFIDENTIAL

UNCLASSIFIED
CONFIDENTIAL

(2) Engineering signal processor.—As a result of a failure in the contour cable, the cable constituent materials were reviewed (IDC 2748.40/1186). Corrective action was started to eliminate reoccurrences of the failure by the use of cables with H film encapsulated with a recommended epoxy. The new versions will be used in the engineering signal processor for SC-5 and up. (See ECRs 297546 and 298345.)

(3) Advanced flight control programmer.—Three advanced flight control programmer versions are contemplated for use in *Surveyor* spacecraft; 284580 for SC-1, SC-2, and SP-1, 284590 for SC-3 and SC-4, and 284550 for SC-5 and up. Version 284580 was designed with the inclusion of noise protection for six nonreversible functions. Also, version 284590 followed the same design as 284580 with the addition of making the latches immune from noise interference. The third version 284550 is currently being designed, extending the previous midcourse correction capability to 102 sec.

(4) Command decoding unit (CDU).—HAC systems engineering has requested that the CDU remain continuously on during flight for SC-1 and subsequent. This is to maintain the interlock circuit's capability (See ECR 333767).

Surveyor *ground support equipment (GSE).* The major additions and modifications of *Surveyor* GSE are reflected by these ECAs:

ECA	Description
112010	Flip-flop card redesign to eliminate threshold noise. Replaces critical and/or all existing flip-flop cards in both STEA and DSIF command generator, programmed automatic telemetry evaluator (PATE) binary comparator.
112046	Logic change to improve tape reader timing in STEA command generator.
112048	Modification of STEA command generator for interface with the computer data system. Design and fabricate new computer data system adapter unit.
112126	Modification of the amplifier card to improve high frequency stability and eliminate high frequency oscillation.
112134	Add pulse delay circuit to generate a pulse on the command sync delayed line to simulate the video processor camera advance pulse. Design new board using integrated circuits.
110723	Update the ground command decoder to spacecraft configuration.

Transmitter low power rf redesign. Redesign of the low power mode of operation in the transmitter was started in November, 1966. The design changes were directed at the A4 T-bar, X6 stripline multiplier, and heatsinking of the transmitter in general. The A4 T-bar consists of three stages of amplification and two X2 varactor multipliers. The design goals are as follows:

(1) To increase low power transmitter output from 100 to 160 mw nominal and to guarantee overall thermal vacuum environmental conditions.

(2) To improve heatsinking of transistors, varactors, and other high dissipation components in new design amplifier multipliers and ECU.

(3) To improve heatsinking of individual subassemblies to transmitter structure.

(4) To reduce internal thermal loss from subassembly attachment points to thermal tray mounting surface.

The new design consists of four modules; a three-stage amplifier, an $\times 4$ multiplier, an $\times 3$ multiplier, and an $\times 2$ multiplier. The power amplifier delivers about 3 w at 95.625 Mc. It is packaged in a sheet metal housing similar to the T-bar construction presently used in the transmitter and receiver.

All three varactor multipliers are connected in shunt. The housings for the multipliers are hogged out of solid aluminum blocks and all of the modules are foamed. The power amplifier (A4) will be mounted in the same location as the original A4 T-bar. The three varactor multipliers will be mounted in the area where the X6 stripline multiplier was mounted.

A breadboard set of modules has been undergoing extensive testing since late November, 1966. Testing of these breadboard modules mounted on a Class III *Surveyor* transmitter will start in February. The test will be performed in a thermal vacuum environment. Prototype hardware is presently being constructed, and will later be mounted on a Class III transmitter and

UNCLASSIFIED
CONFIDENTIAL

UNCLASSIFIED
CONFIDENTIAL

tested in a thermal vacuum environment. All the components for the new design have been ordered. Two RF transistors, 2N3375 and 2N386, are being qualified for the redesigned power amplifier. Most of the machined parts are on order. Drafting is 75% completed.

Radar altimeter and doppler velocity sensor (RADVS). During this period an error was discovered in the corrective factor used for computing the 14-ft mark during unit and system test. This factor compensates for the feed and receiver horn-dish geometry in relation to the boresight balls. The previously used factor was equivalent to 2.95 ft while the correct factor is on the order of 1.7 ft. The AM-4 system at Ryan was recalibrated to accommodate this new correction factor. Both SC-1 and SC-2 RADVS systems were revaluated for specification compliance. Both systems do not have the range smoothing circuit change so that measurement dispersion is greater than in the AM-4 system, which has this change incorporated. The effects of measurement techniques used at Ryan Aeronautical Co. and at HAC are being examined for correlation. Final results of these investigations are not complete.

Study programs in progress at Ryan include the following:

(1) Extended temperature test of the SN-1 klystron power supply modulator (KPSM).

(2) Vibration while ranging test on the SN-1 KPSM and, if feasible, flight units.

(3) Reflectivity accuracy studies.

(4) Additional antenna pattern tests for cross-coupled sidelobe logic study.

(5) Catastrophic failure modes for RADVS after impact.

Three proposed programs for the development and eventual inclusion of double sideband discrimination circuitry into the signal data converter have been evaluated at HAC. Of the three proposals—one for a minimal redesign, one for a moderate redesign, and one for a complete redesign of the signal data converter—the one for a moderate redesign (ECP-10) was selected as the best to pursue for the A-21 *Surveyor* project. The changes in the program plan from that proposed by Ryan were those made to assure that the design and development could be implemented as a completely parallel development with no interference to the existing RADVS program.

The program selected is a three phase development for the electrical redesign of the trackers in the signal data converter. It is the intention to give a go-ahead on this program early in February after the receipt of concurrence from JPL. Delays in authorization or concurrence will result in decreased feasibility of incorporating this change into the A-21 systems.

A proposal for testing the RADVS system under vibration was submitted for evaluation. This plan involves the testing of the RADVS while on a vehicle. The vehicle would be upside down and would be excited through the vernier engine mounts to simulate descent vibration, allowing the RADVS system to operate and radiate into free space. Additional analysis is required to determine if the spacecraft can be rotated and be vibrated upside-down in 1-g field without damage. Use of reflectors and targets are envisioned to provide ranging information. It is planned that this test would be conducted at AFETR, thus providing a final system confidence check. Again dependent on a go-ahead by early February, incorporation into the SC-3 schedule may be possible.

H. Electrical Power Supply

Introduction. Electrical power for the *Surveyor* spacecraft is supplied by a Sun-tracking planar solar panel and a sealed, secondary silver-zinc main battery. An auxiliary battery will be utilized to provide additional peak load capability and increased energy storage capacity during transit and the lunar day; the main battery provides the electrical energy for operation during the lunar night.

The power management system for the first four missions is composed of a boost regulator, a battery charge regulator, and a variety of voltage converters, regulators, and power switches located in other units that provide power management for the various instruments and subsystems. The battery charge regulator unit provides power conversion from the solar panel, main battery charge control, and several switching functions. The optimum-charge regulator circuit provides efficient conversion of solar panel power for use in battery charging. The battery output voltage from the unregulated bus is converted to the main regulated bus voltage by a boost regulator. A main overload trip circuit removes all nonessential spacecraft loads when an overload condition

UNCLASSIFIED
CONFIDENTIAL

UNCLASSIFIED
CONFIDENTIAL

is detected. The main battery charge logic system controls the charging current to the spacecraft main battery. Normally, the system operates in the automatic mode and the main battery is charged until its voltage reaches a predetermined level. A command mode is available whereby the battery may be commanded to be charged.

The auxiliary battery control unit provides battery voltage sensing circuitry, automatic control and selection of either the auxiliary or both batteries, and provision for command override of the automatic control mode. A main power switch provides for disconnection of all spacecraft power.

For the last four missions, the configuration of the power subsystem is modified to provide greater overall efficiency. The optimum charge regulator is deleted, and the solar panel cell layout is changed to provide maximum power output at a lower voltage. Thus, during cruise mode operation, the solar panel output is connected directly to the preregulated bus eliminating the losses in the optimum charge regulator and the booster part of the booster regulator. During lunar operation when the temperature of the panel is high and the output voltage correspondingly low, the solar panel output is connected to the unregulated bus.

Progress summary. Cracked solar cells, identified by visual inspection, have been replaced on two solar panels and a repeat flight acceptance test has been initiated. Visual inspection and replacement of cracked solar cells will be performed on the remaining panels.

A solar cell module-mounting-adhesive evaluation program is under way to investigate alternate adhesives that will eliminate the solar cell cracks. Main battery failure occurred after successful completion of SC-1 solar thermal vacuum mission sequence testing. Investigation is continuing, including power subsystem compatibility testing. Vendor delivery and flight acceptance testing of auxiliary batteries is on schedule. Qualification testing of the T-2N battery with the new separator system has been completed, as well as flight acceptance testing of four additional batteries. Qualification of the T-2N recovery battery with a heater blanket has been completed. Procurement of gondola batteries has begun.

Procurement of solar panels, utilizing a different basic construction as well as a changed output voltage characteristic, has begun. It is expected that the cells on the redesigned panels will not be susceptible to the cracking experienced on the design utilized for the first four spacecraft.

Solar panel.

a. Flight hardware. The status of flight panels is as follows:

(1) Solar Panel 1—flight acceptance testing following diode and temperature sensor retrofit was completed. Repeat flight acceptance testing following replacement of cracked solar cells has begun.

(2) Solar Panel 2—withdrawn from storage for replacement of cracked solar cells. Cracked cells have been replaced; the panel has received an electrical performance test and has been prepared for redelivery.

(3) Solar Panel 3—delivered. Panel to be withdrawn for examination of cracked solar cells by June 1966.

(4) Solar Panel 4—flight acceptance thermal-vacuum testing has been completed.

(5) Solar Panel 5—flight acceptance vibration testing has been completed.

b. Solar cell cracks. A visual inspection technique has been developed for identifying incipient cracks in solar cells which have not exhibited electrical degradation in flight acceptance testing. All solar cells in flight panels with cracks or incipient cracks will be identified, using this inspection technique, and replaced. Replacement has been completed on solar Panels 1 and 2.

c. Systems testing. Strain gages have been installed on the T-21 solar panel substrate to record substrate facing strain during spacecraft drop testing. Analysis of data taken from the first drop test is under way.

d. Alternate solar panel procurement. The design, fabrication and test program for the prototypes of the redesigned solar panels has been initiated with the contractor. The test program includes the fabrication and environmental testing of solar panel samples of approximately 1.5 ft^2 area with selected processes and materials for qualifying the manufacturing techniques for flight hardware. The redesigned solar panel utilizes the same honeycomb construction substrate used for the present panels and will have 3,626 flat mounted cells. The solar cells are 1×2 cm P on N type assembled in flat mounted seven-cell submodules. The submodules will be assembled using a tunnel oven. The solar panel design will consist of three redundant diode-isolated sections. Two of the sections will have two parallel interconnected groups, and the third will have three parallel interconnected groups. Each group will consist of 74 series connected

UNCLASSIFIED
CONFIDENTIAL

UNCLASSIFIED CONFIDENTIAL

seven-cell submodules. A preproduction prototype will be fabricated with 50% of its cell-mounting area covered with electrically interconnected modules. A completely covered production prototype will follow. Both prototypes will be subjected to extensive environmental testing including: thermal vacuum, acoustic temperature/humidity, mechanical vibration and electrical performance. Following the prototypes, a panel will be fabricated for qualifying the design to type approval specification requirements.

Batteries.

a. Main battery. As previously reported, the reliability program conducted at the Electric Storage Battery Company has been satisfactorily completed. All nine batteries met the minimum operational requirements; four are still functioning in extended testing. Publication of the reliability program final report incorporatong results of extended testing awaits the conclusion of the tests. Table 17 shows interim life data.

Table 17. Battery life data—reliability test program

Battery serial number	Specified operating time,[a] hr	Actual operating time, hr	Activated life, days
R9	1630	1990	241
R10	1630	2450	221
R11	1630	1630	157
R12	1630	1630	227
R13	1630	Still operating	—
R14, R15, R16	830	Still operating	—
R17	830	830	104

[a]1630 hr represents launch through third lunar day.
830 hr represents launch through 250 hr of second lunar day.

Main Battery 34 was used on SC-1 for the two back-to-back solar thermal vacuum test sequences. The battery successfully completed the first mission test, which was performed using battery power. During the second mission test, which was performed using external power supplies and the battery in an open circuit condition, the battery developed a shorted cell. The amp-hr history of the battery is shown in Table 18.

Failure analysis performed at HAC by the vendor did not reveal the cause of failure but obvious separator deterioration was found. In addition, discoloration was apparent as a result of a large amount of silver in solution. The condition of the separator was probably a result of the prolonged battery use at elevated temperatures.

Table 18. Ampere-hour history of main battery 34

Charge capacity	Amp-hr
During flight acceptance testing	185
Postsolar thermal vacuum Mission 1	25
Total charge	210
Discharge capacity	
During solar thermal vacuum Mission 1	112
Postsolar thermal vacuum Mission 1	9
Laboratory tests on five cells	62
Stand loss prior to solar thermal vacuum	5
Presolar thermal vacuum use	15
Efficiency losses	7
Total discharge	210

Previously, Battery 29 failed after completing the fourth SC-1 solar thermal vacuum mission sequence test. Examination showed one cell had developed a positive shorting path by means of silver penetration through the separator to the negative plate. This was a typical end of life type failure. A sample of the separator system was examined microscopically. Zinc was found deposited between cellophane layers, which is normal; no foreign material was present. An X-ray fluorescence spectrometer was used to analyze the positive plate. Again, no foreign material was present.

After the failure of Battery 29, power subsystem compatibility tests were initiated. These are discussed in the following section. In addition, a Ag-Zn cell test plan is being prepared. Basic cell tests are required to isolate failure modes under the environments seen by the *Surveyor* battery. Also, some immediate steps are being taken to change the flight acceptance test procedures, namely:

(1) Eliminate complete discharge cycle

(2) Lower float voltage from 27.3 to 26.9 to decrease amount of gas generated during charge.

The changes will aid in extending battery operating life, thus increasing reliability.

b. Auxiliary battery. No problems have been encountered with the auxiliary battery. Deliveries from the vendor and subsequent flight acceptance testing are continuing as scheduled.

c. Batteries for T-2N Vehicles. T-2N main Battery 127 with the new separator system has successfully completed qualification testing. Flight acceptance testing of T-2N

UNCLASSIFIED CONFIDENTIAL

UNCLASSIFIED

main Batteries 128 through 131 has been completed. The T-2N recovery battery with the heater blanket has been qualified. Procurement of four gondola batteries from Willard Battery Company has begun.

Boost regulator. The solar thermal vacuum test with SC-1 spacecraft indicated excessive heating of the boost regulator when command modulation was removed. The problem was reduced to instability of the preregulator under discrete conditions of battery voltage and essential load. The central command decoder constitutes the essential bus load which is removed when command modulation is terminated.

The boost regulator for SC-1 was modified to stabilize the preregulator and the unit was successfully tested over the full range of battery voltage and load conditions in a thermal vacuum environment. Subsequent solar thermal vacuum testing of the spacecraft also indicated satisfactory performance of the boost regulator. The overload trip function was removed from the SC-1 boost regulator to prevent loss of nonessential power during critical phases of the mission. The overload trip function will be retained in units for SC-2 and later spacecraft, but the time constant will be extended to prevent tripping under transient overloads.

Work on the "efficiency" model of the boost regulator (284200) was suspended when it became evident that system noise requirements could not tolerate the characteristics of the redesigned preregulator. These difficulties contributed to the decision to redesign the power system. The redesign on the booster regulator was redirected in December to accommodate the requirements of the new system configuration. The essence of the redesign is to provide the capability of running the preregulated bus directly from the solar panel, thus eliminating the losses in the preregulator for the cruise portion of the mission. Delivery of the first unit (control Item 3024240) is scheduled for August 1966.

Battery charge regulator. A consistent malfunction of the optimum charge regulator during high temperature testing in a solar thermal vacuum regime has been successfully diagnosed and corrected.

As a part of the program to redesign the power system, the optimum charge regulator is being deleted. New logic, to accommodate the requirements of the change, is being incorporated into the battery charge regulator along with the switching function of the A/SPP stepping motors. The new unit, control Item 3024260, is scheduled for August 1966 delivery.

Engineering mechanics auxiliary. During the two recent solar thermal vacuum test performances made with SC-1 spacecraft, readout data showed that spurious and/or improperly timed squib functions were being initiated when the *Centaur* simulator was activated. Investigation and tests indicated that switch contact bounce was amplified by the simulator which produced signals that approximately duplicated normal signals. Since the output of the *Centaur* sequencer is shorted out except prior to the time of use, this would not be a flight problem. The *Centaur* simulator has, therefore, been changed to more closely duplicate the flight vehicle.

System integration testing. Testing of the SC-1 spacecraft has indicated a power subsystem incompatibility. Three simulated transit mission sequence tests were conducted using a subsystem mockup to evaluate the problem in detail in a controlled environment.

In all three tests a Class III boost regulator, battery charge regulator, and a Class IV filter capacitor were used with a wiring harness constructed to simulate the spacecraft harness. A solar panel simulator was used for solar panel power. The first test was run using main Battery 30 mounted on an aluminum plate common with the battery charge regulator and boost regulator. The wiring diagram of the mockup is shown in Fig. 21. The battery current profile throughout the mission sequence is shown in Fig. 22(a) and the amp-hr discharge in Fig. 22(b). At the end of the test, the battery was stored at ambient temperature for 26 hr at which time Cell 14 was found to contain little or no energy. Other cells were discharged and found to contain about 10 amp-hr; 148 amp-hr had been removed in the test as shown in Fig. 22(b). At this time the battery was partially charged at a 2-amp rate and then completely discharged. On subsequent recharge an internal short was detected in Cell 14.

As part of the subsequent failure analysis, the waveform of the battery current was examined and a 5-kc component noted. To remove this component an inductor was mounted in the power bus between the capacitor filter and the battery. A diode was connected in parallel with the inductor. The second transit mission sequence was then performed using main battery 33. The current profile is shown in Fig. 22(c) and the amp-hr discharge in Fig. 22(d). At the end of the test the battery was stored at ambient temperature in an open circuit condition for

UNCLASSIFIED

UNCLASSIFIED
CONFIDENTIAL

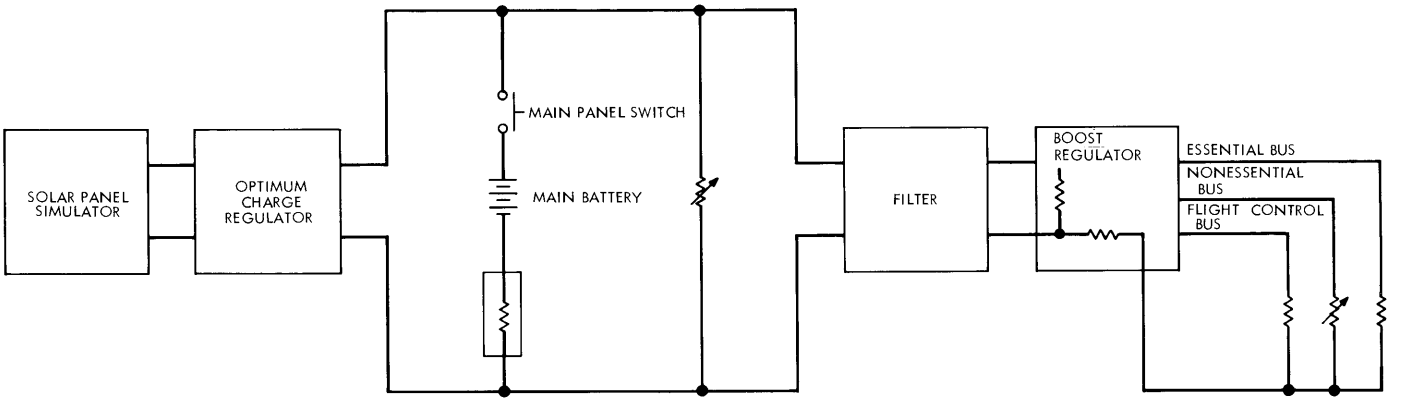

Fig. 21. Power subsystem compatibility test

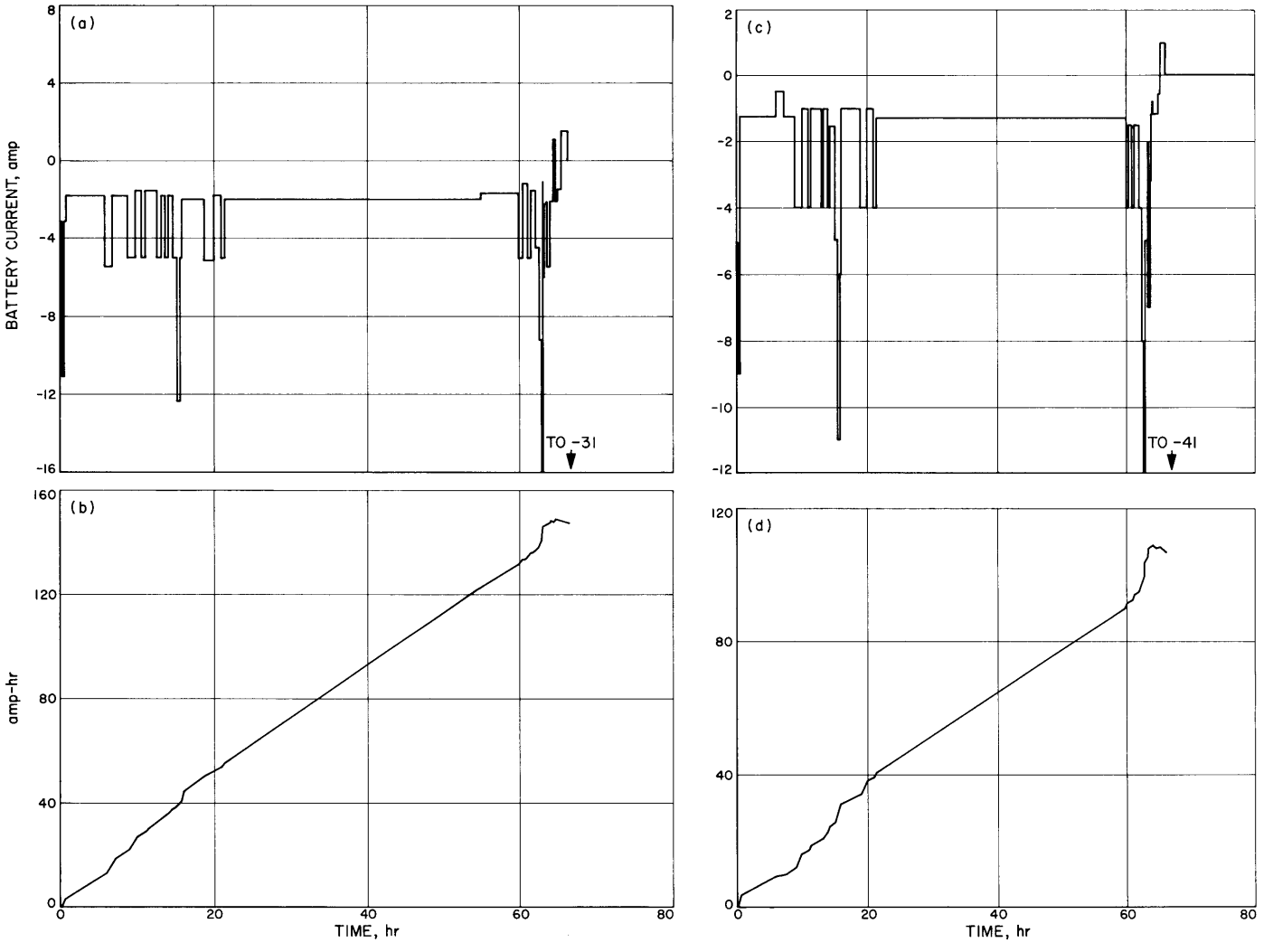

Fig. 22. Power subsystem compatibility test: (a) battery current vs time — Battery 30; (b) ampere-hours vs time — Battery 30; (c) battery current vs time — Battery 33; (d) ampere-hours vs time — Battery 33

CONFIDENTIAL
UNCLASSIFIED

UNCLASSIFIED
CONFIDENTIAL

several days and then discharged with an additional 55 amp-hr removed. One hundred and nine amp-hr had been removed during the test, indicating the battery had contained 164 amp-hr at the beginning of the test. The battery was then fully recharged with no apparent degradation.

The third test was run using main Battery 33 again, but without the inductor. The same current and amp-hr profiles resulted. Again the battery was stored at ambient temperature and then discharged to a minimum voltage. An additional 41 amp-hr were obtained. The battery was subsequently recharged with no apparent degradation and stored for further use.

The three tests discussed indicate that the 5-kc current component alone does not cause battery failures. This has been substantiated by failure of Battery 34 in a recent SC-1 solar thermal vacuum test where the inductor was also incorporated in the power system. This failure was discussed in the previous section. Tests to be conducted will determine if other factors such as high spacecraft compartment temperatures or other complex current components cause battery degradation. Future testing will be performed on one-cell batteries which are typical *Surveyor* battery cells. Each cell will be subjected to different current waveform loads and temperatures.

I. Thermal Control

Introduction. The *Surveyor* thermal control system is comprised of the individual subsystems or unit thermal control systems integrated to provide acceptable thermal environments for all components during all phases of spacecraft operation. The passive and active methods employed include:

(1) special preparation of spacecraft external surfaces to achieve optimum thermal absorption and emission characteristics.

(2) superinsulated compartments to house critical equipment.

(3) electrical heaters and thermal conduction paths controlled by bimetallically operated thermal switches to maintain compartment temperatures within acceptable limits.

System integration of spacecraft thermal control subsystems and thermal compatibility of proposed mission sequence operations are verified; thermal switches and spacecraft coatings are developed; and subsystem thermal vacuum performance is evaluated by hardware tests with the MT-1 vehicle, the thermal control model (S-10), and other thermal models. Qualification of the spacecraft prototype thermal design has been performed on the T-21 vehicle. Mission operation activities are supported by the development of space flight operations facility thermal management procedures.

SC-1 system test support. Two additional real time "back to back" mission sequences have been completed in the solar thermal vacuum flight acceptance testing of the SC-1 spacecraft. The first mission sequence, Phase 6A, was performed at 87% of a solar constant at the test plane and the second, Phase 6B, was performed at 112% of a solar constant. The total solar exposure was approximately 150 hr. Two solar eclipses were performed in the low intensity phase, the second of which was coincident with the terminal maneuver in order to provide an extreme low start temperature environment for the radar altimeter and doppler velocity sensor (RADVS) system. Solar eclipses of 30 and 60 min were performed in the high intensity phase. A special functional test was performed in the 1-hr eclipse. The solar axis of the antenna/solar panel positioner (A/SPP) was allowed to cool down to 0°F to qualify the unit for low temperature operation. It was verified that the sunbulb used for Canopus simulation has only a slight effect on Canopus sensor temperatures. Phase 6C, a 40-hr plugs-out test employing three solar intensity levels (100, 112, and 87%) in sequence, has been completed.

Compartment modifications, incorporated and anticipated, are resulting in increased power dissipation rates. The effect of the additional heat loads on compartment thermal control is being investigated. In the high power mode during test Phase 6B, malfunction of the boost regulator in Compartment B resulted in excessive power dissipation, driving unit temperatures beyond upper allowable limits.

Auxiliary battery cell temperatures obtained during Phases 2 through 6 showed a maximum deviation of 2°F from a linear temperature versus solar intensity correlation. The Phase 1 data point remains inconsistent with respect to the above correlation. The primary cause of this anomaly is felt to be the effect of the warm shadow shrouds during this phase.

UNCLASSIFIED
CONFIDENTIAL

UNCLASSIFIED
CONFIDENTIAL

Prior to test Phase 6A a sunshade was installed on vernier propellant Line 1 to reduce the marginal steady state temperatures on the illuminated regions of line. Results of test Phases 6A and 6B verified that the basic shadow pattern maintained the equilibrium temperatures within the desired 0 to 100°F range and did not compromise the transient capability of these lines. A flight model sunshade was fabricated and installed for test Phase 6C. Temperatures during the plugs-out test (Phase 6C) coincided with those exhibited during Phases 6A and 6B.

Test Phase 6 provided the first opportunity to assess the effectiveness of the relocated thermostat on vernier Line 3. During the low intensity test, line temperatures were considerably higher than anticipated and the heater did not cycle, while at high intensity the heater cycled randomly with respect to both time and temperature range. A post-test examination of the lines revealed that an intermittent short circuit in the heater was the cause of this behavior. The lines in question were replaced, and test Phase 6C data indicate that the heater assembly is operating satisfactorily.

Both helium and nitrogen tanks ran somewhat warmer than during previous phases of like intensities; however, thermal control of the tanks is still adequate. Degradation of the white paint is considered the primary contributor to higher tank temperatures.

A thermostat to control the TV mirror assembly heaters was incorporated in the survey camera before test Phase 6. Prior to this installation, the mirror assembly temperature dropped below the minimum operational limit during camera operation. Satisfactory thermal control was evident during subsequent test phases.

A summary of the temperatures obtained in Phase 6 is shown in Table 19.

A-24 model subsystem thermal analysis and design. Preliminary design analysis computer studies to simulate the touchdown dynamics instrumentation subsystem compartment for day and night landing missions were conducted. The main variables were the surface finishes on the solar collector plate, the canister exterior, and the internal compartment surfaces. The analysis indicated that when the internal surface was coated with low emittance finishes and the external surface of the collector plate was coated primarily with a white finish, that the electronics were maintained at a moderate temperature by the system during transit, and the posttouchdown transient capability would be approximately twice as long as that of the high emittance interior. A more complex model of the compartment has been developed from the simple model used in these studies. Future work will use the more complex model to more accurately predict temperature levels and the transient characteristics of each of the instrument packages.

Surveyor *S-10 vehicle test program.* In accordance with a JPL directive, the S-10 vehicle was shipped to JPL in early December and readied for the JPL test phases in the 10-ft space simulator. Testing at HAC was previously planned to precede JPL testing; however, due to SC-1 schedule slips, the order was reversed.

JPL thermal control has taken primary responsibility in the JPL tests and will analyze the test data. The Phase 1 vehicle configuration was as follows: transit coast mode orientation, shadow shrouds employed, no A/SPP, and spacecraft legs removed. Phase 1 testing consisted of attaining equilibrium conditions with coast mode power applied and a solar intensity of 80 and 100% of one solar constant (as measured by the radiometer) followed by a period of special subsystem tests. Phase 1 testing was initiated January 4 and terminated January 8, 1966.

Phase 2 test configuration included the A/SPP, solar panel, and planar array antenna without the shadow shrouds. The vehicle orientation was that of transit coast mode with the one exception being that the solar panel was rotated down approximately 6 deg from horizontal to reduce the specular solar reflections caused by the solar panel interacting with the chamber optical system. The lines at vernier Engine 1 were wrapped with aluminum foil and the exit plane of the Engine 1 nozzle cone was covered with aluminum foil following Phase 1 and prior to Phase 2 to study their thermal effects. Phase 2 testing consisted of obtaining transit coast mode equilibrium conditions with coast mode power applied, followed by special tests on the compartment system and A/SPP. Phase 2 testing was initiated January 17 and terminated January 19, 1966.

JPL Phase 3 testing was conducted in a simulated lunar night thermal environment to obtain the following: (1) heat loss data on compartment system, (2) heater power requirements for TV cameras, and (3) compartment system thermal switch performance. Phase 3 testing was initiated January 24 and terminated January 30, 1966.

Data obtained during Phases 1, 2, and 3 of JPL testing are currently being analyzed and evaluated by JPL thermal control. The Canopus sensor and inertial reference

UNCLASSIFIED
CONFIDENTIAL

Table 19. SC-1 Phase 6 STV test results—flight sensors (°F)

Subsystem/unit	Allowable unit temperature range, °F	Flight sensor prediction (100% solar constant), °F	SC-1 Phase 6 STV test results—flight sensors, °F		Flight sensor flight predictions, °F	Flight sensor allowable range, °F	Remarks
			Phase A—low level 80% Rad[a] 87% BP[b]	Phase B—high level 105% Rad[a] 112% BP[b]			
Vehicle							
Compartment A							
Upper Tray, V-15[c]	0 to 125[d]	77	75	82	77	0 to 125[d]	
Transmitter A, D-13	0 to 210		73	81		0 to 210	
Transmitter B, D-14	0 to 210		75	82		0 to 210	
Lower tray, V-16	0 to 125	102	101	106	103	0 to 125	
Battery charge regulator, EP-34	0 to 170		132	137		0 to 170	
Main battery, EP-8	40 to 135		105	104		40 to 135	
Radiators (average),[d] V-20, 25, 47		−10 shaded,[e] 54 in Sun	43, 8[f], 24 25[d] (average)	50, 54[f], 32 45[e] (average)	11 shaded,[e] 61 in Sun		
Compartment B							
Upper Tray, V-21	0 to 125	108	73	107	109	0 to 125	
Boost regulator, EP-13	0 to 170		100	135		0 to 170	
Lower Tray, V-22	0 to 125	115	76	113	116	0 to 125	
Radiators (average), V-24, 45, 46		83 (average)	52, 59, 52 54 (average)	84, 92, 84 87 (average)	81 (average)		
Auxiliary battery, EP-26	40 to 130	60	25	67	60	40 to 130	
Vernier propulsion							
Thrust chamber assemblies							
Thrust chamber assembly 1, P-7	0 to 165	62	37	86[g]	80	20 to 125	
Thrust chamber assembly 2, P-10	0 to 165	99	50	91	To be determined	21 to 140	
Thrust chamber assembly 3, P-11	0 to 165	76	42	82	84	17 to 129	
Helium tank, P-17	0 to 100	86	49	92	85	10 to 100	
Main retrorocket engine							
Flight sensors							
Upper case, P-3	20 to 70	60	92/78	77/68	To be determined	To be determined	
Lower case, P-12	20 to 70	51	88/63	74/55	To be determined	To be determined	
Nozzle, P-22			−103	−88	To be determined	To be determined	
Thermocouples							
Safe and arm device	0 to 100[h]	79	49	60	Does not apply	Does not apply	
Head end, RR-21	20 to 70[h]	63[i]	88/74[j]	72/63[j]	Does not apply	Does not apply	
Adjacent to attach point at leg 2, RR-46	20 to 70[h]	37[i]	84/51[j]	64/41[j]	Does not apply	Does not apply	
Adjacent to attach point at legs 1 and 3, RR-34	20 to 70[h]	52[i]	82/59[j]	70/52[j]	Does not apply	Does not apply	
Aft burning surfaces, RR-18	20 to 70[h]	36[i]	78/50[j]	52/41[j]	Does not apply	Does not apply	

CONFIDENTIAL UNCLASSIFIED

Table 19. SC-1 Phase 6 STV test results—flight sensors (°F) (Cont'd)

Subsystem/unit	Allowable unit temperature range, °F	Flight sensor prediction (100% solar constant), °F	SC-1 Phase 6 STV test results—flight sensors, °F		Flight sensor flight predictions, °F	Flight sensor allowable range, °F	Remarks
			Phase A—low level 80% Rad[a] 87% BP[b]	Phase B—high level 105% Rad[a] 112% BP[b]			
Propellant tanks							
Oxidizer 1, P-15	0 to 100	50	33	30	50	0 to 100	At end of 66 hr of exposure to simulated space environment, propellant tanks were within specified temperature limits. Temperatures presented for Phase 6A existed after 80 hr of exposure and illustrate extensive thermal capability of tanks. Phase 6B data represent steady state points. Oxidizer Tank 2 heaters began cycling near end of Phase 6A and continued cycling throughout 6B.
Fuel 1, P-13	0 to 100	55	48	50	55	0 to 100	
Oxidizer 2, P-16	0 to 100	25	19	21	25	15 to 100	
Fuel 2, P-5	0 to 100	25	26	21	25	15 to 100	
Oxidizer 3, P-6	0 to 100	50	31	25	50	15 to 100	
Fuel 3, P-14	0 to 100	55	50	52	55	0 to 100	
Propellant lines							
Leg 1, P-8	0 to 100	23 to 30 (Temperature range represents heater cycling)	23 to 30	32	23 to 30		
Maximum line temperature	0 to 100		65	92	80		
Coil temperature	0 to 100	40	20	65	40		Sunshade reduced line temperature below 100°F. Line temperatures will remain within allowable limits.
Leg 2, P-4			23 to 28	23 to 28	23 to 28		
Maximum line temperature		40	68	100	85		
Leg 3, P-9			50	20 to 58	23 to 29		Flight sensor allowable range has not been determined. Lines 1 sunshade are slightly different from developmental model. Lines 3 have not operated properly since relocating thermostat.
Maximum line temperature			85	88 to 138			Heater on during most of Phase 6A as result of short circuited thermostat. Heater operated intermittently during Phase 6B. All lines remained within specified limits during solar eclipse. Cause was traced to shorted heater, which has been replaced.
Flight control sensor group							
Electronics							
Board 1, FC-44	0 to 165	None	84	110	95	0 to 165	
Board 6, FC-45	0 to 190	None	120	143	130	0 to 190	
Canopus sensor, FC-47	−20 to 130	83	74	107	90	−20 to 130	
Roll Gyro, FC-46	170 to 185	None	180	182	180	170 to 185	Gyro flight sensors location indicate temperatures lower than actual gyro temperatures. This is normal operating condition.
Pitch Gyro, FC-54	170 to 185	None	176	179	176	170 to 185	
Yaw gyro, FC-55	170 to 185	None	179	181	180	170 to 185	
Nitrogen tank, FC-48	−10 to 125	76/90[k]	37	80	60	10 to 115	
Roll actuator, FC-71	0 to 200	100	72	115	103	0 to 200	

UNCLASSIFIED

UNCLASSIFIED

Table 19. SC-1 Phase 6 STV test results—flight sensors (°F) (Cont'd)

Subsystem/unit	Allowable unit temperature range, °F	Flight sensor prediction (100% solar constant), °F	SC-1 Phase 6 STV test results—flight sensors, °F		Flight sensor flight predictions, °F	Flight sensor allowable range, °F	Remarks
			Phase A—low level 80% Rad[a] 87% BP[b]	Phase B—high level 105% Rad[a] 112% BP[b]			
Radars							
RADVS							
KPSM							
Main package, R-8	−22 to 100	47	6	43	23	−12 to 105	
Doppler velocity sensor klystron	−49 to 100	—	0	35	—	—	
Altimeter klystron	−22 to 100	—	3	39	—	—	
Signal data converter							
Low voltage power supply, R-9	−18 to 140	85	45	83	52	—	
Motherboard assemblies	18 to 118	—	—	—	—	—	
Receiver-transmitter antennas							
Altimeter velocity preamplifier	−58 to 122	35	15[m]	55[m]	30[m]	−40 to 110	
Velocity sensor preamplifier	−58 to 122	26	−2[n]	38[n]	19[n]	−42 to 112	
Altitude marking radar							
Electronics, R-7	−20 to 100	None	20	20	6 to 10	−5 to 135	Test data and flight projections apply to steady-state conditions as controlled by thermostatically controlled heaters.
Electronics platform, R-6		None	0	0	0	−20 to 125	
Edge of antenna, R-27	−300 to 250	None	−146	−134	−135	−300 to 250	
Television							
Survey TV	Survival / Operating						
Electronics, TV-16	−285 to 260 / −22 to 150	None	−144	−120	−130 to 0	Same as allowable temperature range	Test temperatures are for steady-state nonoperating condition. Approach and survey camera electronics heated up to approximately 0° and −3°F in 3- and 5-hr periods after heater turnon.
Mirror assembly, TV-17	−200 to 180 / −50 to 180	None	−146	−124	−160 to −15		
Approach TV							
Vidicon faceplate, T-1	−300 to 199 / −22 to 150	None	−28	−28	−30		
Electronics, T-3	−285 to 360 / −20 to 160	None	−124	−104	−110 to 20		
Spaceframe							
Upper, V-27	−140 to 160	73	50	95	To be determined	To be determined	Flight sensor V-27 and V-28 are located on semiilluminated portions of spaceframe, whereas V-35 and V-36 are in regions shaded by solar panel.
V-35	−140 to 160	−72	−82	−61	To be determined	To be determined	
Lower, V-28	−140 to 160	46	30	62	To be determined	To be determined	
V-36	−140 to 160	−18	−30	−7	To be determined	To be determined	

Table 19. SC-1 Phase 6 STV test results—flight sensors (°F) (Cont'd)

System/unit	Allowable unit temperature range, °F	Flight sensor prediction (100% solar constant), °F	SC-1 Phase 6 STV test results—flight sensors, °F		Flight sensor flight predictions, °F	Flight sensor allowable range, °F	Remarks
			Phase A—low level 80% Rad[a] 87% BP[b]	Phase B—high level 105% Rad[a] 112% BP[b]			
Retroattach points							
V-37	−140 to 160	42	25	59	To be determined	To be determined	
V-38	−140 to 160	−25	−36	−14	To be determined	To be determined	
V-39	−140 to 160	44	27	60	To be determined	To be determined	
Landing system leg 2, V-31	−50 to 160	49	30	68	To be determined	To be determined	Landing system extends into zone within chamber where solar intensity is in severe dropoff region.
Crushable block, V-44	−300 to 160	−35	−47	−22	To be determined	To be determined	

[a] Rad = Intensity at test plane as measured by radiometer.
[b] BP = Intensity based on black plate measurements.
[c] Flight temperature sensor number.
[d] When either transmitter is in high power mode, range extends to +160°F in vicinity of traveling-wave tube.
[e] Switch 8 appears to be closed in Phase 6B, but not fully closed in Phase 6A.
[f] Values in prediction columns indicate range to be expected including all radiators. Values in test result columns are average of three flight sensors on radiators partly shaded, partly sunlit.
[g] Installation of propellant line sunshade resulted in lower temperature than observed during Phase 4.
[h] Allowable temperature range applies to time of ignition.
[i] Pretest predictions are based on initial temperature of 80°F.
[j] Indicated temperature range applies to launch and time of ignition.
[k] Flight sensor prediction before/after ultraviolet degradation.
[l] Not enough data available on SC-1 spacecraft. S-10 spacecraft will supply answer.
[m] As measured by flight sensor R-13.
[n] As measured by flight sensor R-10.

UNCLASSIFIED
UNCLASSIFIED

UNCLASSIFIED CONFIDENTIAL

unit data were invalid since the heaters in these units could not be operated.

The *Surveyor* S-10 vehicle was returned to HAC February 1, 1966 and is currently being upgraded to the HAC Phase 1 (hot engine cone test) configuration.

Spacecraft performance analysis and command (SPAC) support. *Surveyor* thermal control participated in the SPAC monitoring of SC-1 STV flight acceptance test Phase 6A December 27 through 31. The test was monitored from approximately 4 to 16 hr-mission time by two thermal performance analysis teams of two men each, using shifts approximately the same as planned for Mission A. In addition, the period of the test from 54 hr-mission time to touchdown was monitored by one thermal specialist. The test pointed out the requirement for deemphasis of mechanical tasks such as data plotting, in order to allow a more thorough analysis of the spacecraft's thermal performance by the participating specialists. To accomplish this goal, it is planned to train a technical aide for use as a plotter during the C tests. It is planned that the *Surveyor* thermal performance analysis group will participate in the C tests schedued for April.

Thermal finishes. The feasibility of repairing inorganic white coatings has been studied, with particular attention centered on the adhesive characteristics of the repaired coating. The conclusions, based on the data obtained during this investigation, are as follows:

(1) Air-dried inorganic paint on base metal (aluminum) has very poor adhesion.

(2) Air-dried inorganic paint over a fully cured (260°F) coating of paint has good adhesion.

(3) Inorganic paint cured at 150°F over base metal (aluminum) has adequate adherence but not quite as good as the 260°F cure.

Various cleaning techniques for the organic white coating have been evaluated to determine if cleaning restored whiteness and if the ultraviolet stability of the coating was affected. Two cleaning procedures performed well. These were solvent cleaning followed by sanding, and cleaning with an abrasive paste.

A cleaning process for inorganic white paint using hard sanding has been evaluated. The sanding restores the whiteness of the coating but appears to increase the absorption on virgin material, while decreasing absorption on degraded surfaces.

Other areas of work on thermal control now in progress include the following:

(1) Evaluation of new organic coatings.

(2) Investigation of metalized pressure sensitive or thermosetting tapes for use in thermal control.

(3) Investigation of fired-on gold and silver and a chemically deposited gold spray (high temperature not required) for use in thermal control.

J. Engineering Mechanics

Introduction. The activities reported in this section include touchdown dynamics, static and dynamic structural analyses, and structural tests. Touchdown dynamics includes the specification, analysis, and testing of the soft-landing system. A significant portion of this work pertains to procurement in the landing gear shock absorbers. A similar activity is the specification of design and test parameters for spacecraft retrorocket engine separation. This section also covers stress and dynamic analyses on major spacecraft structures, the specification of loads and other design criteria, and the determination of structural test requirements. The results of the static and dynamic testing of structural models, including full-scale simulated spacecraft, are reported. This task includes procurement of flight engineering instrumentation, such as accelerometers, amplifiers, deflection potentiometers, and strain gage amplifiers.

Summary. Progress continues toward developing the A-24 shock absorber for application in the A-21 spacecraft. The weld between the gas and hydraulic cylinder has now been removed from the design, and the assembly will be machined as one unit. This leaves one weld on the rod end, which will be welded by the electron beam process. Analyses indicate the A-24 shock absorber design is adequate for Missions E, F, and G; it is currently planned to deliver the first units in June, and thus phase the design into SC-3. A-21 shock absorber type approval test is now virtually complete, and the report is expected in February. Initial conditions have been specified for S-15 three-dimensional drop tests. Evaluation of all-crushable shock absorber design continues. A new stability program written especially for this shock absorber is now complete, and checkout completion is expected in February. Selection of T-21 drop test conditions has been completed and is presented for lunar conditions, together with the equivalent Earth drops.

CONFIDENTIAL UNCLASSIFIED

UNCLASSIFIED CONFIDENTIAL

Preparation continues for S-9 static test. Initial tests started January 28. The upper Compartment B support, which failed on the torsion test, was a high stress, low cycle problem. S-15 drop tests were initiated February 11. The test facility platform and support equipment are ready. A static test, completed on S-2A, demonstrated the structural adequacy of the spaceframe upper tripod support and the antenna/solar panel positioner (A/SPP) torque collar.

Shock absorber procurement. During the A-24 shock absorber design review at National Water Lift (NWL) on December 8, NWL engineering presented a status report on the various technical aspects of the program. Most significant is a unified construction for the hydraulic and gas chambers and the use of electron beam welding to join the gas cylinder and rod end. Some of the development tests were proceeding at a slower pace than previously scheduled. JPL and HAC authorized a change to the specification for the titanium (6AL-4V), allowing a reduction in yield strength required because of vendor difficulties in heat treating the material to expected properties. The material has since been successfully heat treated to the revised specification and was delivered to NWL at the beginning of February.

Present studies indicate the A-24 shock absorber can be used on Missions E, F, and G spacecraft without changes. The A-24 shock absorber will be phased into the program on the SC-3 spacecraft. First deliveries of the new hardware are scheduled for late June, 1966. A-21 type approval tests have been completed, except for the single unit burst-test.

NWL has been instructed to redesignate the SC-3 shock absorber as spare one (SP-1) and to deliver a final set of three for uses on S-9 tests. The units deleted from the SC-3 and SC-4 will be replaced by the improved A-24 shock absorber.

Landing dynamics. To provide shock absorbers for Missions E, F, and G with minimum cost and schedule delays, a study has been carried out to assess the feasibility of using the A-24 shock absorber without alteration. The A-24 shock absorber with no parameter change gives acceptable stability (Fig. 23) and a maximum shock strut load of approximately 8000 lb, and appears to be satisfactory for installation on the A-21 vehicles.

A study of three-dimensional landing stability in support of the S-15 drop tests was conducted using the 3-D

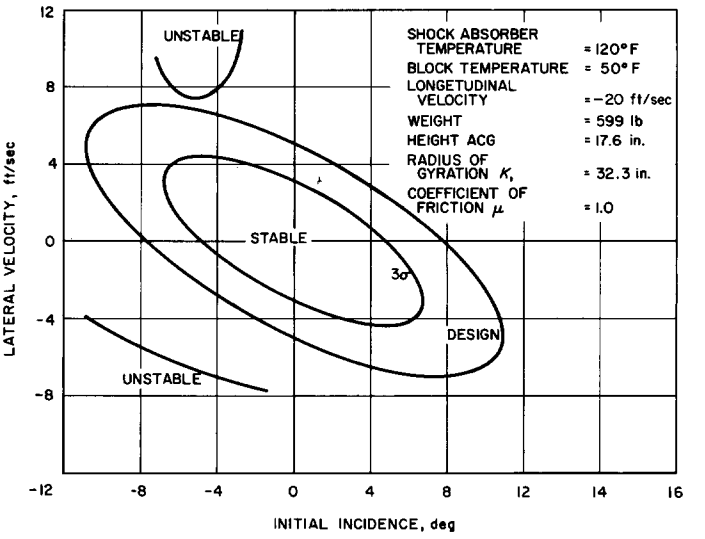

Fig. 23. Stability boundary for A-24 shock absorber on A-21 vehicle

computer program. Table 20 summarizes the drop configurations that have been recommended for the S-15 program. The angles ϕ, γ_β, and γ_v in the table are measured counterclockwise about the lunar vertical passing through the vehicle center of gravity and from a line in the horizontal plane which is the projection of the line of greatest slope of the landing site surface. The angle is measured from the uphill side of the projection.

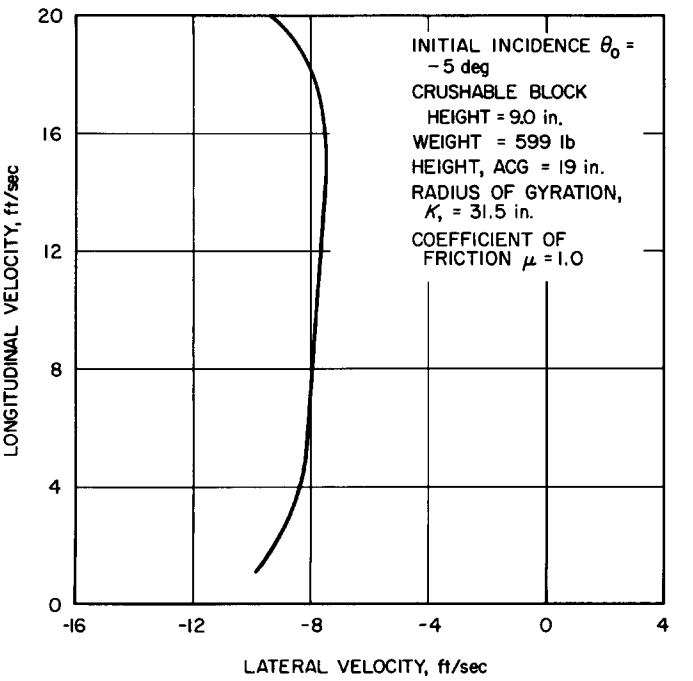

Fig. 24. Stability boundary for all-crushable shock absorber

UNCLASSIFIED CONFIDENTIAL

UNCLASSIFIED

Table 20. Three dimensional touchdown stability

Condition number	Longitudinal velocity X, ft/sec	Lateral velocity V_L, ft/sec	Maximum incidence β, deg	Position of maximum incidence angle γ_B, deg	Position of lateral velocity γ_V, deg	Roll angle ϕ, deg	Site slope, deg	Friction coefficient	Stability[a]
1	20	9	4	120	120	80			U
2	18	9	4	120	120	80			S
3	16	9	4	120	120	80			S
4	12	9	4	120	120	80			S
5	20	9	0	135	135	80			S
6	20	9	4	135	135	80			U
7	20	9	7	135	135	80			S
8	20	7	5	180	180	80			S
9	20	7	5	90	90	80			S
10	20	7	5	45	45	80			S
11	20	7	5	135	135	80			S
12	20	7	5	135	135	0			S
13	20	7	5	135	135	40			S
14	20	9	5	315	135	0			S
15	20	9	5	45	135	0			S
16	20	9	5	225	135	0			U
17	18	9	5	225	135	0			S
18	16	9	5	225	135	0			S
19	20	9	5	225	135	40			S
20	20	9	5	225	135	80	15	0.7	S

[a] U = unstable; S = stable.

With the available touchdown program, a preliminary assessment of the crushable shock absorber concept has been made. Fig. 24 shows a stability boundary for the A-24 vehicle having a shock absorber which deflects under constant crushing force of 6000 lbs. The stability appears to be adequate in relation to specification requirements of a 7-ft/sec lateral velocity capability. With the crushable shock absorber, it is expected that the maximum compression force will not exceed 7000 lb, compared to approximately 9000 lb for the hydraulic shock absorber. These results are sufficiently encouraging to justify a more extensive investigation into the crushable concept. A new IBM program is being written to facilitate this investigation.

Dynamic analyses. The structural response program was used to investigate the elastic response of the T-21 spacecraft on several lunar landings. The entire design ellipse was covered for both single leg uphill and single leg downhill at a longitudinal descent velocity of 15 ft/sec. The three sets of initial lunar landing conditions found to produce the largest elastic responses in the A/SPP compartments A and B, Omniantenna B, solar panel and TV camera No. 3 were selected; by systematic search, three sets of Earth landing conditions, within the constraints of the test setup, were determined which resulted in approximately the same elastic responses as in the three lunar landings, respectively. Table 21, Drop Tests 1, 2, and 3, shows the initial spacecraft velocities and attitudes of the three critical lunar landing conditions and their three corresponding Earth drop conditions. Table 22, Drop Tests 1, 2 and 3, shows the maximum elastic response during the Earth landings found with the help of the structural response program. Table 23, Drop Tests 1, 2, and 3 shows the maximum shock strut loads and body block crushing distance found by the computer solution of the equivalent Earth landings.

Twenty initial lunar landing conditions (Table 24) with the maximum touchdown velocity of 20 ft/sec longitudinal and 4.9 ft/sec lateral were investigated. The landing condition producing the largest elastic responses (Case N of Table 24) was again transformed to an equivalent Earth landing. Table 21 Drop 4, shows this lunar landing and its equivalent Earth drop. The maximum elastic responses found from the structural response

UNCLASSIFIED

Table 21. T-21 Earth drop tests to simulate lunar landing conditions[a]

Drop number	Spacecraft orientation, (single leg in plane of symmetry)	A/SPP position (polar angle), deg	Worst case lunar landing[b]			Equivalent earth drop tests (without horizontal velocity)				
			Touchdown velocities, ft/sec		θ_0,[c]	Slope of surface	Vertical touchdown velocity, ft/sec	θ_0,[c]	Slope of surface	h,[d] ft
			Longitudinal	Lateral						
1	Leg 1 downhill	0	15	0	0	15	13	0	15	2.62
2	Leg 3 uphill	36½	15	−5.5	10.8	15	15.1	10.8	15	3.54
3	Leg 2 downhill	36½	15	−0.3	0.4	15	13.2	0	15	2.70
4	Leg 3 high	36½	20	4.9	−2.7	15	17.5	−16.7	0	4.75

[a] For all conditions the crushable blocks are to impact on a smooth surface; the footpads are to impact a surface of 2 in. wooden blocks.
[b] For lunar landings, lateral velocity is positive in the direction of the single leg.
[c] θ_0 is the initial incidence of spacecraft, positive for single leg above horizontal.
[d] h is the minimum vertical distance between the test article and the surface prior to release.

Table 22. T-21 maximum elastic response during earth drop

Item	Direction of item CG acceleration	Maximum acceleration during drop			
		Drop 1	Drop 2	Drop 3	Drop 4
Compartment A	Out	+2.71	+4.22	+3.90	+7.36
	Tangent	+2.87	−3.79	−3.76	+8.00
	Up	+8.80	+13.9	+10.9	+18.1
Compartment B	Out	+3.88	+8.70	+5.45	+13.9
	Tangent	+2.13	−3.72	−3.31	−11.4
	Up	+9.89	+9.05	+9.79	+8.74
Omnidirectional antenna A	Up	+16.8	+9.26	−9.27	+21.8
Omnidirectional antenna B	Up	+30.8	+25.7	+31.4	−60.3
TV camera 3	Out	+7.80	−12.7	−7.27	+18.0
	Tangent	−2.56	−5.75	−4.92	+13.6
	Up	+8.12	+13.1	+13.6	+19.7
Solar[a] panel	Corner 1 out from panel plane	−22.0	+9.21	+9.33	+14.1
	Corner 2 out from panel plane	+6.57	+20.4	+19.3	+25.6
	Corner 3 out from panel plane	−46.1	−67.6	−73.1	−76.9
	Corner 4 out from panel plane	+52.1	+52.4	−67.6	+73.1

[a] 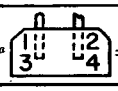 = Solar panel corners.

Table 23. T-21 drop tests maximum shock strut load and body block crushing distance (predicted)

Drop number	Maximum shock strut load, lb			Body block crushing distance, in.		
	Leg 1	Leg 2	Leg 3	Block 1	Block 2	Block 3
1	3810	2180	2180	2.32	1.92	1.92
2	3410	3410	2260	3.45	3.45	2.55
3	3210	3890	2210	1.96	2.31	1.96
4	4100	4100	2720	3.18	3.18	2.35

during this Earth landing are shown in Table 22, Drop 4. Table 23, Drop 4, shows the maximum shock strut loads and body block crushing distances found for this equivalent Earth landing.

Data from an S-2A drop test have been reduced to determine the energy absorbed by the landing system of the vehicle. This is the energy dissipated by the crushable material and the shock struts and the strain energy stored in the compressed shock struts in the final quiescent state after drop. The drop test condition (Fig. 25) shows that the change in potential energy resulting from the drop was 4560 ft-lb and this is the total energy absorbed by the vehicle. Fig. 26 shows calculations for the energy absorbed by the shock struts, including energy dissipated and strain energy stored in the compression struts. Table 25 shows calculations for energy dissipated by the crushable footpads and crushable blocks. Table 26 summarizes the total energy absorbed by the landing system to show

UNCLASSIFIED

CONFIDENTIAL
UNCLASSIFIED

Table 24. T-21 lunar landing conditions investigated for elastic response (predicted)

Lunar landing case	Longitudinal velocity, ft/sec	Lateral velocity, ft/sec	Initial incidence (θ_0), deg	Surface slope (θ_s), deg
A	20	−4.9	10.8	−15
B	20	−4.9	8.1	−15
C	20	−4.9	5.4	−15
D	20	−4.9	2.7	−15
E	20	−4.9	0	−15
F	20	+4.9	0	−15
G	20	+4.9	−2.7	−15
H	20	+4.9	−5.4	−15
I	20	+4.9	−8.1	−15
J	20	+4.9	−10.8	−15
K	20	+4.9	−10.8	+15
L	20	+4.9	−8.1	+15
M	20	+4.9	−5.4	+15
N	20	+4.9	−2.7	+15
O	20	+4.9	0	+15
P	20	−4.9	0	+15
Q	20	−4.9	2.7	+15
R	20	−4.9	5.4	+15
S	20	−4.9	8.1	+15
T	20	−4.9	10.8	+15

Notes:

(1) Lateral velocity is positive in the direction of the single leg

(2) Initial incidence is positive for single leg above the horizontal

(3) Surface slope is positive for single leg uphill and negative for single leg downhill

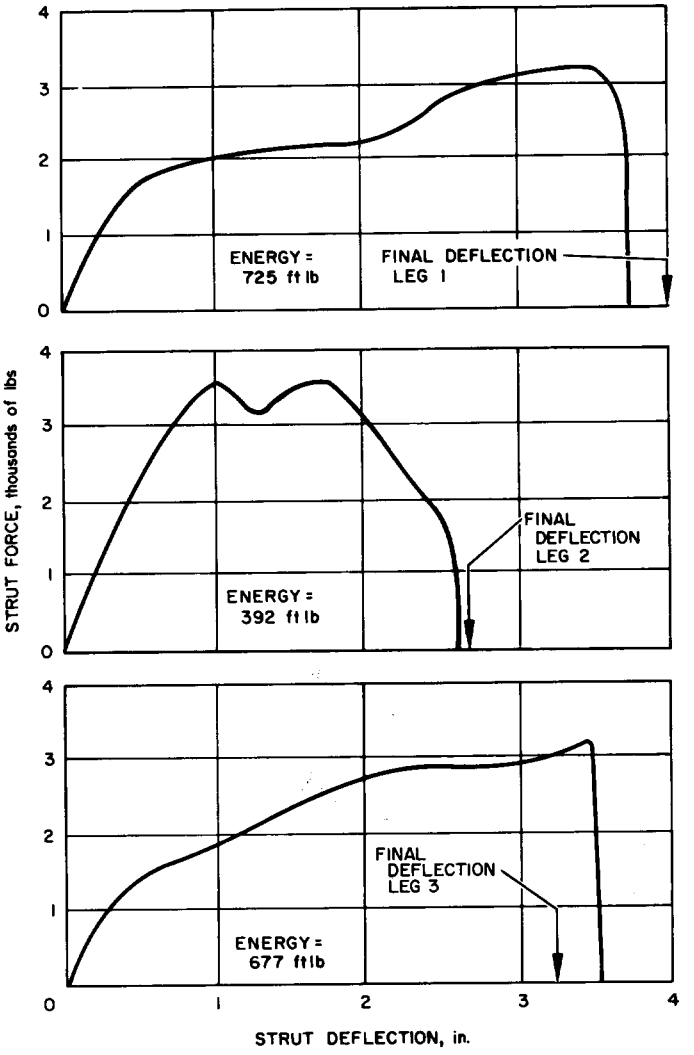
ENERGY = 725 ft lb
FINAL DEFLECTION LEG 1
ENERGY = 392 ft lb
FINAL DEFLECTION LEG 2
ENERGY = 677 ft lb
FINAL DEFLECTION LEG 3
STRUT FORCE, thousands of lbs
STRUT DEFLECTION, in.

Fig. 26. S-2A energy absorption shock absorber force vs deflection (test 2)

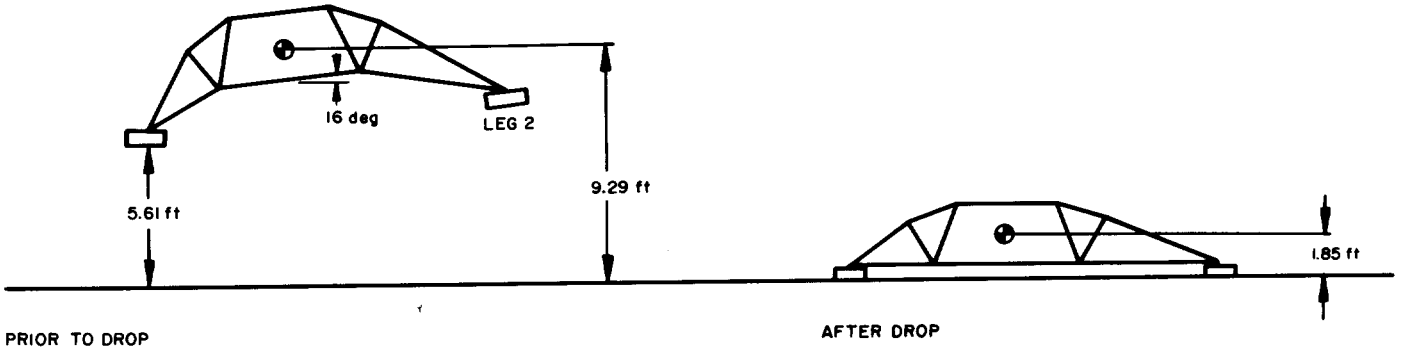

CHANGE IN VEHICLE HEIGHT DURING DROP = 7.44 ft
VEHICLE WEIGHT = 614 lb

Fig. 25. Vehicle potential energy change

CONFIDENTIAL
UNCLASSIFIED

UNCLASSIFIED
CONFIDENTIAL

Table 25. Crushable footpads and crushable blocks energy absorption

Item	Leg	Average crushing force, lb	Deflection, ft	Energy absorption, ft-lb
Crushable Footpads	1	785	0.1875	147
	2	785	0.0934	73
	3	785	0.1667	131
Crushable Blocks	1	1450	0.256	371
	2	1450	0.1282	186
	3	1450	0.237	344
Total energy absorption				1252

Table 26. Total measured energy absorption

Item	Leg	Energy, ft-lb
Shock absorber	Leg 1	725
	Leg 2	392
	Leg 3	677
Crushable blocks and footpads	All legs	1252
Total energy absorption		3046

Note:
The energy unaccounted for is the difference between the change in the vehicle potential energy during the drop and the total measured energy absorption $-4560 - 3046 = 1514$ ft-lb

the total of 3046 ft-lb. The discrepancy of 4560-3046 = 1514 ft-lb is the energy absorbed by the vehicle but not accounted for by the landing system.

It is believed that a significant amount of energy is absorbed by the dynamic structural elastic response of the vehicle. Additional evidence for this belief is obtained by comparison of the results from the rigid body landing program with the experimental results of drop tests. The rigid body landing program traditionally predicts a larger energy dissipation in the crushable material and the shock struts than is actually measured in the drop tests. This discrepancy can be explained by the omission of elastic effects in the rigid body landing program. Studies have begun to include the elastic effects that occur in landing. These effects will introduce a new energy dissipator in the system (structural damping) and should reduce the requirements of the landing system.

Dynamic tests. Preliminary work has been completed on the S-9 test vehicle in preparation for the static load test. Pretest tasks completed include the location of 28 major component centers of gravity, the design fabrication of component loading fixtures, the installation of 36 strain gage bridges on thermal compartment supports, and the attachment of 91 dial gage blocks to the vehicle structure and components. The test vehicle is mounted on test supports and instrumentation is continuing with the installation of the 91 dial gages and 30 deflection beams. Static test loads simulating retro-vernier thrust loading were applied to the vehicle January 28. Static weights will be applied at the 28 load points in increments of 1, 3, 6, 9, and 12 g.

It was concluded that the Compartment B support bracket failure that occurred during the torsion test was a high stress failure. This conclusion was based on the concurring results of: (1) a metallurgical analysis of the failed part, (2) a comparison of type approval test and torsion test acceleration values at the compartment center of gravity, and, (3) a stress analysis which superimposed probable bending and axial stress experienced by the support prior to failure.

Final assembly and adjustment of the mass properties of the S-15 test vehicle have been accomplished, and drop testing for the A-21 touchdown stability study is under way. The ballast for this full-scale drop test vehicle has been located so as to dynamically simulate a flight spacecraft at the minimum landed weight condition. Analytical studies indicate that this minimum weight condition is the most critical from the standpoint of vehicle landing stability.

Calibration of the load-measuring body block support structures has been completed, and the calibration data verify the ability of the structures to measure the crushable block forces and to separate these forces into orthogonal components for comparison with analytical studies. However, minor problems in either the wiring of the strain gages or recording of the bridge output on two of the structures caused erratic calibration curves during several load applications. Work is in progress to correct these discrepancies. It is expected that the measurements made by these support structures will provide useful information about the dynamic crushing properties of the aluminum honeycomb material and also about the friction coefficients in effect during an actual landing.

Modifications and upgrading of the drop test facility at Building 309 have been completed, and the facility will undergo functional checks and calibrations prior to delivery of the vehicle to the test site (Fig. 27). Drag tests

UNCLASSIFIED
CONFIDENTIAL

UNCLASSIFIED

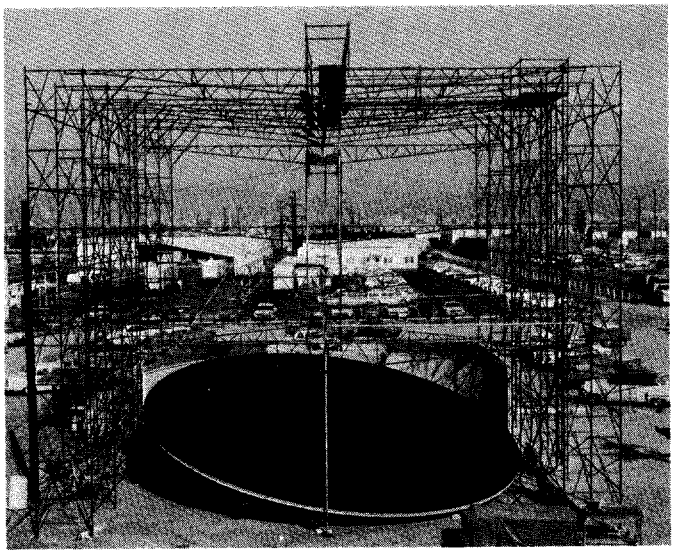

Fig. 27. Modified surveyor drop test facility

conducted on the rubber mat surface covering the landing platform indicate that static and dynamic friction coefficients of up to 0.65 and 0.55, respectively, are attainable.

Flight instrumentation. All accelerometer systems were recieved from Endevco, and the subcontract is now complete. Assemblies for SC-1 through SC-4 and SP-1 are ready for installation. ECA 112130 deleted the accelerometer amplifiers from SC-5 and up, on the basis that the same engineering information will be obtained from SC-1 through SC-4.

Assemblies have been completed for SC-1 through SC-3; units for SC-4 are due February 10. Strain gages have been installed on shock absorbers for SC-1 and SC-2, and on vernier engine brackets on SC-1 through SC-3. Primary calibration of gages on vernier engine for SC-3 will be accomplished next.

Additional testing of the leg position potentiometers is being considered because of recent failures on other potentiometers on *Surveyor* in hard vacuum environments. The leg pots were qualified at 1×10^{-8} mm of Hg but the problem has been found below 1×10^{-9} mm of Hg. Considering that the service life of the potentiometers under hard vacuum is one cycle (at touchdown), 100 cycles after 100 hr exposure to 1×10^{-9} or below could be considered a satisfactory test.

Structures test. The A/SPP mast is supported on the spaceframe by means of two sets of tripods (upper and lower) and a torque-collar (Fig. 28). The upper tripod reacts all of the vertical loads and a portion of the shear and torsional load. Lateral shear loads acting at the center of gravity of the A/SPP are reacted primarily by a couple developed between the upper and lower tripod collars. The purpose of the torque collar at the bottom of the mast is to react part of the torsional load in the mast and render torsional stiffness to the system.

A torsion test was conducted to determine the distribution of torque to the upper tripod collar and the lower torque collar. A secondary objective of the test was to evaluate the stiffness of the mast support structure under maximum landing loads with respect to A/SPP functional requirements. The test was set up to apply a pure torsional couple to the mast and upper collar (Fig. 28). Torsional strain gage bridge 185 was cemented to the mast above the torque collar and calibrated for a pure torque applied to the mast and reacted by the torque collar only. Bending bridges 108, 120, 147, and 148 were used on both ends of upper support Tubes 1 and 2 to measure fixed-end moments. Dial Gages A and B were used to read off rotational and lateral deflections of the mast caused by the applied torque. Dial C was used to record any extraneous lateral deflection normal to the direction of applied loads.

The result of the torque input (in.-lb), to strain gage (185) output, is presented in Fig. 29. The dotted line in Fig. 29 shows output of bridge 185 when 100% of the applied torque is reacted by the torque collar. The solid line indicates the output of bridge 185 when the upper collar is attached to the mast. The ratio of any two values gives the percentage of applied torque reacted by the torque collar. For example:

For P_e = 14,000 in-lb
Strain (calibration) = 9,750 μin.
Strain (lower collar) = 4,550 μin.
Percent P_e reacted by torque collar = $\frac{4550}{9750} \times 100 = 46.7\%$

A permanent set of 31.1-min rotation, 0.0005-in. translation, and 0.0021-in. lateral deflection (direction normal to applied load) resulted after application of 21,000 in.-lb of torque. Fig. 29 indicates that stresses were within the elastic limit and permanent set could be from rivet joint slippage. A final evaluation of test results will be forthcoming subsequent to a detailed inspection of all bolt holes and bearing areas.

UNCLASSIFIED

UNCLASSIFIED

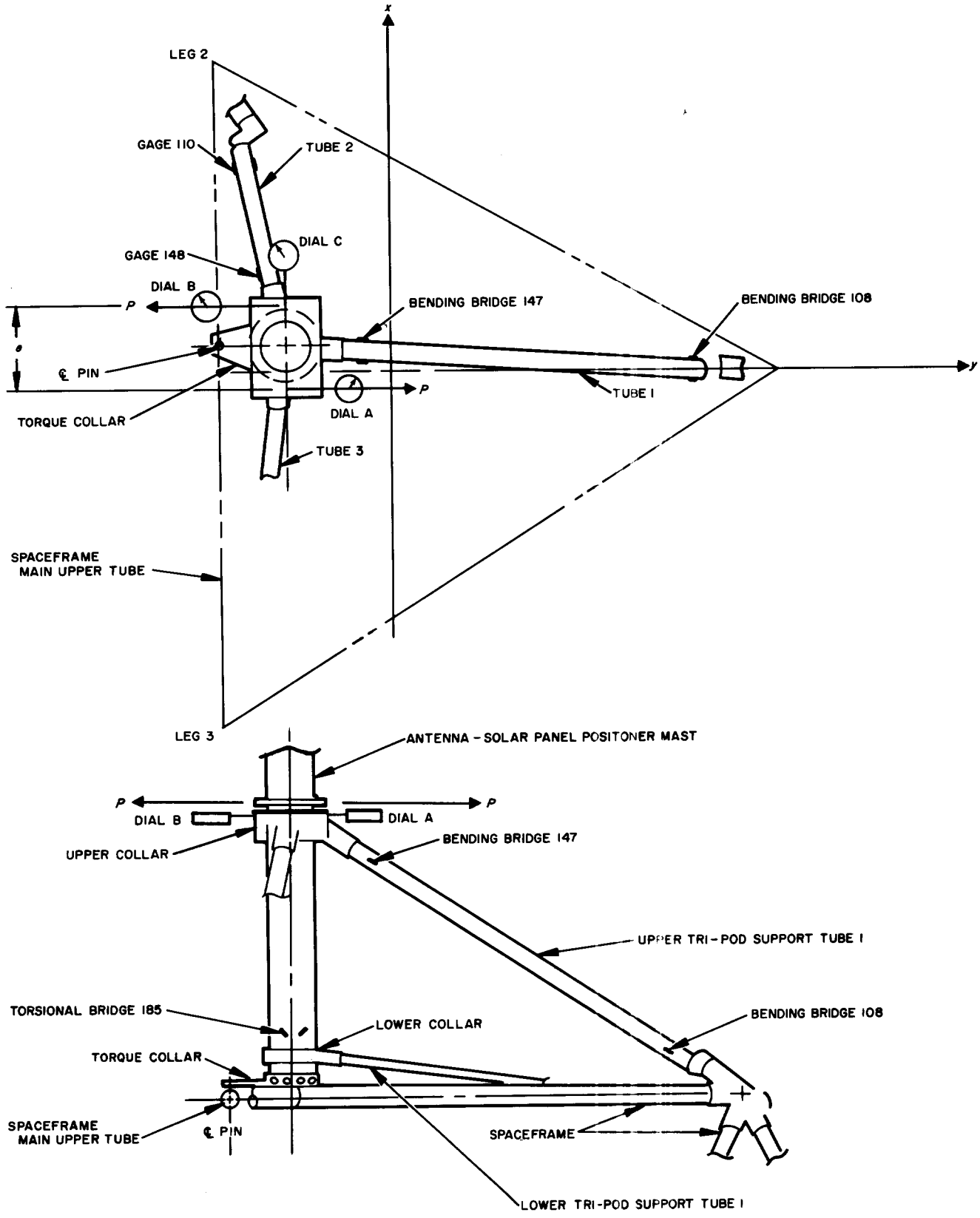

Fig. 28. Test arrangement

UNCLASSIFIED

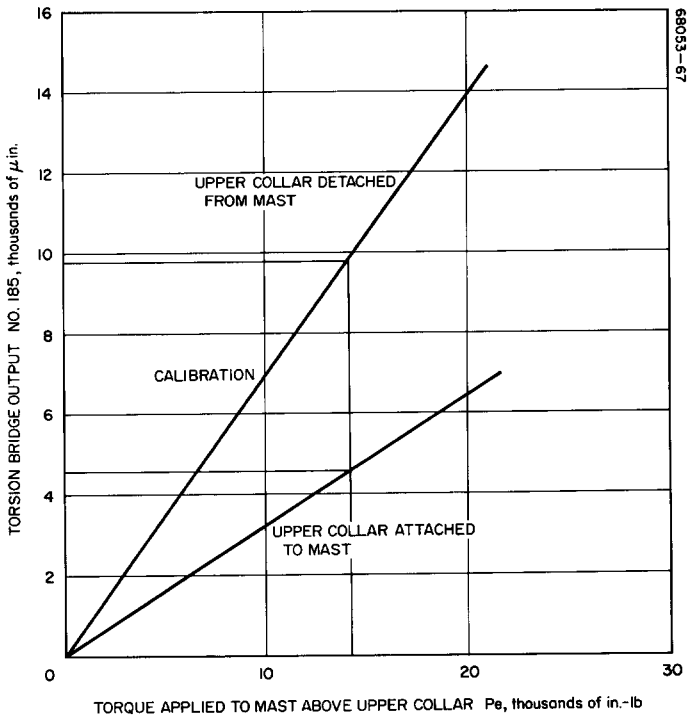

Fig. 29. Torsion bridge 185 output vs torque applied to mast

K. Propulsion

1. Introduction

Propulsion for both *Surveyor* Models A-21 and A-24 spacecraft is provided by a liquid propellant vernier system and a solid propellant retrorocket engine. The retrorocket engine provides primary deceleration during descent to the Moon. The vernier system is used for midcourse maneuver, attitude control during retrorocket firing, and in terminal descent. The feed system portion of the vernier propulsion system was developed by HAC and the thrust chamber assemblies are provided by JPL from Reaction Motors Division (RMD) of Thiokol Chemical Corporation. The Elkton Division of Thiokol developed and provides the retrorocket engine under subcontract to HAC. Due mainly to differing total impulse requirements, there are certain differences in design between the A-21 and A-24 propulsion systems.

2. Progress Summary

a. Main retrorocket engine—A-21. The flight engine for the SC-1 spacecraft is in storage at AFETR, together with an inert engine which was supplied to facilitate spacecraft and equipment checkout. The SC-1 spacecraft spare engine is in storage at Thiokol/Elkton. Extension of the A-21 program to include all of the first seven spacecraft has required a hardware inventory and a cost proposal from Thiokol/Elkton.

b. Main retrorocket engine—A-24. A preliminary design review covering the A-24 nozzle design was held at Thiokol December 16, 1965. A formal design review covering the A-24 retrorocket engine assembly design was held at HAC January 5, 1966.

c. Vernier propulsion system—A-21. Helium tank type approval testing (TAT) was successfully completed, and the type approval test review committee (TATRC) granted acceptance of the helium tank and valve assemblies. With the completion of propellant tank TAT, all system and control item TAT will have been successfully completed. Only two A-21 components, the charging valve and relief valve, remain to be qualified. Tests are under way on these and should be completed by the end of the current reporting period. For the three other A-21 spacecraft added to the contract by Mod 56, it is proposed to incorporate the split helium tank and valve assemblies designed for A-24 as a type of product improvement to decrease assembly difficulties.

d. Vernier propulsion system—A-24. Because of the program redirection stemming from Mod 56 to the contract, effort on A-24 is now scheduled only through completion of control item TAT. Component level TAT is well under way and is complete on several items. Propellant tank shell TAT have proved that the ellipsoidal ends are not susceptible to buckling under design loads.

e. Test vehicle—T-2. An old problem recurred during the first T-2N-2 tether test during this report period: uncontrolled thrust caused by gas in the propellant system passing through the throttle valve. Proven preventative measures were taken, and, on the second tether test, the system performed normally.

3. Main Retrorocket Engine

a. A-21 spacecraft. Flight and flight-spare safe-arm assemblies are presently being processed through the HAC thermal control application procedures. These operations, together with the required flight acceptance vibration testing, will be completed by March 1, 1966.

Current planning is to continue with the processing of the SC-1 spare retrorocket engine, and ship it to the AFETR in time to complete the retroengine checkout and thermal wrapping on a schedule compatible with

UNCLASSIFIED
CONFIDENTIAL

retroengine spacecraft mating operations. If not required to support SC-1, the spare engine will be the first choice for SC-2.

A hardware inventory conducted relative to the use of A-21 retrorocket engines for SC-5, -6, and -7 spacecraft has indicated that sufficient flight cases and safe-arm assemblies are available to cover the A-21 program extension. However, it will be necessary to procure flight nozzles, case insulation, struts, and collars. Peripheral equipment, including a diffuser for the Thiokol altitude facility, safe-arm shipping containers, and shock recorders will also be required in order to replace those items which have been damaged in the course of A-21 development and qualification programs.

The launch schedule for the extended A-21 program may require the use of retrorocket engines that are over 12-mo old. Although the 12-mo storage life is specified as a minimum requirement, confirmation of extended storage-life capability will be obtained. This qualification of storage-life extension shall be accomplished by test-firing one or more of the four unused A-21 qualification engines in the Thiokol altitude facility. Since all of these engines were cast in May to June of 1964, an 18-mo storage-life confirmation is presently available. A further extension of capability to 40 mo is also being considered. This could be accomplished by testing one of the unused A-21 qualification engines.

Further evaluation of the main retrorocket solar thermal vacuum post-transit propellant temperature gradient data accumulated during the SC-1 spacecraft series has resulted in a modification to condition the retrorocket engine and spacecraft to 70 ± 5°F and then raise the conditioning temperature to 85 ± 5°F for a 2-hr period just preceding launch, in order to lower the posttransit bulk mean retropropellant temperature by 15°F. It is planned to verify this conditioning sequence in the thermal control model solar thermal vacuum test series. Consideration of the tolerances involved, however, indicates that the modification may not be sufficient to lower the retropropellant temperature to the predicted level, applied in the A-21 development and qualification programs. The possibility of combining a high-temperature gradient with the 18-mo storage life confirmation firing discussed above is, therefore, being considered.

b. A-24 spacecraft. A preliminary nozzle design review was conducted at Thiokol December 16, 1965. During this review, the Elkton and Wasatch Divisions of Thiokol presented the results of their nozzle thermal and stress analyses, and the planned fabrication sequence was presented. As a result of the information presented, Thiokol was authorized to proceed with the fabrication of two overtest truncated nozzles (25:1 expansion ratio) and components for three others.

A formal design review covering the A-24 assembly design was held at HAC January 5, 1966. A full presentation of the ballistic, thermal, and stress analyses was made. As a result of the meeting, Thiokol was authorized to proceed with the case-forging operation. Final fabrication of the cases will be authorized after a review of additional information requested during the meeting.

4. Vernier Propulsion System

a. System dynamic performance data. Surveyor vernier propulsion dynamic performance data were acquired during the vernier propulsion feed system TAT conducted on the S-6 and S-7 vehicles. A report summarizing these data and resulting conclusions was issued this report period. A short summary of the findings follows.

The vernier propulsion systems (VPS) tested were representative of the *Surveyor* A-21 configuration. The S-6 system was operated through two real-time simulated mission profiles at extremes of thermal environment (0° and 100°F). The S-7 system was operated through one real-time simulated mission (including a second midcourse firing) while subjected to TAT level vibrational environment. Both systems were commanded to the same midcourse and lunar descent firing profiles, except that the S-6 program did not include the second midcourse firing. Both systems performed extremely well, indicating that the VPS is well qualified to perform its intended mission.

The frequency response of both systems at high thrust levels was generally the same on either saturated or unsaturated propellants. At low thrust levels, the frequency response on unsaturated propellants was generally the same as at high thrust, but decreased somewhat with saturated propellants. The step response of the systems was slightly slower with saturated propellants than with unsaturated propellants, especially the response to step decreases in thrust.

Computer studies and closed-loop testing of a VPS combined with a simulated flight control system demonstrated that the dynamic performance of the S-6 and S-7 vehicles is more than adequate for vehicle stability, even at low thrust levels on saturated propellants. A similarly performing VPS in a flight spacecraft could successfully complete any planned *Surveyor* A-21 mission.

UNCLASSIFIED
CONFIDENTIAL

UNCLASSIFIED
CONFIDENTIAL

Table 27. Propellant tank test data

Test No.	Type of test	Requirements	Remarks
1.	Vibration	Variable-frequency sine wave (with tank response limited to 12 g) from 10 to 1500 cps (1) octave per min and superimposed random 6.75 g from 100 to 1500 cps along three axes, one sweep up and one down. Tanks filled with Freon and pressurized to 300 psig.	Slight loosening of bolts on thermal standoff and chipping of plastic insulator noticed after last axis of shake. The problem was attributed to improperly torqued bolt on assembly. This problem had no effect on test results and had no effect on flight type tanks.
2.	Thermal vacuum	Vacuum of 10^{-6} mm Hg for 66 hr at 100°F and at 66 hr at 0°F tank filled with Freon and pressurized to 800 psig.	Performed well.
3.	Acceleration	Constant acceleration of 10 g for 4 min and 5 g for 8 min. Tanks filled with Freon and pressurized to 300 psig.	Performed twice due to 200 psi loss on first test (facility problem). Second test was successful.
4.	Expulsion	11 expulsion cycles; 10 cycles at 90 to 95% expelled, 1 cycle at 100%. Eight cycles at ambient temperature, two cycles at 100°F and one at 0°F (100% expulsion cycle), one tank filled with MMH fuel and other with MON-10 oxidizer, and both pressurized to 730 psig. Average rate of expulsion 250 $in.^3$ per min.	(These tests were in progress on one tank at close of report period. Results of expulsion tests on both tanks will be fully reported in next issue.)

b. Propellent tank assembly TAT (Table 27). An oxidizer tank assembly (PN 287004-3, SN 2) and a fuel tank assembly [PN 287001-3, serial number (SN) 2] were subjected to four major environments for the type approval program. Leak tests for both gas and liquid in the tanks were made during and after each major test.

c. Helium tank and valve assemblies TAT. Type approval tests were successfully completed last report period. Subsequently, on December 21, 1965, the assembly was exposed to 100 functional cycles as an endurance test. After this test series, the assembly was torn down and inspected. (Fig. 30). Examination of sealing surfaces, K-seals, O-rings, and all components indicated no visible signs of excessive wear or obvious weakness (Figs. 31 through 35). The relief and charging valves from the assembly were then assigned to component level TAT. When these are tested (near the end of the current reporting period), all levels of the A-21 propulsion system (component, control item, and system) will have completed TAT.

In a meeting on January 13, 1966, the TATRC granted acceptance of the helium tank and valve assemblies test results.

d. A-21 vehicles (SC-5 through -7). Mod 56 to the contract requires delivery of three additional A-21 vehicles (SC-5 through -7). The vehicles will be substantially similar to SC-1 through -4 spacecraft, except that they may incorporate a mechanism to vent residual propellants after lunar landing, and the split helium tank and valve assemblies developed for A-24 may be adopted. The latter consists of relocation of the relief and check valves (with housings) as two separate assemblies.

A system for venting the propellant after lunar landing is being developed. Two alternate approaches are being considered. One incorporates the squib valve planned for use on the A-24 lunar dump system, operated by an Earth signal. The other is a Woods metal disc contemplated for inclusion in each propellant tank standpipe port that would melt, either due to solar heating or remote controlled applied heat. A decision on which heat source will be used is pending.

e. A-24 spacecraft. Contract Mod 56 deleted, for the time being, a requirement for A-24 spacecraft. However, development of components and control items for the propulsion system is to continue through control item TAT. Also, all specification effort needed to complete the program, as originally planned, will continue.

The redesigned helium regulator, with its ports relocated to facilitate the isolation of the helium tank and valve assemblies from the check and relief valve package, has successfully completed TAT. Hardware deliveries are nearly complete.

The lunar dump components are in process of TAT at the vendor, and engineering models of both the check valve and dump squib valve have been delivered. Complete evaluation will not be concluded until S-6A/S-11 testing begins. However, preliminary functional checkout as a mockup system is contemplated in the next report period.

Both propellant tank and helium tank shell TAT are nearing completion. Propellant tank shell buckling, which was of concern with the elliptical-end design, has been evaluated by analysis and test, and the design proved satisfactory.

CONFIDENTIAL
UNCLASSIFIED

UNCLASSIFIED
CONFIDENTIAL

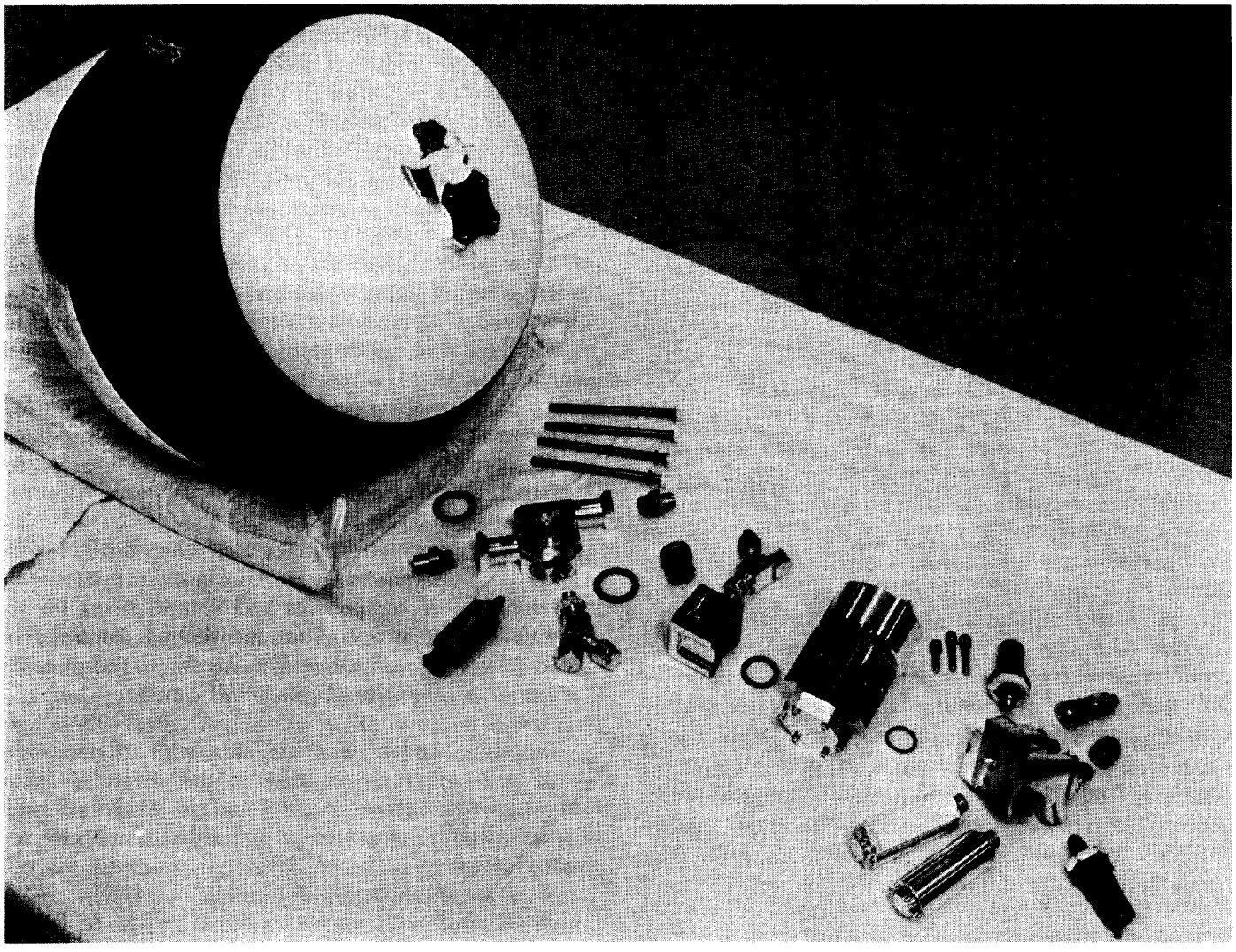

Fig. 30. Helium tank and valve assembly 262789-1 SN 2 disassembled

UNCLASSIFIED
CONFIDENTIAL

UNCLASSIFIED
CONFIDENTIAL

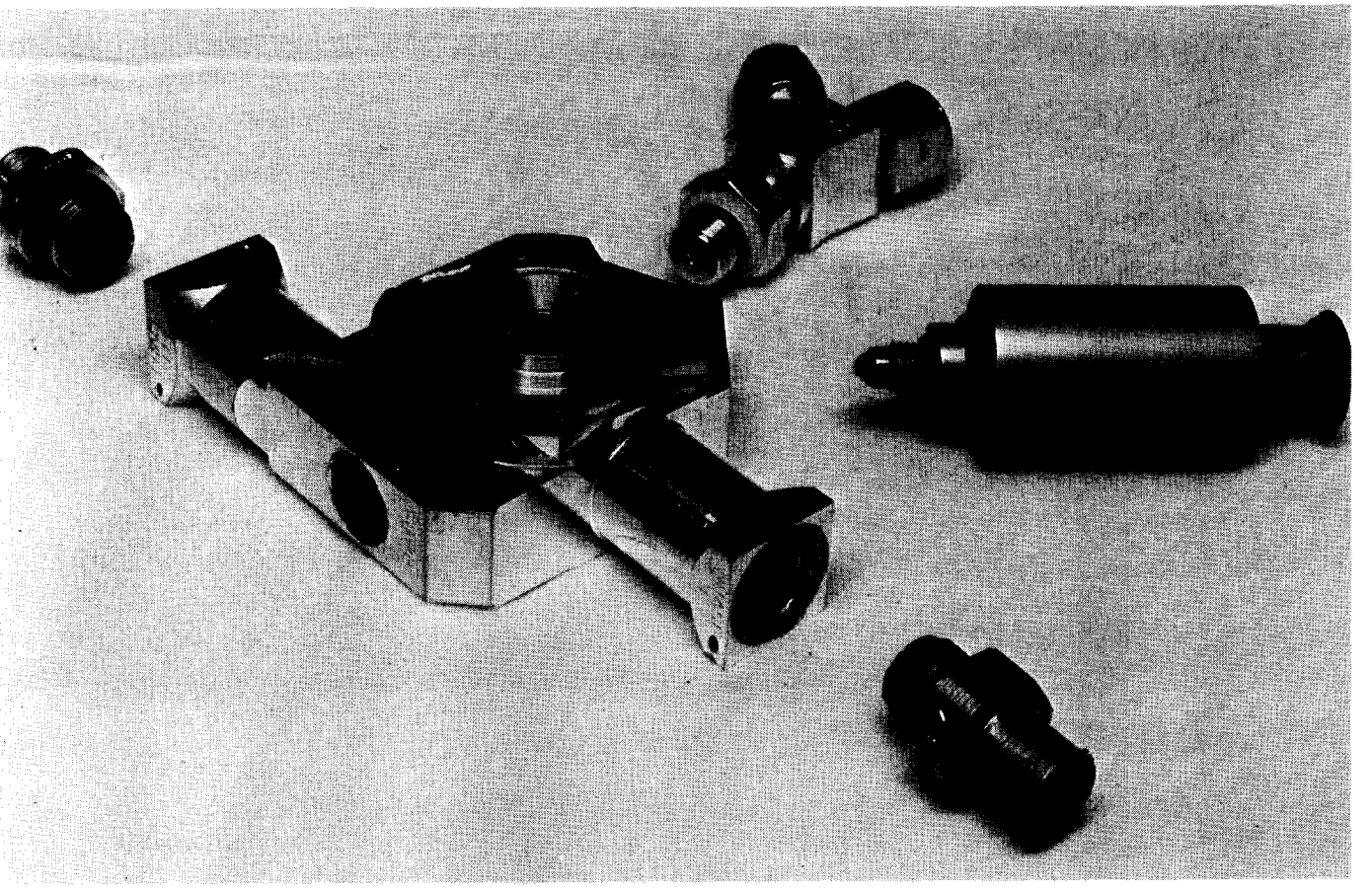

Fig. 31. Squib valve assembly showing fired squibs, charging valve, and transducer

UNCLASSIFIED
CONFIDENTIAL

UNCLASSIFIED
CONFIDENTIAL

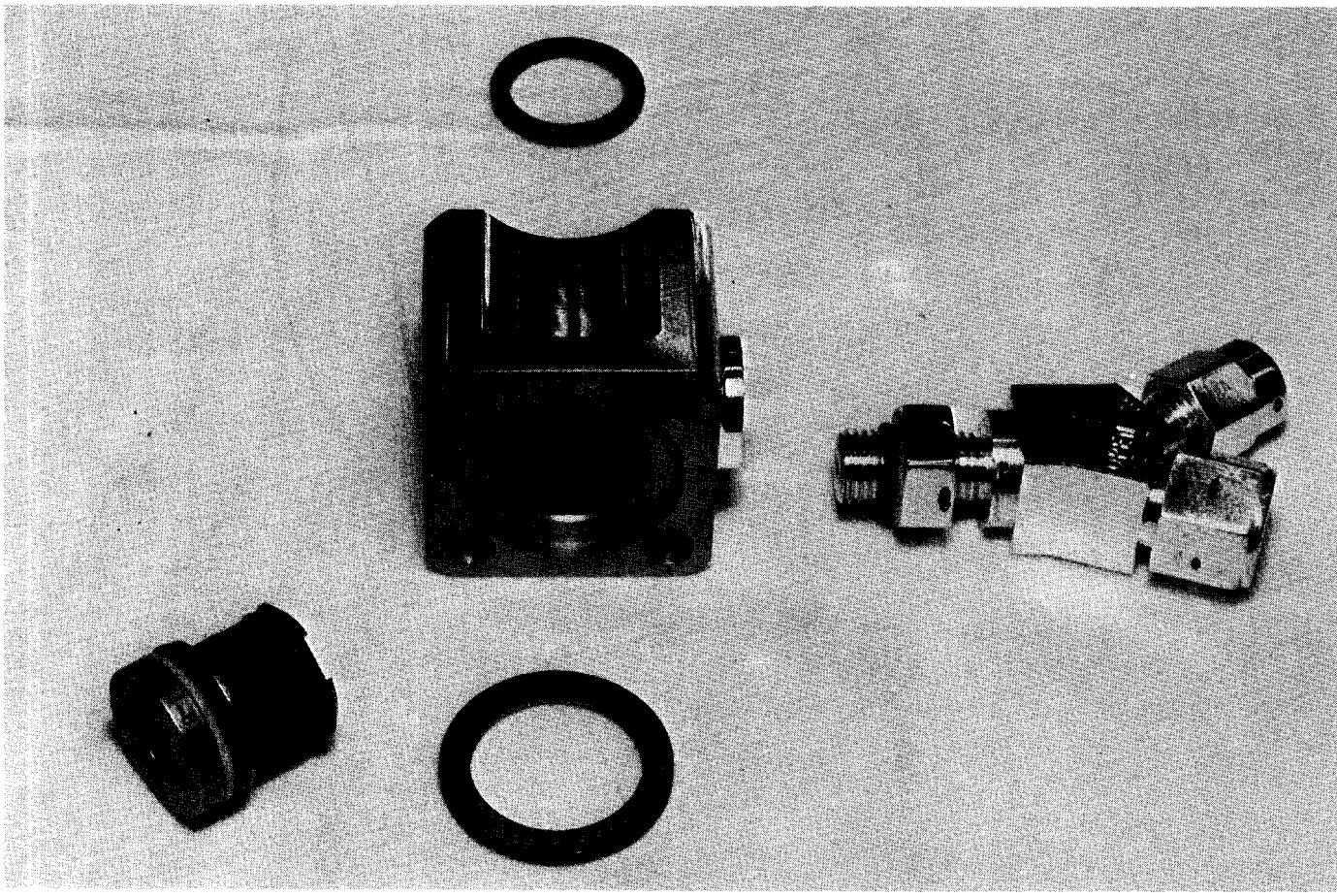

Fig. 32. Filter housing, K-seals, charging valve, and filter element

CONFIDENTIAL
UNCLASSIFIED

UNCLASSIFIED

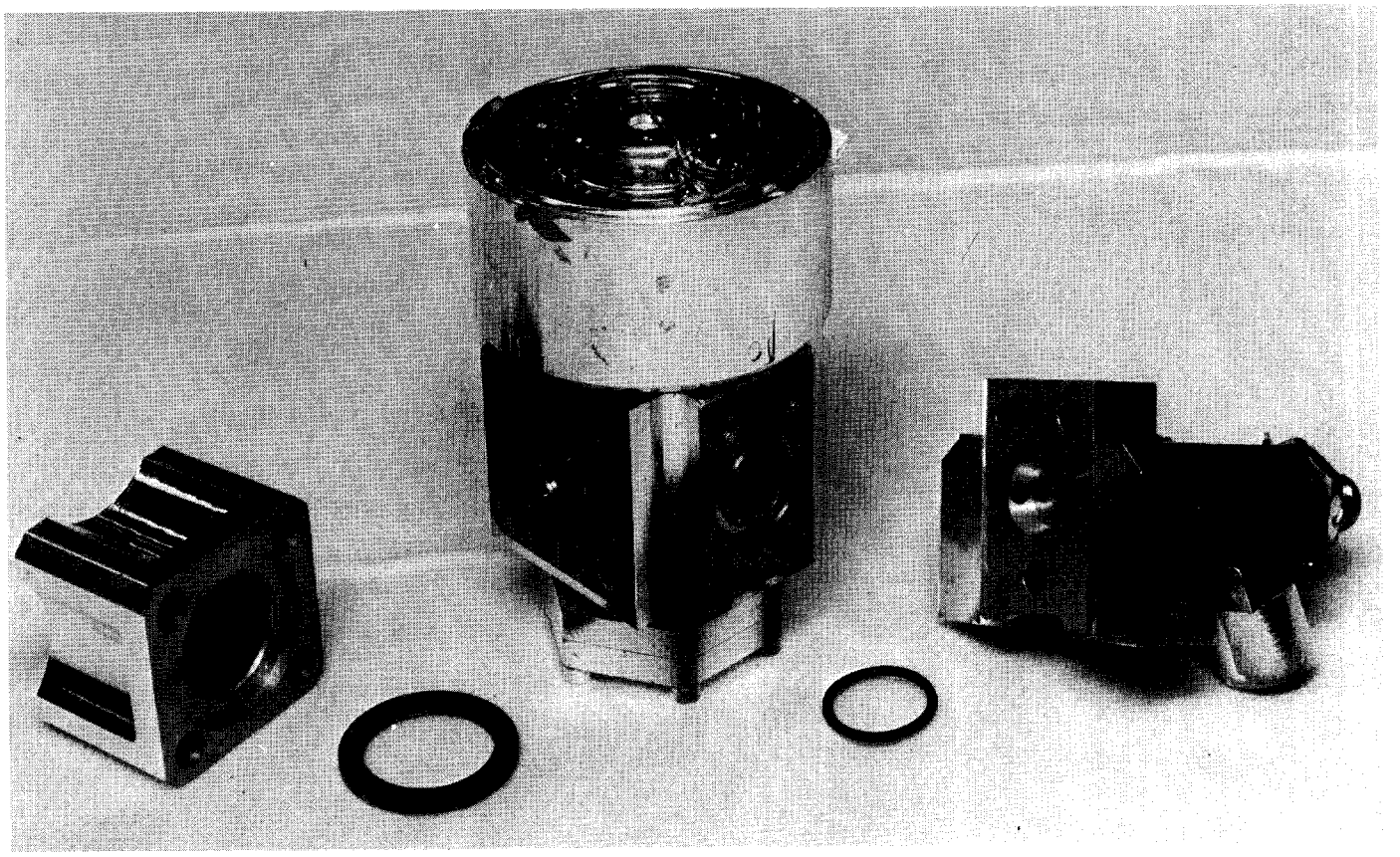

Fig. 33. Filter housing, regulator, check valve housing, and seals

UNCLASSIFIED

UNCLASSIFIED
CONFIDENTIAL

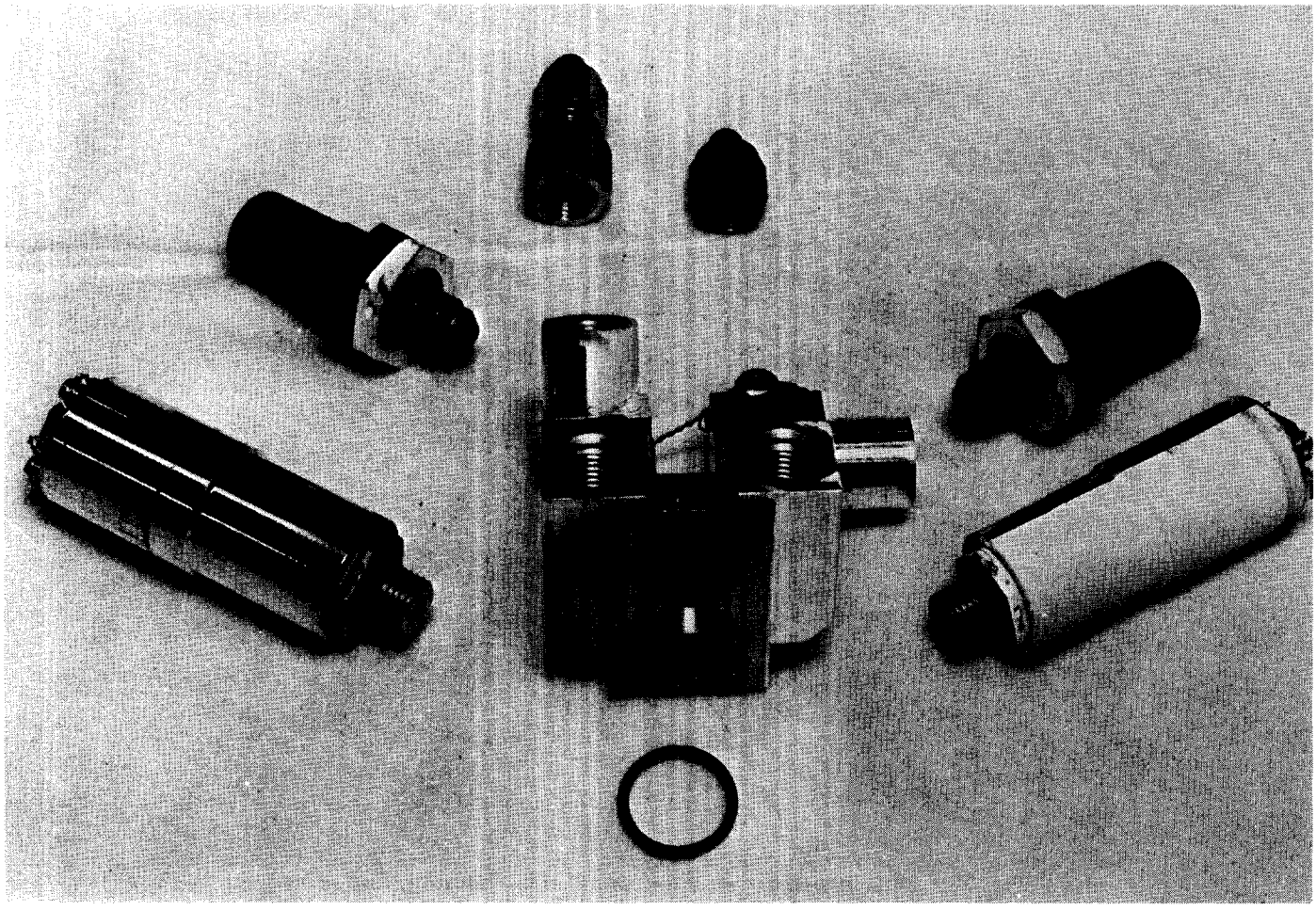

Fig. 34. Check valve housing with relief valves, quick disconnects, and test connections

UNCLASSIFIED
CONFIDENTIAL

CONFIDENTIAL
UNCLASSIFIED

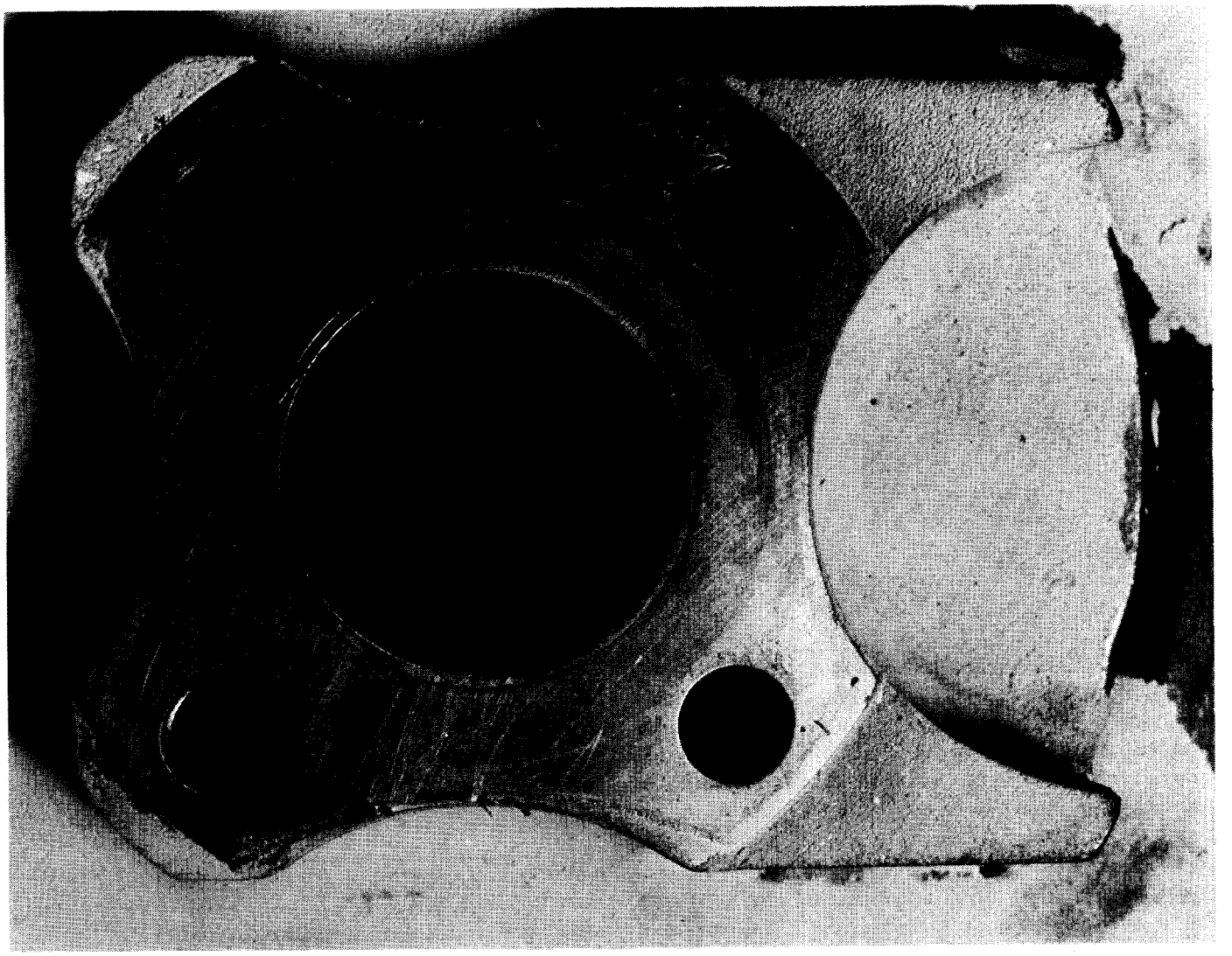

Fig. 35. Closeup view of helium tank mating flange

CONFIDENTIAL
UNCLASSIFIED

UNCLASSIFIED
CONFIDENTIAL

S-6A and S-11 testing is not contemplated until 1967, if go-ahead is given. However, test procedures and test specifications will be completed by mid-1966.

f. T-2N descent test vehicle. The first tether test on T-2N-2 was performed, but was only partially successful due to uncommanded thrust excursions caused by gas bubbles in the propellant system. Post tether engine flow test indicated oxidizer clogging. This is not related to the uncommanded thrust excursions but appears to be caused by reaction of oxidizer remaining in the injector after a test with moisture to form nitric acid, which in turn forms nickel salts by corrosion of the injector manifold. Prior to the next tether test, continuous injector vacuum purging pretest was instituted (to preclude acid and salt formation). The system was also checked before test to make sure all gas had been bled from the propellant system. The propulsion system performed satisfactorily on the second T-2N-2 tether test.

g. Thrust chamber assemblies. The design of the propellant valves in the Reaction Motors Division of Thiokol (RMD) thrust chamber assembly does not provide a completely leak-tight seal. There will be a minute trace of oxidizer leakage at all times when the system is loaded with propellants and pressurized. This miniscule amount, when combined with available moisture from the air, forms a solution of nitric acid. The action of this acid on the nickel injector forms salts, and these, when in sufficient quantities, tend to clog the injector holes.

JPL supplies these thrust chambers and is conducting tests on the thrust chamber assemblies to evaluate the magnitude of injector clogging to be expected on flight spacecraft during holds at the AFETR. Should it be determined necessary, JPL has considered providing a desiccant-filled blowout cover for the thrust chamber assemblies.

As a parallel effort, HAC is conducting tests to determine the relation between humidity levels and corrosion of nickel when exposed to the vapors of *Surveyor* oxidizer (MON-10). Preliminary results indicate that relative humidity must be below approximately 10% to avoid corrosion deposits. Humidity levels in the shroud enclosing the spacecraft at the AFETR are maintained at 45 ±5%. The tests being conducted by JPL on thrust chamber assemblies are intended to determine if salts form under conditions simulating those to which the thrust chambers will be exposed during usage on spacecraft. Results of these tests will indicate if special precautions have to be taken to avoid corrosion deposits.

5. New Technology

A majority of spacecraft propellant positive expulsion systems in use in the United States use a Teflon bladder collapsed by pressurized gas. This works well enough in most applications; however, Teflon is permeable to gases. Thus, under storage conditions, enough gas permeates the bladder to soon saturate the propellant. These saturated propellants cause sluggish response to throttling. Also, subsequent temperature changes can cause gas to come out of solution and form gas pockets or bubbles that, if entrained in the propellant, might have adverse effects on the propulsion system's performance. Another disadvantage to permeable bladders is that permeation of propellant vapor through the bladder often causes compatibility and sealing problems in the upstream pneumatic system.

Because of these disadvantages and because of the possibility of experiencing pressure-bubble symptoms (occasionally causing erratic retrorocket engine performance) in the *Surveyor* vernier propulsion system, development of a low permeation bladder[4] was investigated. This investigation culminated in a joint effort between HAC and Dilectrix Corp., Farmingdale, New York, to perfect a metallized Teflon bladder. This effort resulted in a bladder design not only about 30 times less permeable to helium and 100 times less permeable to N_2O_4 than an all pure Teflon construction, but also with substantially similar endurance capability in repeated expulsion cycling.

A cross-section of the metallized bladder is shown in Fig. 36. For comparison, a cross-section of a typical all-Teflon bladder is also shown. The layer of TFE Teflon

[4]Innovator, William Mascenik.

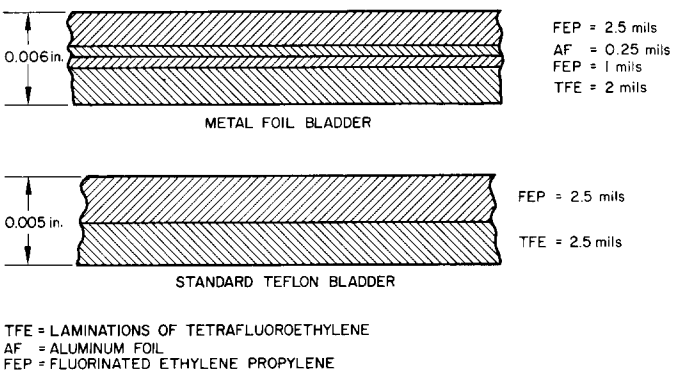

Fig. 36. Propellant expulsion bladders cross-section

UNCLASSIFIED

UNCLASSIFIED
CONFIDENTIAL

provides a majority of the flex life and strength, and the FEP forms a permeation barrier to liquids. However, both are quite permeable to gases, especially helium. (Helium, being light and inert, is an attractive and widely used pressurizing gas in spacecraft.) Hence, in the HAC-Dilectrix metallized bladder, a thin layer of aluminum foil is sandwiched in between FEP layers. The layer is fabricated from three thin sheets of aluminum foil having overlapping seams (a cylindrical center section and gored hemispherical end sections). The aluminum provides a highly effective gas barrier and yet is pliable enough to remain intact in repeated expulsion cycles. This endurance capability was proven in tests in October through mid-December, 1965 on two metallized bladders. The bladders were manufactured by Dilectrix to a HAC specification (HAC 287149) and drawing (HAC PN X287150) and were the same size and shape as the *Surveyor* vernier propulsion system bladders. The purchase order for these bladders was placed May 24, 1965, and they were delivered to HAC in early August. Testing of the bladders took place at the HAC Propulsion Department's Placerita Canyon Test Facility.

One of the bladders was installed in a *Surveyor* propellant tank and soaked in the *Surveyor* oxidizer, MON-10 (90% N_2O_4 and 10% NO), for 38 days. During that period, the bladder was exercised through ten expulsion cycles. Each of the cycles went to 90% (10% of oxidizer left in the tank), and the operating pressure was 800 psig (approximate *Surveyor* operating pressure). The first 8 cycles were at ambient temperature and the last two were at 100°F. No leak was detected after any cycle except after the last; then only a small pinhole was found. This is considered excellent performance because in normal usage it is only necessary that the bladder remain intact through one complete expulsion. This bladder posttest is shown in Fig. 37.

Early in the soak period, the permeation rate for helium was measured. The pressuring gas in the test setup was helium, and helium partial pressures that resulted from permeation through the bladder into solution with the oxidizer were recorded as a function of time. Fig. 38 is a graph of the results. Also shown on the graph is the measured permeability of a typical all-Teflon bladder (*Surveyor* bladder). Fig. 38 shows that the all-Teflon bladder relatively quickly allows helium saturation of the oxidizer side of the bladder. A substantially longer time is required before the oxidizer retained within the metallized bladder is saturated with helium. Hence, a much longer interval is available in which temperature fluctuations may occur with the metallized bladder without the possibility of helium coming out of solution and forming a bubble.

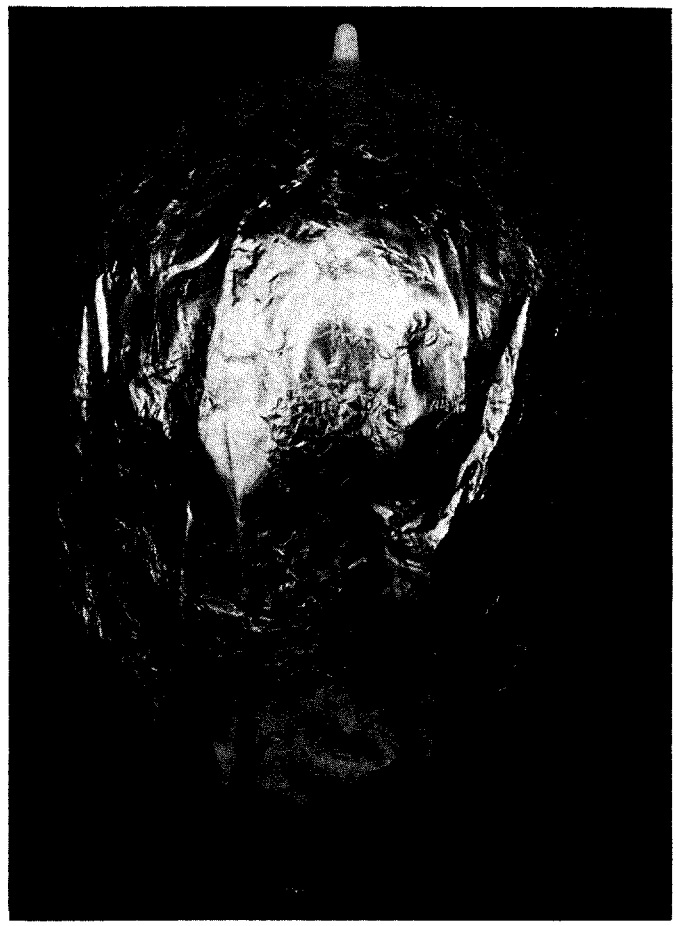

Fig. 37. Test bladder following ten expulsion cycles

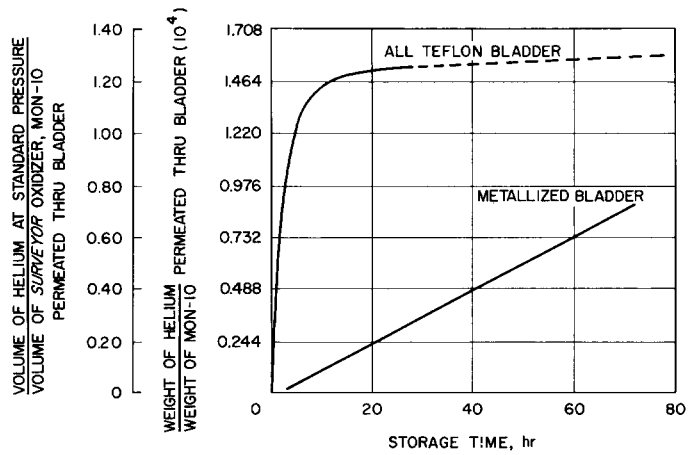

Fig. 38. Helium permeated as function of storage time

UNCLASSIFIED
CONFIDENTIAL

UNCLASSIFIED
CONFIDENTIAL

The helium pressurant gas permeated the metallized bladder and went into solution with the oxidizer at a rate of 0.00265 lb in 72 hr, which compares with 0.00265 lb in 2.5 hr for the all-Teflon bladder.

The other metallized bladder was installed in a *Surveyor* propellant tank filled with water and exercised through three complete expulsions (99.7, 99.7 and 99.8% of the water expelled). A pressure of 50 psig was used. There were no leaks in this bladder posttest. This is also considered excellent performance due to the very severe creasing and crumpling that the bladder sustains as it approaches 100% expulsion. The posttest bladder is shown in Fig. 39.

To supplement the above bladder tests, swatches of material with the same cross-section were checked for N_2O_4 permeability, physical characteristics and compatibility with the *Surveyor* propellants and certain solvents used on *Surveyor* (Genesolv D freon and isopropyl alcohol). The physical properties compared well with the all-Teflon material, and, as expected, the permeability of the metallized bladder material to N_2O_4 was so low that in a 48-hr test no permeation by N_2O_4 could be detected. The threshold of the detection equipment used was 1 mg. For comparison, an all-Teflon piece of material under the same test conditions would have permeated about 100 mg in the same period of time. Hence, the metallized bladder is at least 100 times less permeable to N_2O_4 than the all-Teflon bladder.

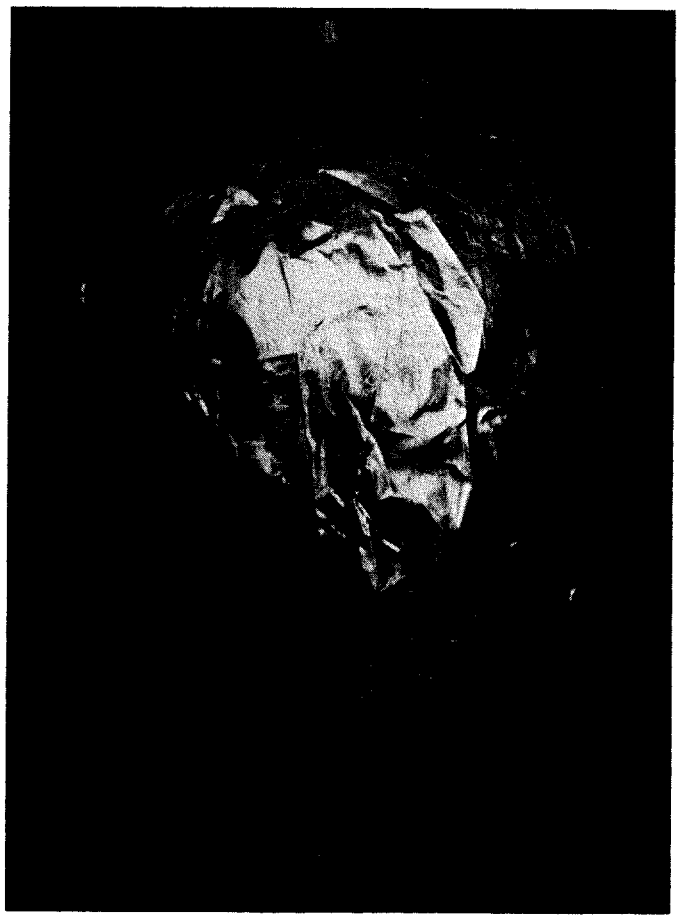

Fig. 39. Test bladder following three nearly 100% expulsion cycles

The compatibility swatches indicated no problems with the *Surveyor* fuel (MMH-H_2O) or with either of the solvents. However, the swatches placed in the *Surveyor* oxidizer (MON-10) became delaminated. The bladder which underwent ten expulsions after 38 days of exposure to MON-10 also showed evidence of delamination in the form of several blisters of about 1½-in. in diameter. Subsequently, a number of swatches representing a new bonding technique were received and tested at JPL. They were found to remain intact after soaking in N_2O_4 for 30 days. Similar results would be expected for exposure to MON-10. Therefore, it is concluded that any future bladders of this type will utilize the new bonding technique, which will eliminate the delamination problem.

The metalized bladder is not currently planned for use on *Surveyor*, since the present propulsion system functions extremely well. If the vernier engine response rates need to be increased for later spacecraft, these bladders would allow considerable improvement in the present system response.

6. *Thrust Chamber Assembly Evaluation*[5]

The evaluation of the *Surveyor* vernier engines (RMD Model No. TD-339) was continued with three tests being performed at JPL's environmental test facility during the latter part of January and February, 1966. The test summary, which follows, is arranged according to test goals.

Group	*Test No.*	*Test date*	*Purpose*
18	A-295	Dec 22	Launch shock
19	DD115, 118	Jan 7–Feb 4	Thrust vector
20	DD116, 117	Jan 14–Jan 25	Hard vacuum storage
21	F10 thru F14	Jan 12–Feb 25	Material compatibility

[5]Prepared by JPL Technical Section 384.

CONFIDENTIAL
UNCLASSIFIED

UNCLASSIFIED

a. Group No. 18. Following exposure of Serial No. (SN) 535 thrust chamber assembly (TCA) to static acceleration (*SPS 37-37*, Vol. I, p. 32), the engine was subjected to a simulated launch vehicle shock environment which consisted of four pulses (about 3 sec apart) in each of three orthogonal axes, one of which was along the spacecraft thrust axis. The pulse form, developed by the JPL environmental requirements group, consisted of the sum of two exponentially decaying damped sine waves, as expressed by the following equation

$$x = 45e^{-70t}\cos 3454t + 3e^{-3.5t}\cos 170t$$

where x is expressed in g's; t is expressed in seconds ($0 \leq t \leq 0.2$).

Fig. 40 shows the TCA attached to a hard-mount adaptor, which, in turn, is connected to the vibration fixture used to generate the shock environment. Also shown is the auxiliary equipment used to fill the engine manifolds with solvents and to hold the solvents under pad pressure (260 psi) during test. Response accelerometers were mounted on the fixture at appropriate points to record the actual applied pulse shape.

The tests (A-295-1, -2, and -3) were successfully completed December 22, 1965. Data reduction, describing the form of the shock pulses, is presently in process. Solvent flow tests, before and after the shock tests, indicated no change in the throttle valve calibration or the operability of the shutoff valve. No leakage points developed.

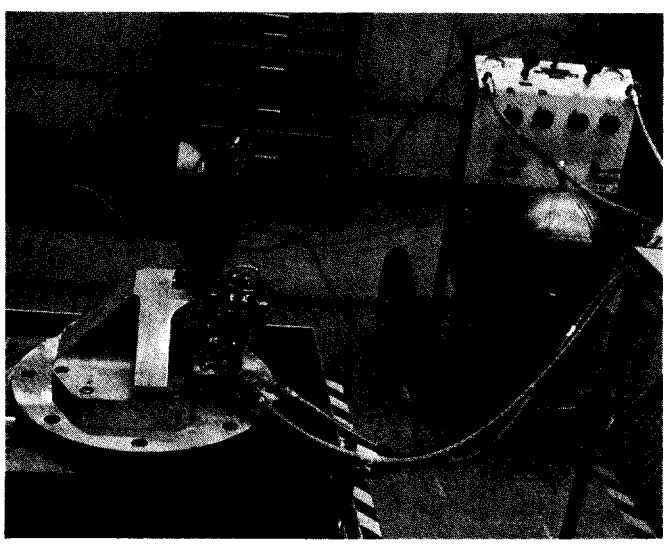

Fig. 40. Thrust chamber installation—launch shock (tests A295-1, -2, and -3)

b. Group No. 19. During the latter part of 1965, work was initiated on a program to measure the side force developed by the TCA. A thrust vector deviation stand (TVDS) was available as *Surveyor*-purchased equipment from a previous contract with the Space Technology Laboratories, Inc. (STL). This stand had been designed to test the STL vernier engine and had not been used in tests at the time of its delivery to JPL. The stand is designed to measure the force perpendicular to the thrust center line, in two planes, by deflecting a balanced beam a measured angle. This deflection is resisted by coiled propellant lines serving as springs in both trunnion axes.

Fig. 41 is a photograph of the TVDS mounted in the hyprox facility at JPL's Edwards Test Station. As illustrated the system is calibrated by hanging a small weight from the nozzle exit and recording the arm deflection in degrees and the arm position in millivolts (output of potentiometers at the fulcrum).

The TVDS used in the tests described herein is designed to circumvent the interaction problem inherent in a direct force measuring system by measuring position instead of force. The TVDS measuring system provides an angular position of a spring-centered, swinging assembly in a force-field generated by the lateral component of thrust. The lateral component of the thrust vector reacts at 90 deg to the support arm causing the arm to rotate about the gimbal center. The amount of rotation of the support arm is a function of the magnitude of the lateral component, the arm length, and the system spring rate.

The system spring rate depends on the stiffness of the propellant lines and instrumentation leading into the support arm through the gimbal axes. This spring rate would normally be made as low as possible, consistent with space limitations of the test installation. The system center of gravity offset is adjusted to zero using a counterweight. Knowing the spring rate, the position of the arm during engine operation can be translated into a magnitude of the lateral thrust component which can, in turn, be translated into thrust vector deviation. The ability of the system to rotate against a constant spring rate is assured by passing the lines and instrumentation along the gimbal axes, and by keeping the system CG offset at zero.

Arm position is sensed by rotary potentiometers located on the gimbal axes. The large permissible motion of the arm enhances the relative accuracy of the system. Longitudinal and rotary dampers may be added as required to diminish undesirable dynamic effects.

UNCLASSIFIED

UNCLASSIFIED
CONFIDENTIAL

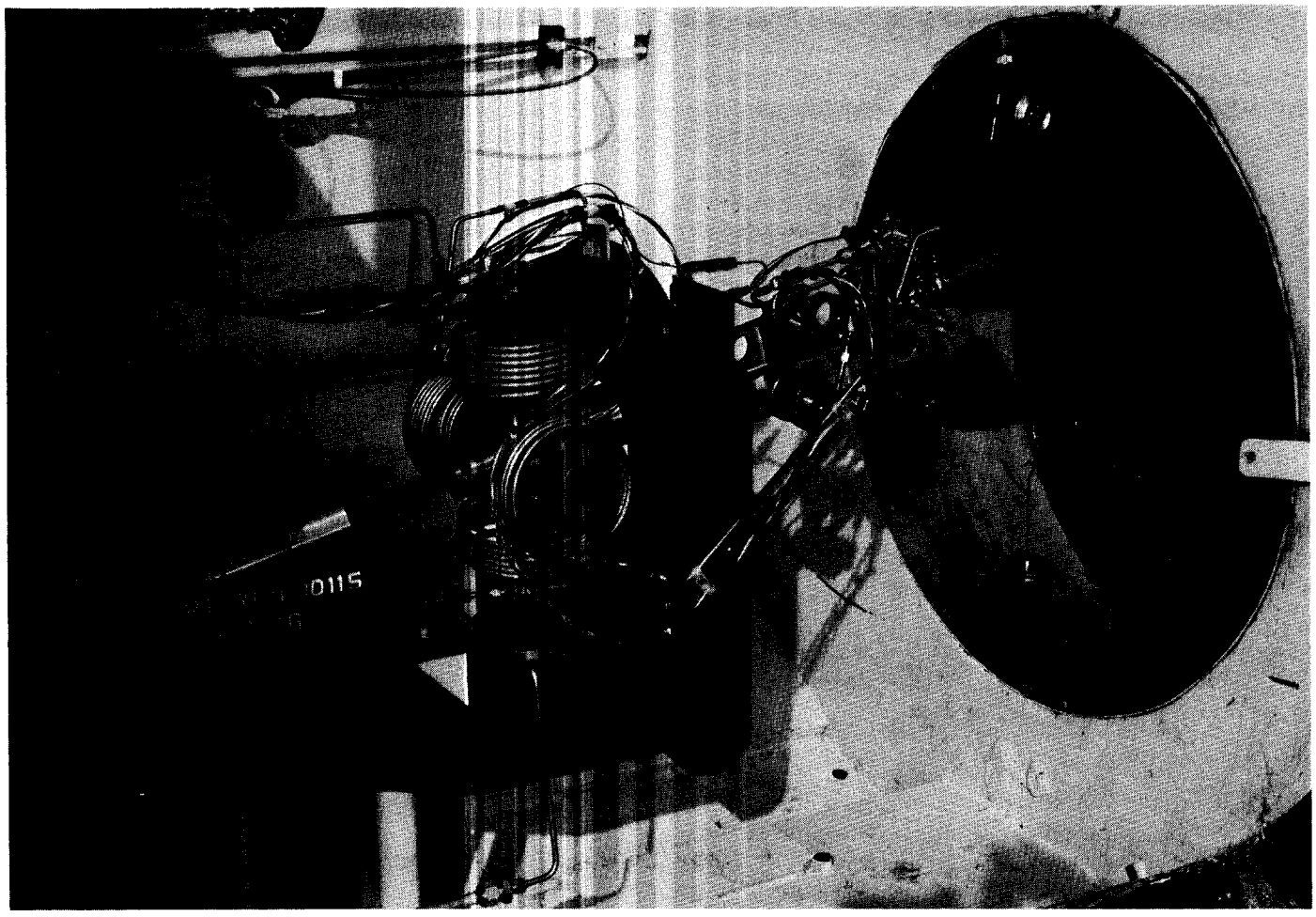

Fig. 41. Thrust vector deviation stand (tests DD-115, -118)

For the thrust vector measurement tests the TCA was mounted on the stand and an alignment tool was installed in the nozzle. The TCA was then aligned optically with the TVDS arm by use of a precision transit and a vernier angle gauge. The precision of the alignment is believed to be within 0.005-in.

The stand was calibrated to the left, right and up by hanging a weight on a swivel-mounted pulley which was adjusted to pull perpendicular to the original center line of thrust at each calibration point. Suitable corrections were applied to the recorded weight to account for the change in angle from the normal to the thrust axis. An angle of about 4 deg corresponded to a side force of about 0.2 lb.

The thrust vector alignment program was conducted with two engines. Initial tests were performed with SN 538 TCA to demonstrate the suitability of the equipment and technique. These tests were followed by tests of SN 535 TCA, as a part of the engineering type approval test (TAT) program of the *Surveyor* engine.

Test DD115. The test firing of SN 538 TCA was performed January 7, 1966. The engine was fired for 30 sec at the midthrust (zero ma) level. Both horizontal (X-force) and vertical (Y-force) side forces were measured. These forces changed less than 0.025 lb from their nominal value during the steady portion of the test. The stand required 4.5 sec to reach its steady-state deflected position (approximately 4 deg in the vertical plane), indicating that the system is close to optimum damping.

One problem observed during test was a large amplitude pressure oscillation in the TCA inlet lines. Both pressures were ringing at 14.4 cps with oxidizer line pressure amplitudes of 600 psi (peak-to-peak) and fuel line pressure amplitude of 30 psi (peak-to-peak). High-speed

UNCLASSIFIED

UNCLASSIFIED
CONFIDENTIAL

movies showed the propellant line coils oscillating in an accordion fashion and moving approximately ¼ in. These same oscillations were present during flow bench tests at midthrust but disappeared at higher flow levels.

Test measurements, recorded at 10 and 28 sec after initiation of the test, indicated that the side force in the horizontal plane was essentially zero. The predominant side force was that measured in the vertical plane and acted in a downward direction.

The measured force is not the true side force of the nozzle but represents a fictitious force applied at the nozzle exit, the calibration point.

There are several corrections which must be considered in extracting the actual side force from the measured data. These are (1) the effect of momentum forces in the fluid streams acting upon the TVDS, (2) the effect of changes in weight distribution which take place during a firing as compared to the weight distribution during calibration, and (3) the effect of transferring the force from the nozzle exit, which is the calibration plane, to the plane in the nozzle at which all side forces may be assumed to be concentrated.

Analysis indicated that the forces created by the change in direction of the confined fluid streams near the gimbal point would have a small effect on arm position and the accuracy of the side force measurement. With the system pressurized during calibration, there was no zero shift in the TVDS. It was concluded that no correction is needed for the slight changes in static pressure or for the fluid velocity effects which take place during system operation.

Considering the weight distribution effects, the TVDS is calibrated with all volumes in the engine to the shutoff valve filled with propellants. The major change in weight distribution during a firing is the weight of propellant occupying the injector manifold. This weight (0.0135 lb) acting at the injector manifold (20 in. from the fulcrum) is equivalent to a force of 0.0113 lb acting downward at the assumed point of application (23.75 in. from the fulcrum) of the side force in the nozzle. This equivalent weight must be subtracted from the measured side force (acting downward in a vertical plane) to give the true side force.

The point of application of the side force in the nozzle was determined by calculating the pressure forces acting on the nozzle wall (in a direction perpendicular to the nozzle centerline) over several incremental lengths of the expansion cone and then establishing (by moments) the location of the resultant force. This calculation indicated that the nozzle side forces may be considered to be effectively concentrated at a plane located 1 in. downstream of the throat (5.25 in. from the nozzle exit). The measured side force is then corrected (increased) by the ratio of the moment arms [29/(29 − 5.25)] to give the true side force of the nozzle.

Examination of the above ratio indicates that a small error in the calculation of the location of the resultant side force will have a small effect on the accuracy of the final answer.

Considering the two major corrections, the true side force and thrust vector angle calculations are given in Table 28.

Table 28. True side force and thrust vector angle calculations

Item	Time from fire signal	
	10 sec	28 sec
Measured force—Fy, lbs	0.207	0.227
Point of application correction ($Fy' = Fy \times 29/23.75$), lbs	0.253	0.277
Propellant weight (injector manifold) correction, lbs	−0.011	−0.011
True side force ($Fy'' = Fy' - 0.011$), lbs	0.242	0.266
Axial thrust[a] ($F = I_{sp} \times W_t$), lbs	66.4	66.1
Thrust vector angle (arctan Fy''/F), deg	0.21	0.22

[a]SN 538 TCA did not have a P_c tap. Based on recorded flow rates and assuming a nominal I_{sp} of 281 sec, the axial thrust was calculated.

Test DD-118. SN 535 TCA was successfully tested for thrust vector alignment February 4. The firing profile called for a 60-sec test at three discrete thrust levels. The engine was cycled twice to each thrust level to provide thrust vector data at various stages of thermal equilibrium. Prior to the test, the coiled feed lines were stiffened by shims (mounted between the coils) in an attempt to reduce the feed system oscillations present in the previous test.

Measurements indicated the presence of a side force acting in the vertical plane in a downward direction. Side forces in the horizontal plane were about 10% of the force in the vertical plane. Propellant line pressure oscillations, although considerably damped from the previous test, existed at the midthrust level but not during minimum and maximum thrust conditions. The oscillations at the midthrust level were considerably reduced at the second step to this level.

UNCLASSIFIED
CONFIDENTIAL

CONFIDENTIAL

The true side force (correction terms included) and the thrust vector angle for each of the three thrust levels are noted in Table 29.

Table 29. True side force and thrust vector angles

Item	Time interval, sec					
	0-10[b]	10-20	20-30	30-40	40-50	50-60
Measured force—Fy, lbs	0.26	0.28	0.11	0.21	0.28	0.11
Point of application correction ($Fy' = Fy \times 29/23.75$), lbs	0.32	0.34	0.13	0.26	0.34	0.13
Propellant wt (injector manifold) correction, lbs	−0.01	−0.01	−0.01	−0.01	−0.01	−0.01
True side force ($Fy'' = Fy' - 0.01$), lbs	0.31	0.33	0.12	0.25	0.33	0.12
Axial thrust[a] −F, lbs	66	107	25	66	107	25
Thrust vector angle (arctan Fy″/F), deg	0.28	0.18	0.28	0.22	0.18	0.28

[a]Thrust level estimated from chamber pressure measurement.
[b]Questionable data because of feed system pressure oscillations at the start of the test.

The average thrust vector angle for the last 30 sec of the test, covering a thrust range from 25 to 107 lb, is 0.23 deg. This agrees closely with the thrust vector angle of 0.22 deg for SN 538 TCA.

As indicated in the above discussion, the side force measured in each test was primarily in a vertical downward direction. It is not clear whether this is a coincidence or is caused by some factor which is not obvious at the present time. Additional tests are planned to further explore this question.

Certain gravity and moment correction terms have been applied to the measured data to provide the true force data. These corrections are small, however, compared with the raw data. It is believed that the measured side force in Test DD-118 is accurate to ±0.04 lb, based upon the amount of zero shift exhibited in this 60-sec test.

The two tests (DD-115 and DD-118) show that the thrust vector angle of the TD-339 TCA is well within the allowable 0.3 deg.

c. Group No. 20. Following exposure of SN 535 TCA to launch shock, the engine was subjected to a program of thermal-vacuum storage. The first storage period was planned to be at a nominal temperature of 0°F for 66 hr, followed by a 5-sec engine firing. The second storage period was to be at a nominal temperature of 165°F for 100 hr, again followed by a 5-sec engine firing. During both storage periods, the engine was scheduled to be under a vacuum of about 10^{-6} torr.

Since this program was designed to simulate the conditions during injection and transit, the engine was stored with propellants under nominal tank pressures of 720 psi. The TCA was encased in the hard vacuum environmental chamber previously illustrated in *SPS 37-37*, Vol. I, p. 32, and used in hard vacuum start tests DD-111 to DD-114 inclusive. This equipment included an insulated and temperature-conditioning feed system.

SN 535 TCA was successfully stored under hard vacuum from 11 a.m. January 14 to 3 p.m. January 17, and then test fired (Test DD-116) for 5 sec. The engine was stored in the temperature range of 10 to 25°F for 15 hr and in the temperature range of 0 to 10°F for 51 hr for the required total of 66 hr. The engine was under full tank pressure (720 psi) for 63 of the scheduled 66 hr. A facility gas leak necessitated lowering pressure to about 130 psi for 3 hr to effect repairs.

The average vacuum during storage was 3×10^{-5} torr. Engine ignition took place at a vacuum of 3.5×10^{-4} torr and with propellants at a temperature of 0 to 5°F. Both start and shutdown transients were normal.

Following the above storage program, the temperature conditioning system was changed for the high-temperature storage program to follow. Inspection of the engine indicated its suitability for entering the second phase of the program.

The engine was successfully stored under hard vacuum from 11 a.m. January 21 to 3 p.m. January 25, and then test fired (DD-117) for 5 sec. The engine was stored at a temperature in excess of 165°F for the entire period. Certain thermocouples monitoring the temperature of the TCA and propellant lines acted erratically during the initial portion of the storage period. Secondary junctions existing along the leads were found to be giving erroneously low temperatures. Following repair, the thermocouples indicated temperatures closely comparable to those indicated by the thermocouples monitoring the hot water system. Based upon these latter readings it is concluded that the storage temperature was between 170 and 180°F for the entire storage period.

The engine was under full tank pressure (720 psi) for 100 hr. The average vacuum during storage was 5×10^{-5}

UNCLASSIFIED CONFIDENTIAL

UNCLASSIFIED
CONFIDENTIAL

torr. Engine ignition took place at a vacuum of 4×10^{-4} torr with propellants at a temperature of about 164°F. Both start and shutdown transients were normal.

Following test, the engine was leak and flow tested. The solenoid valve was found to be inoperative because of gas leakage by one of the seals. The valve was replaced to permit additional testing of the engine and the faulty valve returned to RMD for failure analysis.

Posttest flow measurements showed a slight plugging of the oxidizer injector with a shift in mixture ratio from the nominal 1.5 to the range of 1.30 to 1.46. Following a hot water flush, flow tests indicated the engine to be essentially back within mixture ratio limits. The plugging was apparently due to salt formation, which has been experienced under postfiring conditions on other engines.

d. Group No. 21. As indicated in *SPS 37-37*, Vol I, p. 34 (Group 15—Lunar survival storage tests), the fuel poppet of the shutoff valve revealed severe disintegration of the Nylon-101 seat following 5 days of exposure to the *Surveyor* fuel, monomethylhydrazine hydrate (MMH-H_2O), at a temperature of 300°F. Fig. 42 is a photograph of the badly-cracked seat following test. Based on the results of this experiment, additional compatibility tests of the Nylon-101 with fuel were scheduled. These tests were planned to determine the limiting conditions of temperature and exposure time for Nylon-101 in *Surveyor* fuel. Other materials were also to be tested in a search for improved properties.

The two environmental boxes used in lunar survival testing of the TCA were moved to F Stand. A number of type 347 stainless steel containers were made from 12-in. lengths of 1-in. diameter tubing and so arranged in the boxes that certain of the material samples could be stored in the fuel under pressure, while other samples would be immersed in the fuel under vapor pressure only. The fuel was to fill 50% of the container volume. Finally, some samples were to be suspended in the box (not exposed

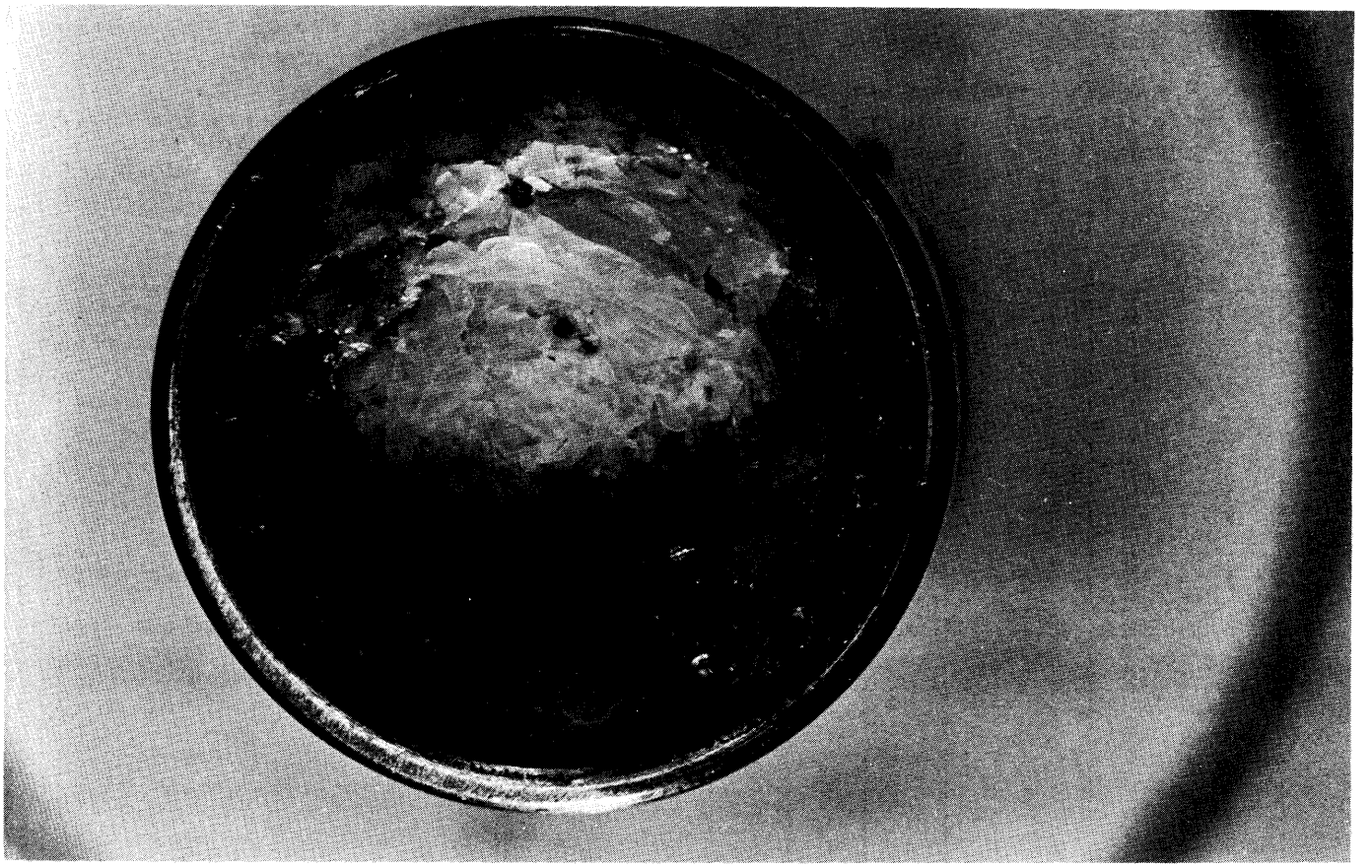

Fig. 42. Nylon-101 fuel poppet after 5-day fuel exposure at 300°F (test E-39-4)

CONFIDENTIAL
UNCLASSIFIED

UNCLASSIFIED
CONFIDENTIAL

to the fuel) to determine any degradation resulting from exposure to the high-temperature gas (nitrogen) in the box.

Nylon-101 tests. Testing of the Nylon-101 samples was initiated January 12th. Ten samples of the material, each ¾-in. diameter by 3/16-in. thick, were prepared. Each sample was weighed and tested for shore hardness prior to and following test. Five samples were tested at 230°F with exposure times of 2, 5, and 15 days. The other five samples were tested at 280°F with similar exposure times. Some samples were stored under 850-psi nitrogen gas pressure and others under fuel vapor pressure only.

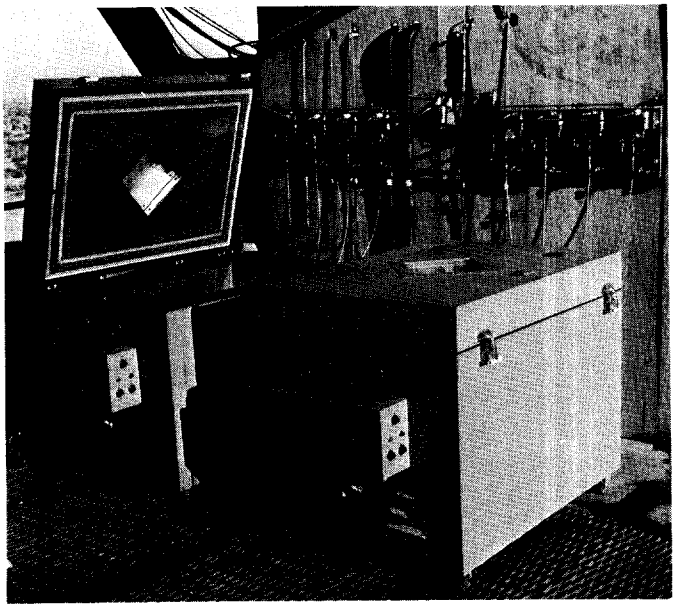

Fig. 43. Temperature conditioning boxes for material compatibility testing (tests F-10 to F-14)

Fig. 43 is a photograph of the conditioning boxes and auxiliary pressurization equipment used in the experiment. Test results are presented in Table 30.

As indicated in the above tabulation, prolonged exposure at 230°F caused cracking in the material. No cracks were visible in the two-day sample whereas there were many cracks in the 5-day and 15-day samples. Also of note is the larger weight gain of those samples stored under pressure as compared with samples stored under the fuel vapor pressure. There appears to be a considerable amount of absorption of the fuel in the Nylon.

Finally, it is to be noted that the fuel in which the 280°F samples were immersed was murky in appearance and contained a chalk-like substance. By contrast, the fuel containing the 230°F samples (2 and 5 days) was clear, although the murky appearance developed after 15 days of exposure at 230°F.

Table 30. Nylon-101 fuel compatibility test conditions and results

Box No.[a]	Sample No.	Temp, °F	Pressure, psig	Exposure time, days			% wt change	Hardness, Shore D		Visual observations, posttest	
				2	5	15		Initial	Final	MMH • H_2O	Sample
1	1	230	Vapor pressure (20)	X			+2.60	83	74	Clear	Unchanged
1	2	230	850	X			+5.51	82	74	Clear	Unchanged
1	3	230	850		X		+7.90	83	70	Clear	Several cracks, sample intact
1	4	230	850			X	+7.40	83	*	Milky	Several cracks, some crumbling
1	9	230	Ambient			X	−0.19	83	85	GN_2 exposure	No cracks, color change to tan
2	5	280	Vapor pressure (40)	X			+4.70	83	*	Milky	Several cracks, sample intact
2	6	280	850	X			+9.35	83	*	Milky	Numerous cracks, crumbling
2	7	280	850		X		+8.36	83	*	Milky	Numerous cracks, crumbling
2	8	280	850			X	+6.4	83	*	Milky	Numerous cracks, crumbling
2	10	280	Ambient			X	−0.24	83	85	GN_2 exposure	No cracks, color change to brown

*Nylon disc crazed to the point that hardness measurements could not be made.
[a]Test F-10, Box 1; test F-11, Box 2.

CONFIDENTIAL
UNCLASSIFIED

UNCLASSIFIED

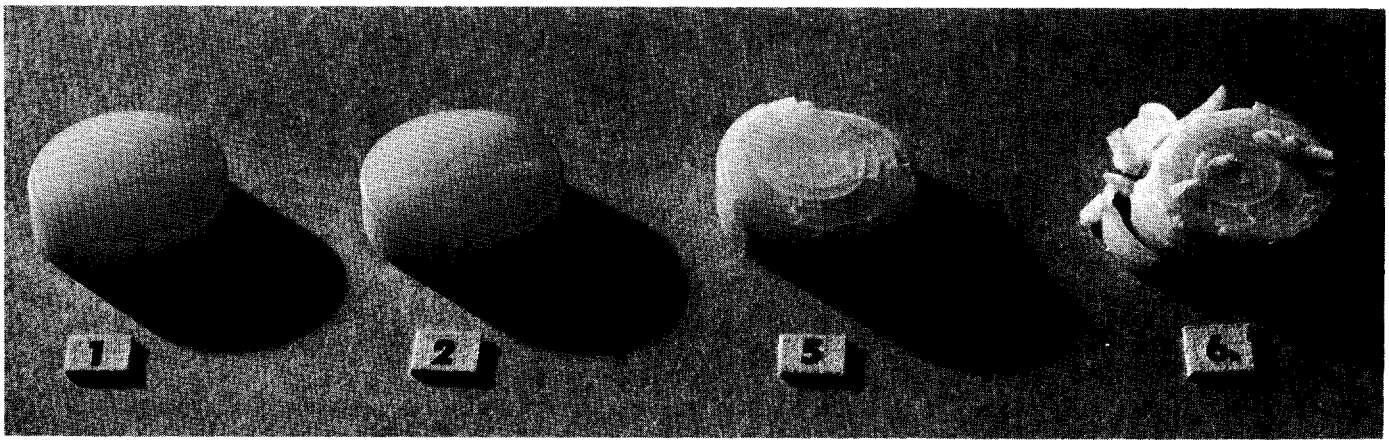

Fig. 44. Nylon-101 samples after 2-day fuel exposure at 230°F (1 and 2) and 280°F (5 and 6) (tests F-10 and -11)

Fig. 44 is a photograph of the 2-day Nylon samples, after their removal from the fuel. Samples 1 and 2, exposed at 230°F, are unchanged in appearance. The degree of cracking in samples 5 and 6, exposed at 280°F, is clearly indicated in the photograph.

It is concluded that Nylon-101, when exposed to MMH • H_2O at elevated temperatures (230–280°F) for an appreciable length of time, undergoes severe degradation.

The results of this sample investigation clearly explain the inability of the TCA to survive "lunar survival" conditions when exposed to the fuel.

Improved materials—Group 1. The failure of the Nylon-101 samples in *Surveyor* fuel prompted a search for substitute materials to meet "lunar survival" conditions. Three materials were initially selected. These were Teflon, Kel-F and an improved Nylon called "VESPEL." According to the suppliers, all of these materials should be useable over a wide temperature range with an upper limit in excess of 330°F. The compatibility of the VESPEL with the fuel would have to be established.

Two samples of each material were placed in fuel storage February 2nd at a temperature of 310°F and a pressure of 850 psi. It was planned to remove the first sample of each material after two days and the second sample after five days storage. The results of the experiment are presented in Table 31.

Fig. 45 is a photograph of the 2-day Teflon and Kel-F samples after their removal from the fuel. Both samples were originally white. The Teflon retained its original color and was essentially unaffected by exposure to the fuel. The change in color of the Kel-F from a translucent appearance to black is evident. The VESPEL samples

Table 31. Material fuel compatibility test conditions and results (Test F-12)

Material	Sample No.	Temp, °F	Pressure, psig	Exposure time, days		% Wt change	Hardness, Shore D		Visual observations, posttest	
				2	5		Initial	Final	MMH • H_2O	Sample
Teflon	12	310	850	X		+0.13	57	56	Milky	Unchanged
Teflon	13	310	850		X	+0.16	56	56	Clear	Unchanged
Kel-F	14	310	850	X		*	78	*	Dark brown	Black, expanded and cracked
Kel-F	15	310	850		X	*	77	*	Dark brown	About 50% expanded, cracked and black
Vespel	16	310	850	X		*	84	*	Dark brown	Sample disintegrated
Vespel	17	310	850		X	*	84	*	Dark brown	Sample disintegrated

*Material badly degraded. Determination of weight and shore hardness changes not possible after MMH • H_2O exposure.

UNCLASSIFIED

UNCLASSIFIED
CONFIDENTIAL

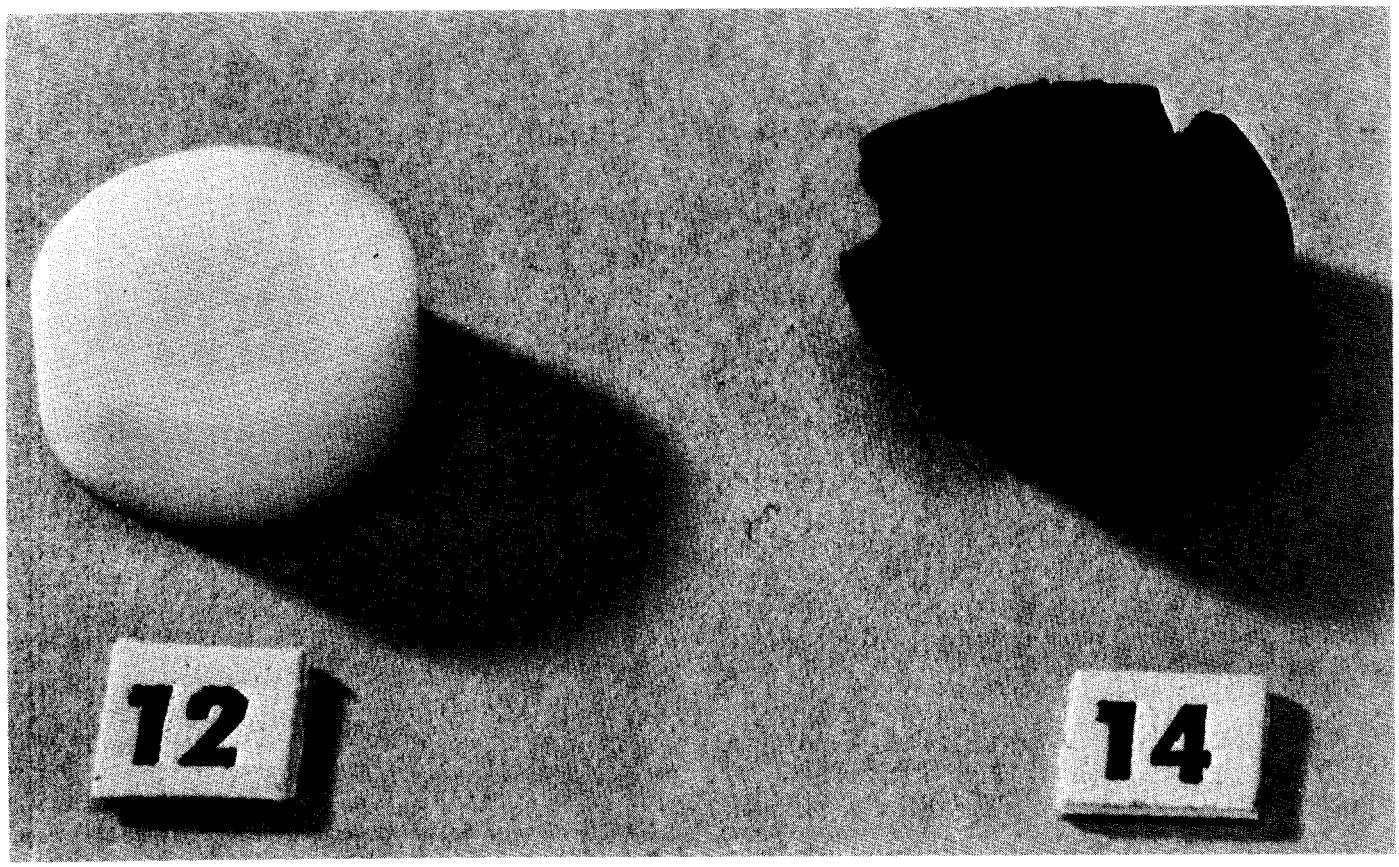

Fig. 45. Teflon (12) and Kel-F (14) samples after 2-day fuel exposure at 310°F (test F-12)

were completely disintegrated and reduced to a powdered solid after exposure to the fuel. The VESPEL disintegrated in the fuel producing no reaction or pressure buildup.

About 9 hr after the start of the test, a pressure rise took place in the Kel-F sample tubes, indicating a reaction with the fuel. Thereafter, the Kel-F sample tubes were periodically vented of excess pressure. The results of the Kel-F storage tests were unexpected and thus were repeated with another stock of material (Test F-13, Samples 19, 20, and 21). Identical results were obtained, the material reacting with the fuel, expanding and turning black.

Testing of this group of materials indicated that Teflon, which had previously been eliminated as the valve seat material for other considerations, appears to be the only common material which is compatible with *Surveyor* fuel at elevated temperatures and pressures.

Improved materials—Group 2. The results of exposure of Teflon to *Surveyor* fuel at 310°F for 5 days indicated its potential as a substitute material for the fuel poppet. Its durability under cyclic loads at low temperature (0°F), however, is questionable. Accordingly, it was considered that Teflon reinforced with a filler (ceramic or glass fibers) might represent an improved material capable of meeting both the functional requirements of the shutoff valve and the lunar survival conditions currently under investigation.

Samples in the form of valve seats (used in Jamesbury Ball Valves) were selected for test under the same conditions as the "Group 1" materials. At the same time, two other new materials (polyphenylene and polyphenylene oxide) were included in the test program.

Testing of these materials was initiated February 14th. Eight samples, four of the reinforced Teflon (two identified by red filler color and two identified as an improved filler, which is black), and two each of the polyphenylene group were tested for 2 and 4 days at 310°F. Test results are presented in Table 32. Based upon these tests and the previous Group 2 tests, it is concluded that either the pure Teflon or the filled Teflon (red filler) is the most promising seat material to meet the lunar survival needs.

UNCLASSIFIED
CONFIDENTIAL

UNCLASSIFIED

Table 32. Material fuel compatibility test conditions and results (Test F-14)

Material	Sample No.	Temp, °F	Pressure, psig	Exposure time, days		% wt change	Hardness, Shore D		Visual observations, post-test	
				2	4		Initial	Final	MMH • H_2O	Sample
Polyphenylene oxide	22	310	850		X	+11.1	80	72	Light amber color	Color unchanged, considerable physical distortion
Polyphenylene oxide	23	310	850	X		+17.0	80	72	Light amber color	Color unchanged, considerable physical distortion
Polyphenylene	24	310	850	X		*	75	*	No fuel left	No color or apparent physical change**
Polyphenylene	25	310	850		X	+0.26	75	74	Light amber color	No color or apparent physical change**
Teflon black filler	26	310	850	X		+0.14	60	60	Light amber color	No color or apparent physical change
Teflon black filler	27	310	850		X	+0.07	60	60	Moderate amber color	No color or apparent physical change
Teflon red filler	28	310	850	X		−0.58	60	60	Clear	No color or apparent physical change
Teflon red filler	29	310	850		X	−0.70	60	60	Clear	No color or apparent physical change

*No data obtained because of premature loss of fuel.
**It was observed that this material was quite brittle both before and after test.

7. Surveyor Vernier Engine Pressure Transducer Line Resonance and Heating[6]

a. Summary. An analysis has been conducted to determine the cause of large magnitude oscillations in chamber pressure transducer output and severe heating of the chamber pressure tap which has occurred during some vernier engine ground testing. The tube between the vernier engine combustion chamber and the pressure transducer is apparently driven at its natural frequency by the 400 cps dither in the throttle valve command, causing large magnitude oscillations due to the very low damping in the tube. The hot gas flowing in and out of the tube causes severe heating. Changing the natural frequency, increasing the damping, or decreasing the volume should reduce the heating problem.

The most satisfactory solution appears to be filling the tube with a stainless steel stranded wire.

b. Introduction. Transducer chamber pressure line heating and burnout, which has occurred on some engines, has been attributed to the apparent large amplitude oscillations in chamber pressure. These oscillations cause hot gas to flow in and out of the line. Fig. 46 shows large

[6]Prepared by JPL Technical Section 384.

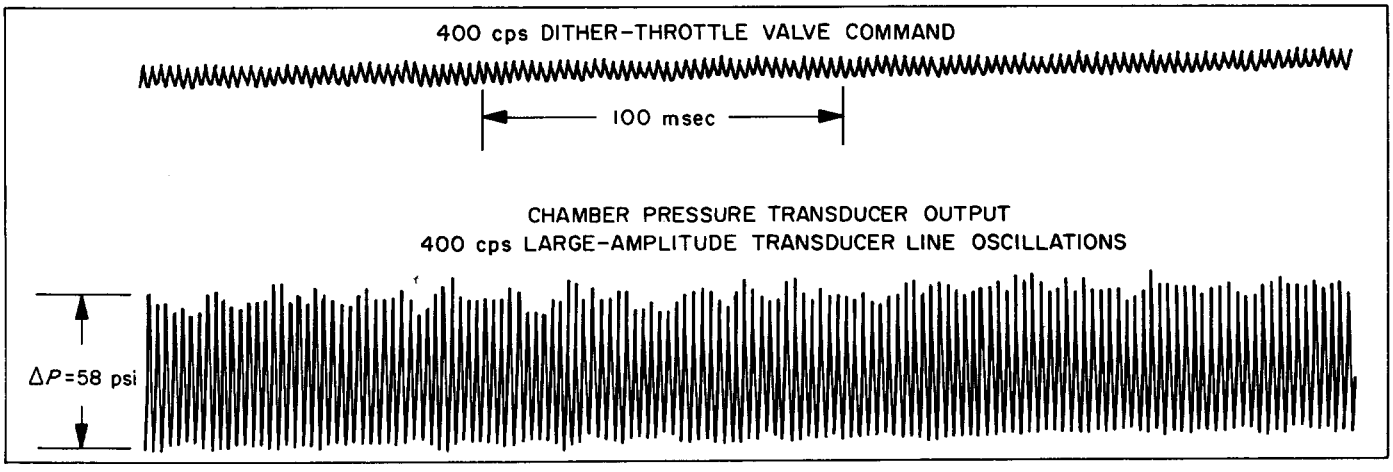

Fig. 46. Throttle valve command and transducer line oscillations displaying identical frequencies

UNCLASSIFIED

UNCLASSIFIED
CONFIDENTIAL

amplitude oscillations which caused severe chamber pressure line heating during S-7 tests. The command current to the throttle valve is also shown on Fig. 46. Note that the frequency of the oscillations is exactly the same as the 400 cps dither signal in the throttle valve command.

Engines with low-hysteresis fuel regulators are ineffective in appreciably damping the 400 cps dither signal at low thrust levels and, therefore, this signal reaches the combustion chamber where it drives the transducer line at its resonant frequency (near 400 cps). This condition causes large-amplitude pressure oscillations inside the transducer line because of the apparent low damping ratio (0.012) which, in turn, is apparently responsible for the constant pumping in of high-temperature combustion gases. Fig. 47 shows typical response of a transducer mounted in a standard adapter with simulated connecting line, whose configuration is very nearly that used during *Surveyor* vernier engine firings. Several response tests were made with the transducers connected to a shock tube at the Edwards Test Station. Static pressure prior to impact of the pressure step was 150 psi, with approximately a 160-psi pressure step in all cases. The rise time response, the lower ringing frequency (basically that of the connecting line), and the higher or diaphragm frequency were approximately 1 msec, 400 cps, and 20,000 cps, respectively. The damping ratio was calculated to be approximately (0.012).

Heat transfer calculations indicate that the volume of the transducer line is such that there is sufficient total thermal energy available from the high temperature gases entering the line during the oscillating conditions to maintain the line walls near a temperature of 2000°F. Sustained temperatures of this magnitude can only result in line failures during sufficiently long intervals of low-thrust operation.

c. Test results. Most of the testing associated with this analysis was directed to find ways of either significantly increasing the damping ratio or changing the natural frequency. Either change would markedly decrease the amplitude of the pressure oscillation inside the line which, in turn, would lower the tube wall temperature. Of the many tests conducted, several modifications appear to provide sufficient correction in either damping ratio or natural frequency to insure less heating. One method consists of installing an 0.050-in. diameter orifice at the combustion chamber end of the line. This configuration appears to significantly increase the damping ratio (Fig. 48), as desired, but also doubles the rise time. Another approach to change the natural frequency is to either shorten or lengthen the present transducer tube.

Presently, the best and least expensive solution appears to be the insertion of a 4½- to 5-in. length of about 0.090-in. diameter stranded stainless steel wire into the pressure transducer line. This configuration appears to slightly decrease the natural frequency and perhaps increases the damping ratio (Fig. 49). Most significant, however, is the 90% reduction of gas volume in the line. Calculations indicate that with such a volume reduction the highest

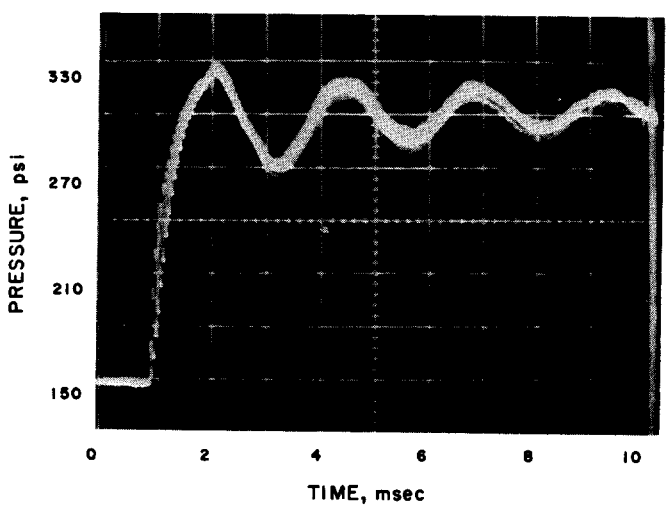

Fig. 47. Typical response of transducer mounted in a standard adapter with simulated connection line

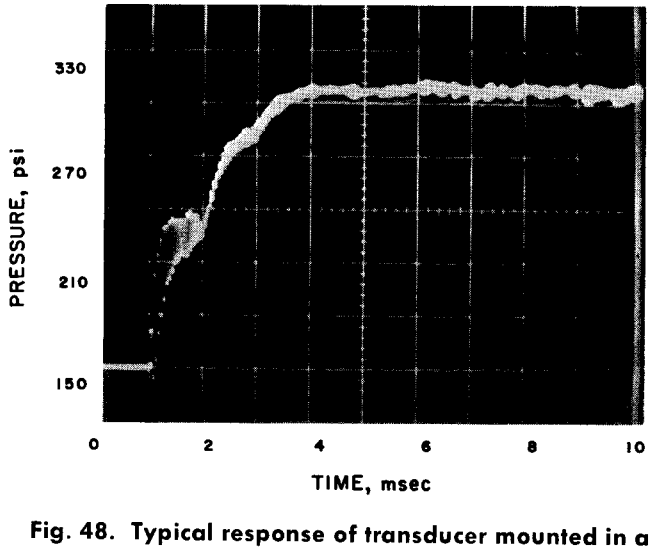

Fig. 48. Typical response of transducer mounted in a standard adapter with simulated connecting line having an 0.052-in. diameter orifice at combustion chamber end

UNCLASSIFIED

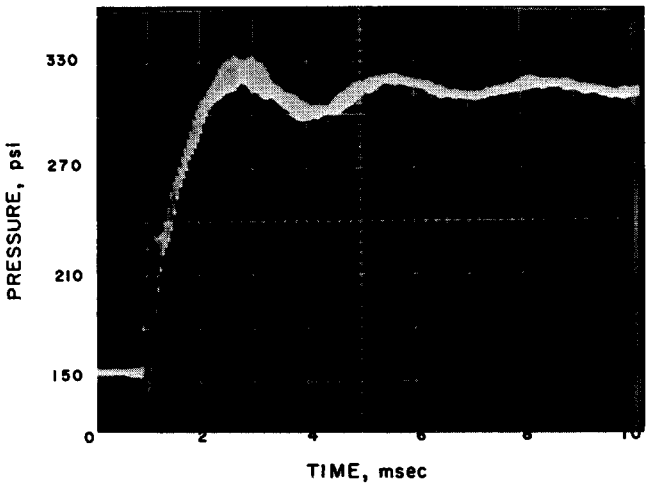

Fig. 49. Typical response of transducer mounted in a standard adapter with simulated connecting line filled with an 0.095-in. diameter aluminum rod

expected tube wall temperature will be, on the average, about 150°F.

d. Conclusions. Because the response of the transducer-line configuration with and without the inserted 0.090-in. diameter wire appears nearly identical, and also because heat transfer calculations definitely show that a significant gas volume reduction in the line will reduce the tube wall temperature, it is concluded that the most advantageous solution is to insert a proper length of 0.090-in. diameter stranded stainless steel wire into the transducer line.

A vernier engine with previous history of transducer line heating will be tested first at the thrust level and dither signal frequency, which should produce significant wall heating and will then be retested at these same conditions after installation of the stainless steel wire. It is expected that the stranded wire insert will prevent chamber pressure tap heating in the future.

8. Lunar Surface Contamination Due to Surveyor Vernier Engine and Main Retrorocket Exhaust Products[7]

a. Summary. An analysis of the *Surveyor* vernier and retrorocket engine exhaust product impingement concentrations on the lunar surface during the entire spacecraft descent is presented. Such information will aid in evaluating soil and lunar atmosphere experiments. The results of this analysis indicate that 98% of the total surface contamination by exhaust products occurs during the final descent, from 50 ft to vernier engine cutoff, 10 ft above the lunar surface.

b. Analysis. For easy analysis the *Surveyor* descent trajectory was divided into three phases, as listed in Table 33.

Table 33. *Surveyor* mission phases

Mission phase	Engines operating	Altitude, ft	Acceleration control
Retroengine descent phase	Retrorocket and verniers	320,000–38,000	≈ Constant thrust
Vernier descent phase	Verniers	38,000–50	Preprogrammed velocity altitude profile
Final descent phase	Verniers	50–10	Constant velocity

Gas impingement concentrations on the lunar surface due to exhaust gases of one vernier engine were estimated during the final 50 ft of terminal descent. During this time, the *Surveyor* spacecraft will descend with a constant velocity near 5 ft/sec and each engine will be operating at about 30 lb of thrust.

The local free stream density along the centerline of the jet is assumed to vary inversely with the square of the distance from an apparent source point. This is a good approximation for that portion of the flow field of interest in this analysis. Rocket plume fields calculated for the *Surveyor* engine show that beyond an exit radii of 50 the flow appears to display free molecular characteristics.

Thus,

$$\rho/\rho_o = K(Z/r_t)^{-2} \qquad (1)$$

where

K = 1.0 for $Z/r_t \geqq 600$[8]

ρ = free stream density

ρ_o = stagnation density

Z = distance from apparent source

r_t = rocket engine throat radius

The range of Z/r_t in this analysis is from about 600 to 2000.

[7]Prepared by JPL Technical Section 384.

[8]K is based on the results of flow field calculations for the *Surveyor* vernier engine.

UNCLASSIFIED

The mass flow rate of exhaust gas which impinges on a unit area is expressed as

$$\frac{w}{A} = \rho V \tag{2}$$

where

w/A = mass flow rate per unit area

V = free stream velocity

The total mass per unit area (M/A) of exhaust gas which impinges upon the lunar surface can be expressed as:

$$M/A = \int \frac{w}{A}\, dt = \int \rho V\, dt \tag{3}$$

Because the free stream velocity does not appreciably change from one point in the flow field to another, the velocity V in Eq. (3) can be assumed constant and equal to the effective nozzle exit plane value V_e where

$$V_e \approx g I_{sp} \tag{4}$$

and

g = gravitational constant

I_{sp} = specific impulse

Also, because the spacecraft descends at constant velocity during the final 50 ft, then

$$dt = -\frac{dZ}{v} \tag{5}$$

where

v = spacecraft descent velocity

The combination of Eqs. (1), (3), (4), and (5) result as

$$M/A = \frac{-g I_{sp}\, \rho_o\, r_t^2}{v} \int \frac{dZ}{Z^2} \tag{6}$$

Integrating Eq. (6) and assuming that at 50 ft above the surface $M/A = 0$, the final expression for mass concentration during the final 50 ft of descent is

$$M/A = \frac{g I_{sp}\, \rho_o\, r_t^2}{v}\left(\frac{1}{Z_{co}} - \frac{1}{50}\right) \tag{7}$$

where Z_{co} = vernier engine cutoff altitude.

The impingement concentration level of combustion products on the lunar surface again due to one vernier engine during the preprogrammed descent from 38,000–50 ft was estimated by using actual velocity and altitude profiles.

Again combining Eqs. (3) and (1) observe that

$$\frac{M}{A} = V_e\, \rho_o\, r_t^2 \int \frac{dt}{Z^2} \tag{8}$$

and

$$dt = \frac{dV}{a} \tag{9}$$

But "a" is nearly constant along the preprogrammed descent trajectory. Therefore,

$$\frac{M}{A} \approx \frac{V_e\, \rho_o\, r_t^2}{a} \int \frac{dV}{Z^2} \tag{10}$$

Four separate and distinct line segments approximate the constant deceleration curve from 38,000 ft; therefore, the total vernier engine impingement concentration down to 50 ft is

$$\left[\frac{M}{A}\right]_{50\,\text{ft}}^{38{,}000\,\text{ft}} \approx \frac{V_e\, \rho_o\, r_t^2}{a}\left[\sum_{i=1}^{4} \int \frac{d\,[V_i|Z|]}{Z^2}\right] \tag{11}$$

where $V_i|Z|$ in each case is a linear function of Z.

The calculations using Eqs. (7) and (11), and assuming 100% absorbance, are shown in Table 34.

Table 34. Exhaust product surface contamination

Distance above lunar surface, ft	One vernier engine Gas products, gm/cm²	Main retroengine	
		Gas products, gm/cm²	Solid products, gm/cm²
38,000–50	21×10^{-6}		
50–10[a]	1090×10^{-6}		
At 25,000		1.5×10^{-6}	2.5×10^{-6}
Exhaust product constituents	H_2O, N_2, CO, CO_2, H_2, H, OH, NO, O_2, O	H_2, CO, HCl, H_2O, N_2, H, CO_2, Cl, OH	AL_2O_3
Total impingement contamination due to all effects (3 vernier engines and retroengine)	3337×10^{-6} gm/cm²		

[a] Lowest vernier engine cutoff altitude. This value could be as large as 19 ft, in which case the contamination would be less than that shown above.

UNCLASSIFIED
CONFIDENTIAL

The gas impingement concentration level of the main retroengine was conservatively calculated from Eq. (8) by assuming that the total propellant supply was expended at the lowest possible burnout altitude (25,000 ft)[9]. Calculated concentration levels, assuming 100% absorbance, are shown in Table 34.

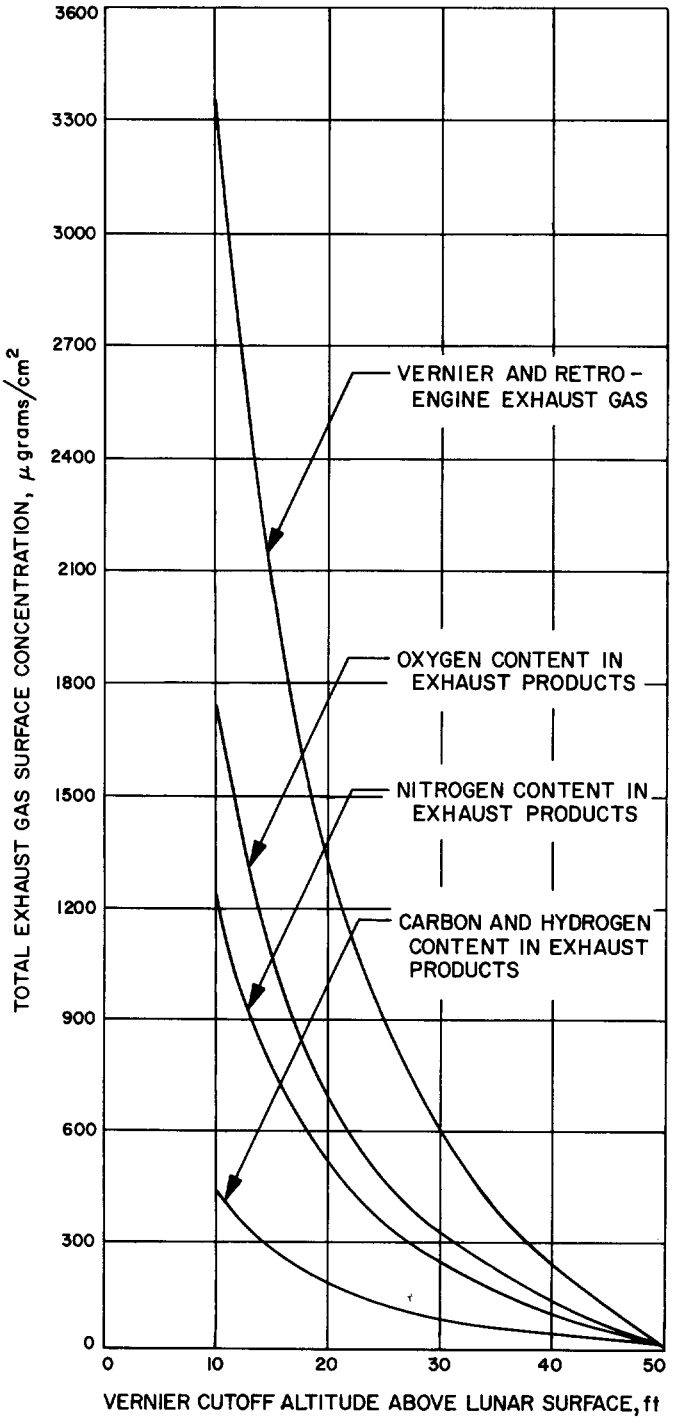

Fig. 50. Total lunar-surface contamination due to retroengine and all vernier engine exhaust products

The solid particle (Al_2O_3) impingement concentration due to main retroengine exhaust was conservatively estimated, assuming again that the total retroengine propellant supply was expended at the lowest possible burnout altitude (25,000 ft). The average size of solid particles has been shown to be about 4 μ; for this engine the solids account for 29% of the total exhaust products. An appropriate particle expansion angle was determined for this size particle. Again assuming 100% absorbance, conservative estimates are shown in Table 34. Assuming that the entire descent is vertical and that the centerlines of all the jets are coincident, the maximum surface contamination is estimated to be about 3 mg/cm^2.

Fig. 50 shows the expected concentration levels of all exhaust products as a function of the vernier engine cutoff altitude above the surface.

c. Conclusions. It is seen from Table 34 that the main retroengine contributes negligibly to the total combustion product concentration level, even under the most conservative assumptions, and that almost all of the contamination results during the final descent from 50 ft to vernier engine cutoff.

Presently there appears to be no way to reduce significantly the amount of contaminants impinging on the lunar surface. Fig. 50 shows that a modest increase in cutoff altitude would not appreciably decrease the surface contamination.

L. Spacecraft Vehicle and Mechanisms

A-21 flight and test vehicles. In response to an action directive from JPL, the Mod 56 program redirection for *Surveyor* was initiated. This change has added three additional flight vehicles to the A-21 program. They are engineering payload configurations and are similar to the present A-21 models, with certain modifications. The

[9] This value was used in the calculations instead of 38,000 ft so as to remain as conservative as possible and still show negligible retroengine contamination levels when compared with those contributed by the vernier engines.

CONFIDENTIAL
UNCLASSIFIED

UNCLASSIFIED
CONFIDENTIAL

major items to be accomplished by these modifications are as follows:

(1) Design of the thermal compartments will be improved to allow quick access to internal components and test connectors. To accomplish this a simplified thermal shell and insulation blanket will be incorporated. The thermal shell will be removable, a single unit attached with screws and plate nuts (Fig. 51). Another common attachment method utilizing sheet metal hinges and removable pins is being evaluated to further enhance ready access. The insulation for the compartments is a mylar blanket made from 75 sheets of 0.25-mil material faced with 1-mil material and stitched with nylon thread to form a single part that affords easy handling. This configuration is also less susceptible to damage than the present design. After removal of the thermal shell the vertical sides of the blanket are folded to rest above the top of the compartment, thus exposing all components and test connectors.

(2) Compartment trays are to be revised to improve component mounting. The difficulties encountered with the present Delron fasteners will be eliminated by incorporating Keensert fasteners installed in tray bosses. These bosses are simple cylindrical aluminum parts, approximately 0.50 in. in diameter, that are installed along with the core material between the tray face sheets to form the bonded tray assembly.

(3) The thrust chamber assembly bracket for vernier Engine 1 will be redesigned to provide $\pm$12-deg gimbal instead of the $\pm$6 deg now provided. This change will permit use of a single part configuration in place of the multipiece reinforced bracket on existing vehicles.

(4) Necessary harness redesign will be made to accommodate unit circuit changes. In addition, a solution to the problem of harness-to-connector strain relief is required. During this reporting period, a number of designs were evaluated and

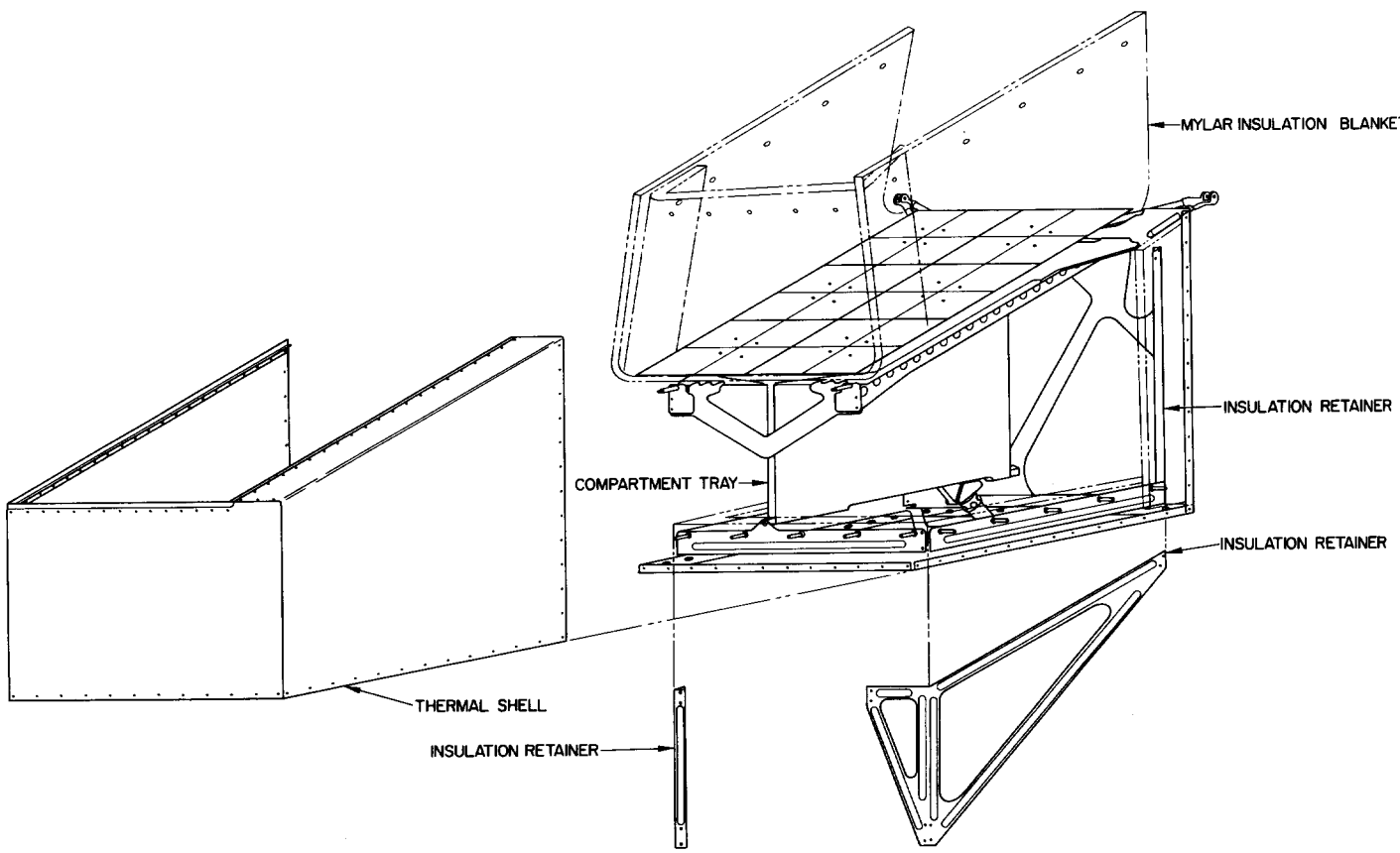

Fig. 51. Thermal shell

UNCLASSIFIED
CONFIDENTIAL

CONFIDENTIAL
UNCLASSIFIED

two types were chosen on the basis of weight and retrofit capability; these are a shrink boot type and a hardware type (Fig. 52). Further evaluation is necessary and tests will be conducted during the next reporting period.

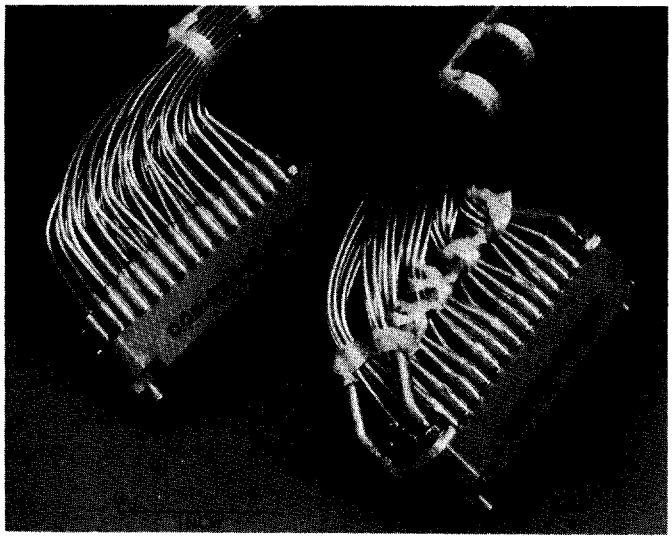

Fig. 52. Harness to connector with and without strain relief

(5) TV Camera 4 will not be flown on these three vehicles. This will delete the camera substructure and will require extensive changes to the substructure, spaceframe, and general arrangement drawings.

(6) Structural revision may be necessary for the installation of new higher torque motors for the antenna/solar panel positioner (A/SPP).

(7) The S-9 vehicle (structural test model) will be upgraded to agree with the above changes.

These and other changes, as required, are being incorporated through the formal change control and will be further delineated in future progress summaries.

S-9 engineering payload structural test model and S-10 thermal test model. The S-9 vehicle is now undergoing static loading in the structural laboratory while S-10 is at JPL for solar thermal vacuum testing.

A-24 flight and test vehicles. These vehicles were previously designated Model A-21A. Almost complete engineering emphasis was transferred to *Surveyor* Model A-21 during the first part of this reporting period. Status of the A-21A program at that time consisted of the completion of approximately 75% of all flight vehicle engineering with a number of test vehicle engineering drawings in work. In addition, a majority of the test vehicle engineering planning specifications were in the final stage of release.

Antenna/solar panel positioner (A/SPP). The A/SPP provides mounting, positioning, position indicators, and launch and landing locks for the planar array antenna and the solar panel. The antenna support structure includes controllable axes for roll, elevation, and solar and polar rotations. The drive for each axis uses a solenoid stepper motor for power and a wirewound potentiometer for position indication.

A formal design review of the A/SPP has been conducted. It was determined that a major design revision of the A/SPP be undertaken for effectivity on SC-5. The most significant change to be incorporated in this version of the A/SPP is a jackscrew and nut in the polar axis drive instead of a worm and sector gear. Additional modifications are an improved bearing support for the elevation axis, a modified solar axis with the elimination of one locking device, improved locks throughout, and the incorporation of a high torque stepper motor and planetary gear drive in each axes. Part number 293300 has been assigned to this model of the A/SPP, and intensive design and development effort has been under way since mid-January. Tests have been initiated in the components and materials laboratory to determine the best choice of materials and lubrication for the screw and nut. Some subassemblies of the new model have been released for fabrication of development hardware. Four concepts of the structure surrounding support of the planar antenna have been under study, and design is progressing on a selected configuration. Kinematics analysis of the solor axis has led to a modification of the torque tube and solar panel arms in order to relieve excessive loads that might have reflected into the drive under some conditions. Weekly meetings are being held on this A/SPP development to promote good communications with all concerned departments at HAC and with resident JPL engineers. Specific design features, overall progress, stress analysis, and schedule are covered.

Since the almost totally new A/SPP design entails some risk in being available for SC-5, a decision was also made, following the January design review, to conduct a parallel effort on a backup design. Part number 293275 has been designated the backup model. The design embodies the minimum changes to the existing A/SPP and corrects known areas of concern, including improved

CONFIDENTIAL
UNCLASSIFIED

UNCLASSIFIED CONFIDENTIAL

locks for the elevation and roll axes, strengthening of the web of the sector gear and the antenna support tube, and incorporation of high torque motors. This design effort has also been initiated with emphasis on the locking devices; the other changes are relatively simple and straightforward.

During this reporting period, a limited program for the A-24 Model was conducted. The prime items in work were (1) the development and fabrication of the M-14 mockup (Fig. 53), (2) the continued development of the touchdown dynamics instrumentation subsystem lunar contact switch and landing gear leg potentiometers and, (3) limited engineering on thermal compartments A, B, and touchdown dynamics instrumentation subsystem.

Early in January two drives in the SC-2 A/SPP failed, because of binding gear trains. One cause of failure was traced to rework of the train's aluminum gears, which actually removed dry lubricant and anodized at the extremities of the gear bores in order to ensure existence of a radius. A second, and more significant, problem was disclosed to be the lack of radial support to the first stage of the planetary gear drive, which had only two planet gears. This situation caused excessive misalignment between the drive motor pinion shaft and the planet gears. A design change has been incorporated (effective with SC-2) calling for the addition of a ball bearing in the planet carrier which maintains pinion and gear alignment within required limits. During investigation of the failure, the gear trains of all drives were examined for other potential areas of weakness. Consequently, the microseal lubricant was changed to Lubeco 905, a predominantly molybdenum disulfide base lubrication. In addition, harder materials were selected for both the aluminum and steel pins used to support gears, and

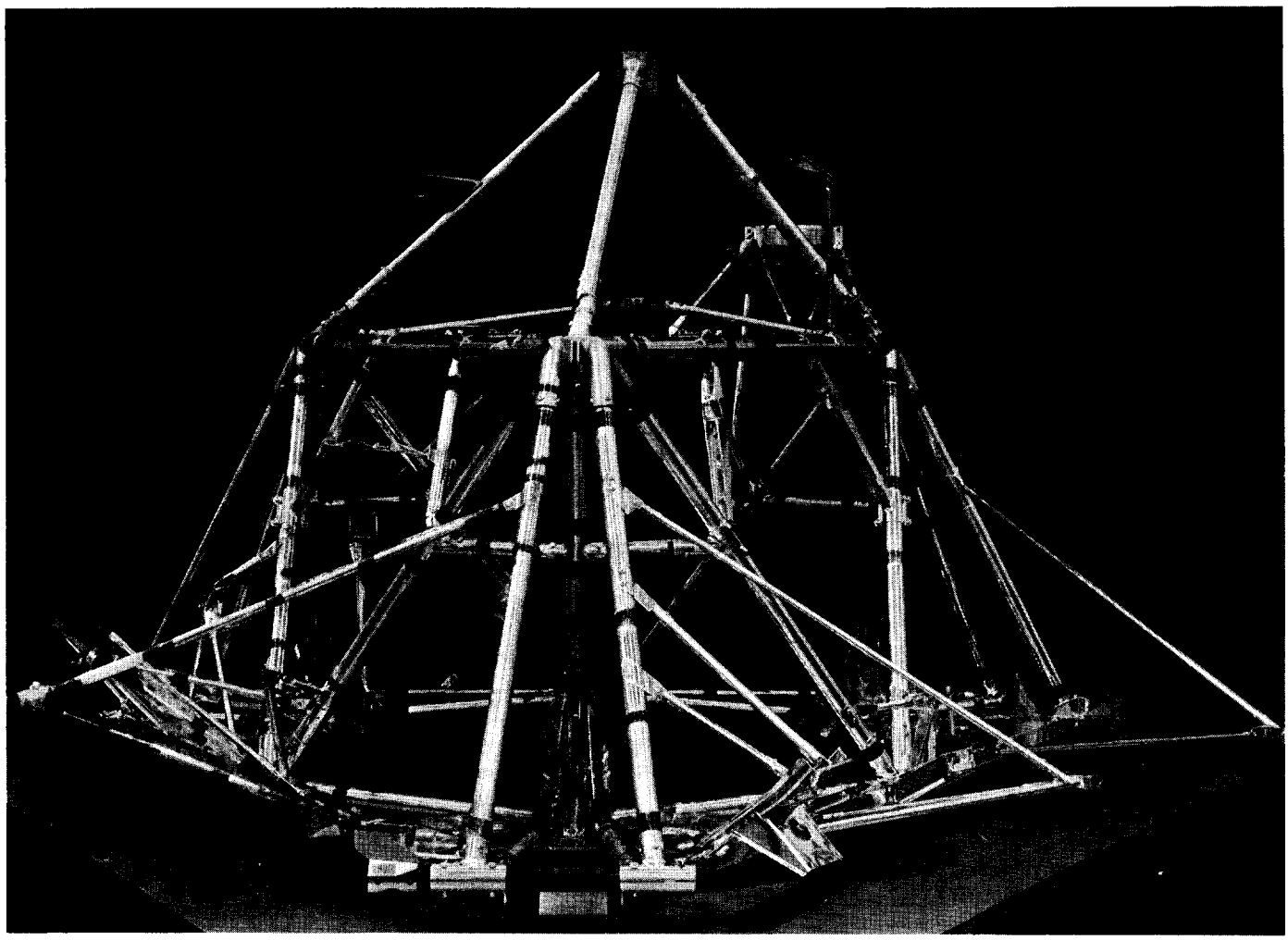

Fig. 53. M-14 mockup

UNCLASSIFIED CONFIDENTIAL

CONFIDENTIAL UNCLASSIFIED

harder surface treatments were applied to the pins. As a final measure, a stabilizing ball bearing was added to the first gear stage to prevent dislocation of the planet gear carrier. Six new drives have been built, four for the SC-2 A/SPP and two for engineering tests. The A/SPP has been reassembled and has nearly completed flight acceptance testing. One of the engineering drives has demonstrated satisfactory life and performance at ambient, low, and high temperatures.

A fixture has been completed for testing the cone worm and sector gear used in the polar axis drive of the A/SPP. The fixture permits controlled misalignment of driver and driven member and observation of performance under load. Still to be tested is performance in a vacuum at cold temperature.

A major design change to the lockpin puller arrangement has been made consisting of combining the lockpin and indicating switch into a module that can be preadjusted as a subassembly. Self-alignment is another feature of the new lockpin module; when the pin is in lock position, a small degree of freedom at the point where the pin attaches to the pulling device permits self-alignment. This configuration has been designed for all seven A/SPP locking locations and for the three operational modes: manual, test, and flight. In addition, the engineering team has designed all tools necessary for adjusting and installing the lockpin-switch modules. The design is planned for early release, with verification tests to follow on developmental hardware.

Tests on modified stepper motors are now applicable to developmental models. Results have been verified with a life test on a Class IV (production) stepper motor, and life test of a second production motor is nearly complete. These motors incorporate a double ball bearing roller detent with protective sleeves on the ball bearings. A vibration test to be performed during the next reporting period will complete the evaluation of this design improvement.

High-torque stepper motor. In support of these new A/SPP models, a dual effort is continuing in pursuit of a stepper motor that will reliably produce three to four times the torque of the existing A/SPP drive motor. A HAC-conceived solenoid type stepper motor is being fabricated in breadboard form to prove basic magnetic and mechanical features. Flight version drawings of the motor have been completed, and fabrication is pending. Suppliers of stepper motors have been presented with revised specifications; initial response indicates that at least a few vendors may offer a motor suitable for alternate choice in A/SPP drives. The entire motor effort has been placed in a control systems laboratory equipment development group in order to provide rapid expansion of the effort devoted to *Surveyor* mechanisms and to relieve continuing *Surveyor* mechanisms activities.

Thermal switches. Thermal switches, mechanical devices mounted on the spacecraft's electronic A and B Compartments, provide temperature control through bimetallic action on a thermally conductive contact. These mechanisms connect or disconnect a highly reflective surface to the mounting surface.

An improvement in thermal switch performance appears feasible through the first of silvered reflection mirrors having vicor glass bases. Engineering data have been completed on this type of mirror, and an order has been placed with a vendor for an initial quantity. Delivery is expected, and design verification and type approval tests will be performed.

The first of four thermal switches subjected to a performance check following prolonged (3 mo) storage, operated within specified tolerances on its first cycle. This test is an attempt to discover any tendency for the thermal contact to stick after long periods of closure.

Omnidirectional antenna mechanisms. The two omnidirectional antenna mechanisms (A and B) are tapered fiberglass cloth tubes bonded to aluminum hinge bracket assemblies. They deploy and lock the two omnidirectional antennas into operating position before separation from *Centaur*. Omnidirectional antenna mechanisms A and B for SC-3 were delivered to bonded stores. The units for SC-4 are in process, and delivery is expected.

Separation sensing and arming devices. Three separation sensing and arming devices per spacecraft provide redundant actuation of the postseparation squib firing circuits and vernier engine solenoid circuit after the spacecraft separates from *Centaur*. Units of the three-switch design have been reworked to a (-1) configuration, which ensures no binding at the internal actuator arm pivot point. This configuration has been retrofitted to the SC-1. Units for SC-2 are in bonded stores.

Pyrotechnic devices. Because consumption of the basic pin puller squib (236472-1) has greatly exceeded the original estimate, an additional quantity was requisitioned. Proposals received from eight vendors were reviewed and evaluated, resulting in the award of a

CONFIDENTIAL UNCLASSIFIED

UNCLASSIFIED
CONFIDENTIAL

subcontract to the Hi Shear Corporation of Torrance, California, for the manufacture and qualification (type approval) testing of 2500 squibs. The part number was changed to 293162 to reflect an increase in the postfiring resistance to ground specification. Twelve additional sets of pyrotechnic devices for the T-2 vehicles have been flight acceptance tested for shipment to Holloman Air Development Center.

M. SC-1 Transit Thermal Model

A number of IBM 7094 computer programs have been under development in the Space Flight Operations Department of the *Surveyor* project at HAC space flight operations facility for use in the JPL space flight operations facility (SFOF) data processing system. These programs will be used during missions A and B to assist members of the spacecraft performance/analysis/command (SPAC) team to evaluate spacecraft performance during actual flight.

The development cycle for the Mission A programs has been completed and these programs are being used during space flight operations facility (SFOF) tests as part of the normal SPAC operation. Scheduled for use during Mission A are a data reduction program, which processes raw data into engineering units; a calibration curve fit program, for DSIF receiver automatic gain control (AGC); a telecommunications prediction program for predicting signal levels and minimum margins throughout the mission; a tape read/write program for recovering data which have been lost due to computer outages; and an attitude determination program, for establishing the spacecraft attitude after landing.

For Mission B, a number of additional programs are scheduled for use. These are a power management program, to bookkeep the battery condition and predict spacecraft power requirements; a thermal management program to predict potential thermal problems; a command sequence bookkeeping program, to establish times for status events for the other management programs; a command preparation program, to construct new or revised command sequences to control the spacecraft; and a command transmission program, to format a series of commands prepared by the command preparation program for transmission on the teletype lines to the DSIF stations and verify their transmission. Development of all Mission B programs is substantially complete at this time and operational experience is being gained in a series of special tests prior to their being used in the Premission B testing phase.

Thermal management program function description. The thermal management program was developed to utilize the mathematical thermal model (which is an electrical analog of the spacecraft heat transfer problem, spacecraft telemetry, operational sequence, and power dissipation data) in order to solve a system of differential equations that describe the thermally controlled compartments and other equipment aboard the *Surveyor* spacecraft that are temperature-critical. The program routine is designed to handle a spacecraft surface to which electrical or heat generating units are mounted. When thermal nodes can be selected, a statement can be made that the sum of heat into and out of a node is zero, assuming that the nodes are thermally interrelated. Therefore, a system of differential equations can be written for which the solution yields the temperature of the node as a function of time.

In order to solve the spacecraft thermal problems, two types of information are required:

(1) Geometry data—i.e., how many nodes and how the nodes are thermally related for the physical body in question.

(2) Thermal parameters of the nodes—i.e., heat into/out of the node due to electrical energy dissipation and/or due to solar and lunar radiation and conductance between related nodes.

Basically, the thermal management program for *Surveyor* Mission B is divided into the transit, lunar day, and lunar night phases. The geometry and thermal parameters for each phase are contained in separate models such that the operator may select any or all of these models to be solved for a particular computer run.

Two modes of computation are available: the update mode and the predict mode. In the update mode, the program will take the actual spacecraft temperature values and use these data to compute future temperature values. In the predict mode, the program will forecast the temperature values at a specific time based on a set of previously computed values. In addition, the program has the option of predicting temperatures using the minimum nodal time constant of a model to predict all nodal temperatures or to predict nodal temperatures at some desired time using each node's individual time constant. Fig. 54 shows the functional flow for the thermal management program. Operations are not necessarily shown

UNCLASSIFIED

UNCLASSIFIED

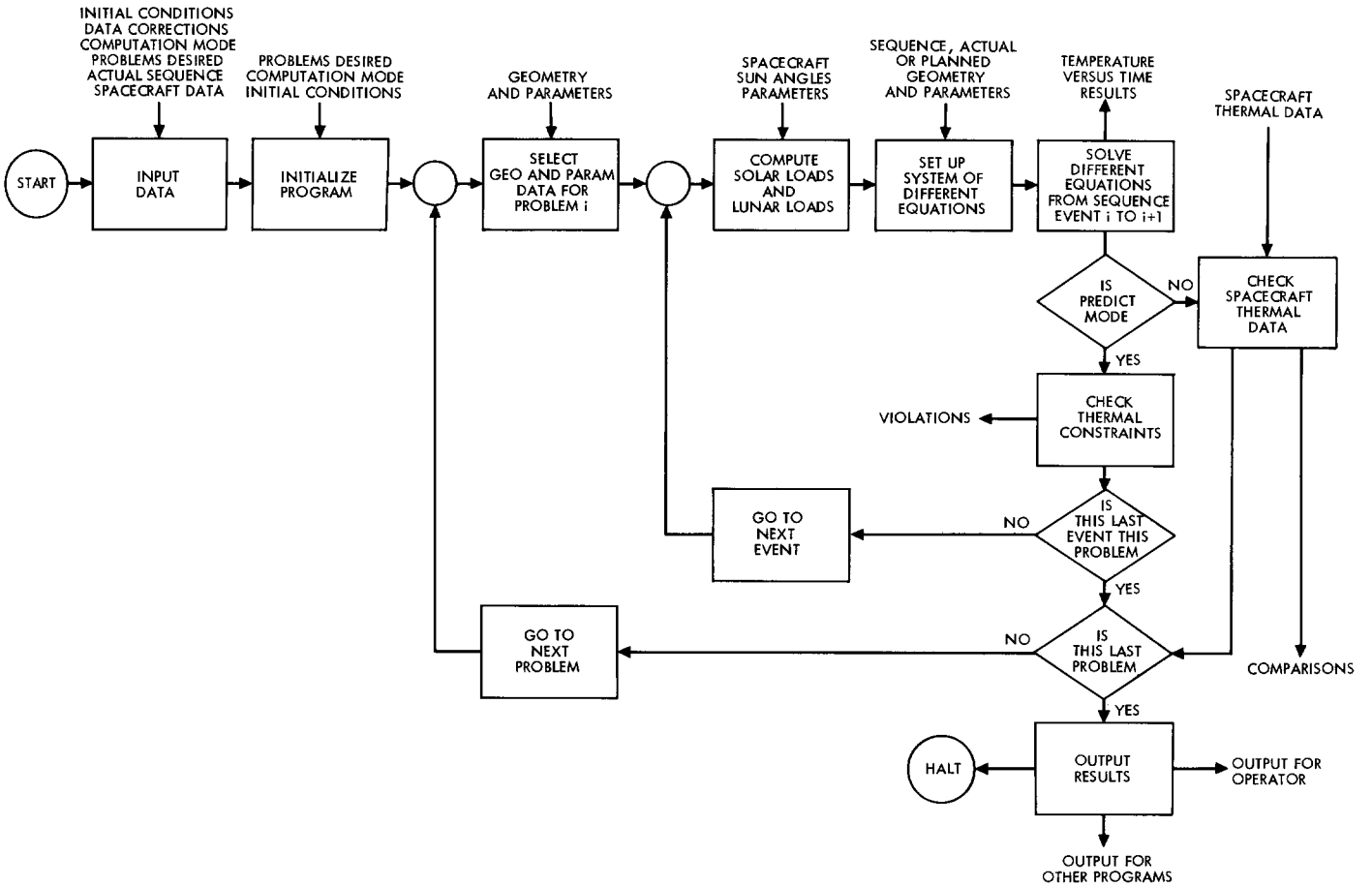

Fig. 54. Thermal management computer program functional flow diagram

UNCLASSIFIED

UNCLASSIFIED
CONFIDENTIAL

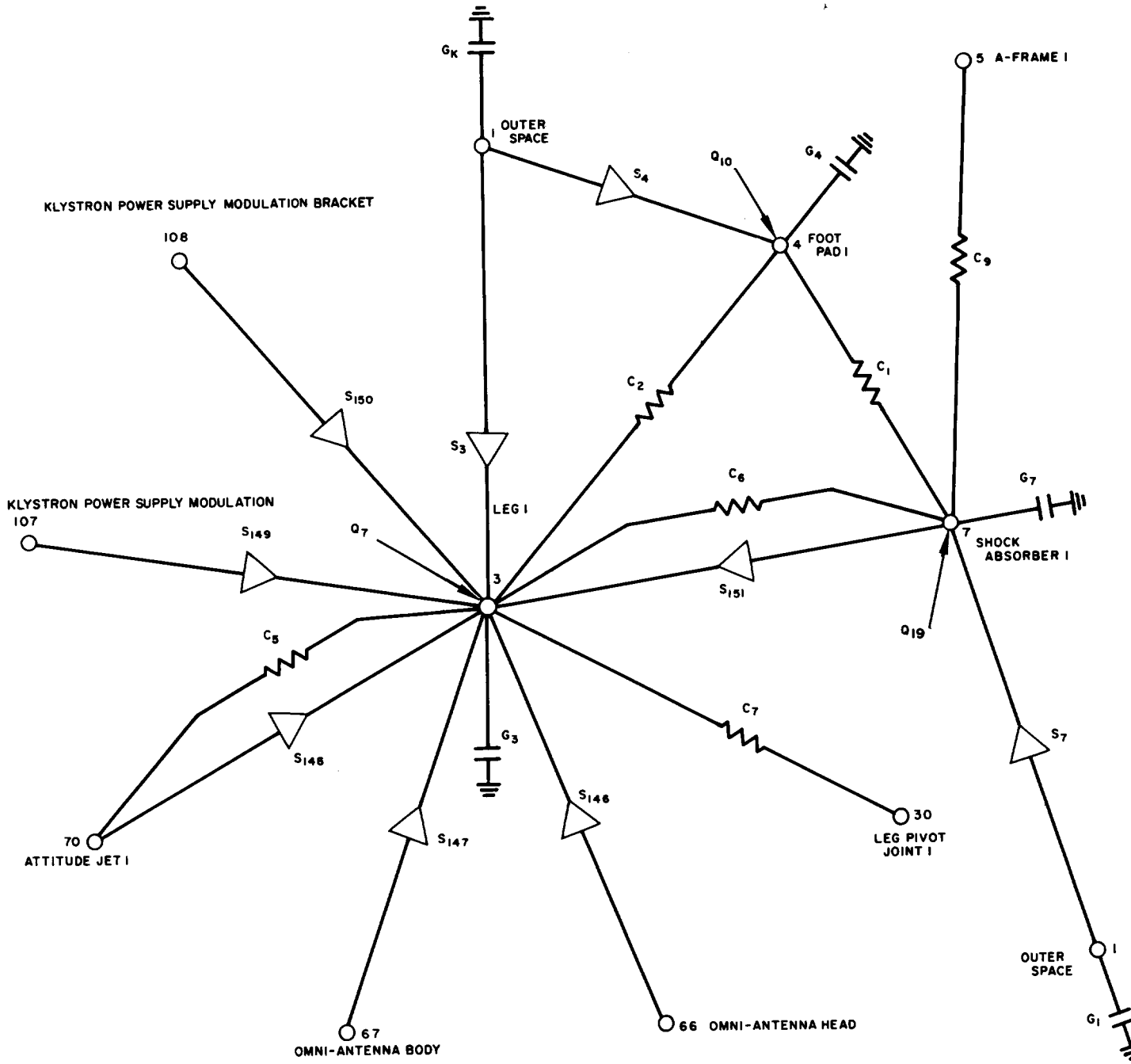

Fig. 55. Eleven-node electrical analog model

UNCLASSIFIED
CONFIDENTIAL

CONFIDENTIAL

in the order in which they are performed. Arrows into the blocks show data used by a function. Arrows out of the blocks indicate data saved for output.

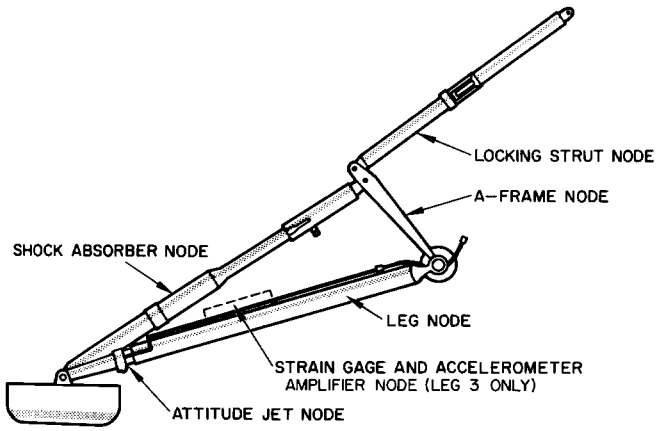

Fig. 56. Landing gear assembly

Transit thermal model fundamental analysis. Ref. 1 fully presents an initial model which is used to study the effects of parameter variation and subsystem isolation on the overall program stability and validity. An eleven-node electrical analog model (Fig. 55) of the landing gear assembly (Fig. 56) is presented and analyzed over a ten iteration period from launch through approximately the first hour of flight. The computing interval of 346.0581 sec is derived from the minimum nodal time constant of leg 1. The computing interval is based on the assumption that a maximum temperature of 200°F can be experienced by any node. Two time-varying data functions are used in this model:

(1) Cosine of Sun incidence angle used to determine solar heat inputs to leg 1, footpad 1, and shock absorber 1 (Fig. 57).

(2) Effective sink temperatures of surroundings (Fig. 58).

The eleven-node electrical analog model was initially run at the JPL computer facility on November 18, 1965, using the certified thermal management program load tape 1100. At this time, two significant deficiencies were uncovered: (1) the program would not operate satisfactorily when the print interval was in the vicinity of the value of the minimum nodal time constant; and (2) the program would not accept a nonintegral print interval.

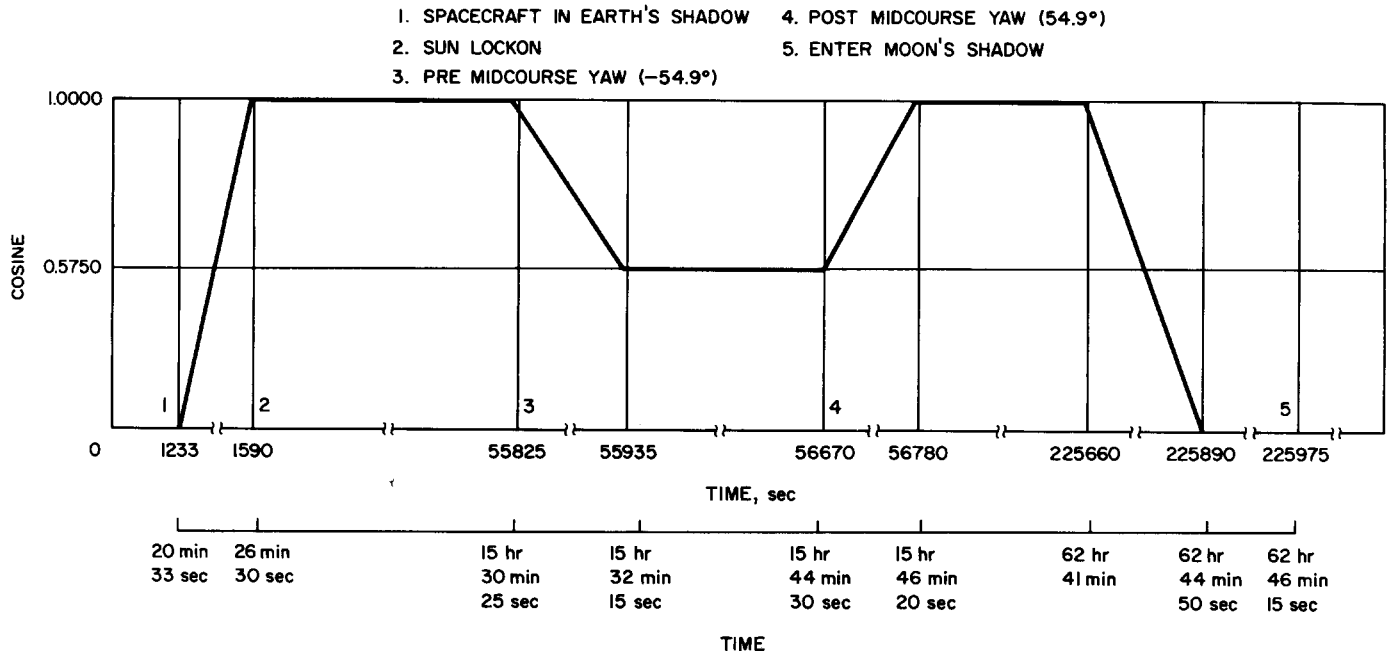

Fig. 57. Cosine of Sun incidence angle

UNCLASSIFIED

UNCLASSIFIED

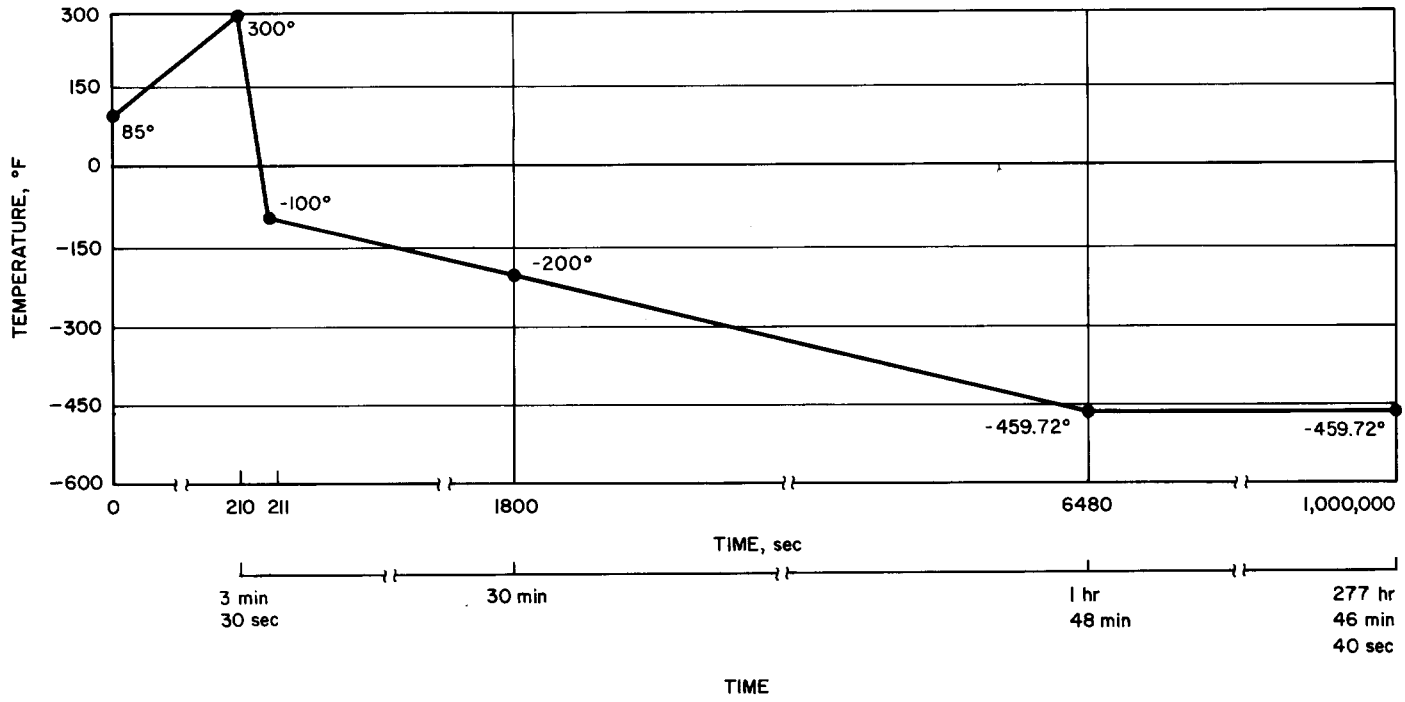

Fig. 58. Effective sink temperature of surroundings

These deficiencies have been corrected in thermal management program load tape 2130.

Transit thermal model conclusions. At launch, all nodes are assumed to be at 85°F. The initial disturbance to the system is effected by the sink temperature of the surroundings. From its time plot (Fig. 58), this temperature is seen to vary linearly from 85°F at launch to 300°F at 210 sec. At 210 sec, it is assumed that spacecraft nose fairing jettison occurs and the temperature falls to −100°F in about 1 sec. From the temperature plots in Fig. 59, it is interesting to note that the difference between the machine computations and the hand computations (which neglected the 300° peak) amount to about 10° at the steady state. Steady state normally occurs after about the tenth iteration (first hour of flight). Because the heat buildup prior to release of the nose fairing is neglected in the hand computation and because the actual nodal temperatures are higher, temperatures associated with these computations can be considered the minimum expected nodal temperatures.

As shown in the temperature plots in Fig. 59, the temperatures are reduced until just prior to the fifth iteration (1730.2905 sec), when they increase as a result of solar radiation applied to the spacecraft after emergence from the Earth's shadow during the fourth computing interval. At 1590 sec, and still during the fourth iteration, Sun lockon occurs and the solar heat input remains constant until the premidcourse velocity correction occurs (at about 15 hr and 30 min). During the remaining iterations, the slopes of the curves are decreasing, and, hence, the nodes are approaching steady-state temperatures.

Although the results of this analysis can be considered questionable, due to the choice of nodal time constant and the simplicity of the model used, an academic approach of this type is essential for a satisfactory understanding of the system with regard to both the spacecraft and its thermal behavior.

N. Aerospace Ground Equipment

System test equipment assembly (STEA) equipment. Design of the STEA equipment for the new screen room in Building 350 has been completed. The new equipment is in fabrication and will be ready for electromagnetic interference tests on SC-2 spacecraft. A *Centaur* programmer from combined systems test was incorporated into the STEA for the last solar thermal vacuum test on SC-1 spacecraft. The purpose of using an actual *Centaur*

UNCLASSIFIED

UNCLASSIFIED
CONFIDENTIAL

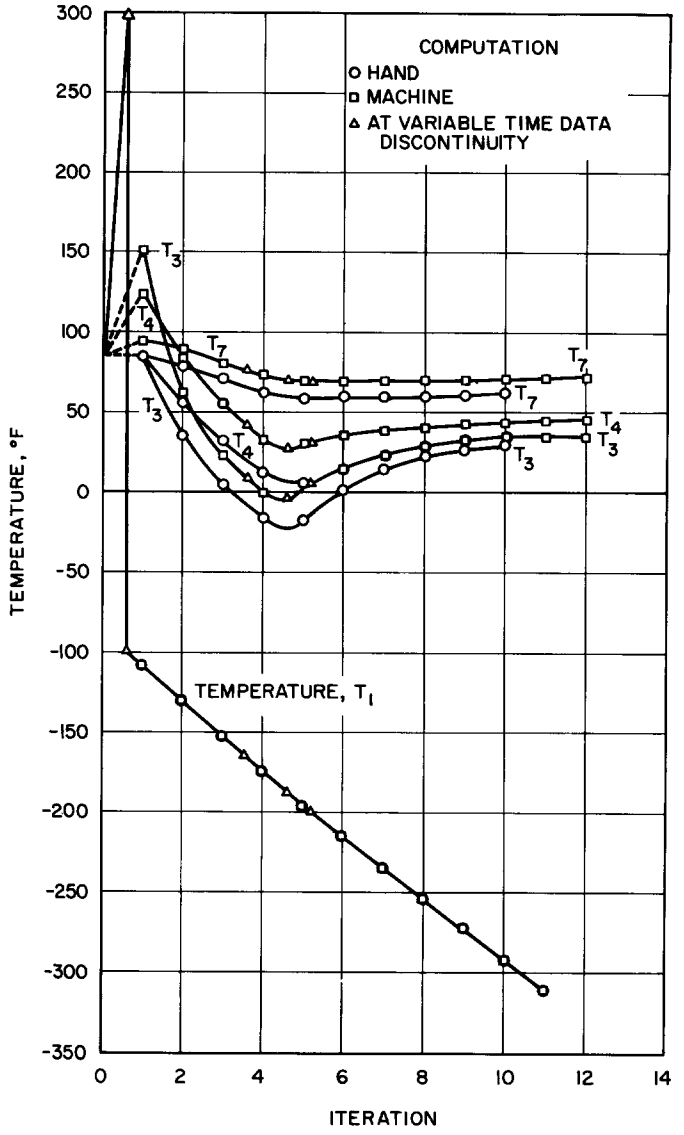

Fig. 59. Node temperatures

programmer was to determine if spurious signals might be generated which could fire spacecraft squibs.

Spacecraft testing. A plugs-out relay box was designed and built for the SC-1 spacecraft plugs-out test in the chamber. The box was to open all leads into the umbilical connector within 3 ft of the spacecraft, simulating actual spacecraft configuration after separation from *Centaur*. Provision is being made to monitor the voltage of each cell in the spacecraft main battery while it is mounted in the spacecraft. The monitoring will be done with the JPL supplied power scanner.

STEA 3 report. The T-21 drop tests, utilizing the STEA 3 trailer installation at El Segundo, were completed Saturday, January 15, 1966. During this series of tests the portable AGE equipment provided continuous support to T-21, which was subjected to three drops on the simulated lunar surface. Thus, the T-21 tests were accomplished without interfering with other spacecraft or other AGE equipment in Buildings 350 or 365.

On completion of the T-21 drop tests, an extremely tight schedule required immediate shipment of the STEA 3 equipment to General Dynamics/Convair (GD/C), for installation and use with SC-1. All components were inventoried and documented jointly by AGE, HAC quality control, and JPL quality control. Conditions of components were visually verified, several complaints were worked off, and the trailer was serviced for the trip to San Diego. Several TFRs were cleared from the equipment that had been used through the T-21 tests and this equipment was included in the scheduled shipment. Portions of the STEA 3 equipment not permanently attached to the trailer were shipped separately by van. The trailer arrived at GD/C January 18, 1966.

Reference

1. Rona, J. M., *Fundamental analysis, SC-1 Surveyor Spacecraft, Transit Thermal Model, Eleven Node Thermal-Electrical Analog, Leg No. 1 Landing Gear Assembly*, Report SSD 68029R, Hughes Aircraft Co., Culver City, California, January 24, 1966.

UNCLASSIFIED
CONFIDENTIAL